Intention Estimation and Control of a Wrist Rehabilitation Exoskeleton

Yihui Zhao

University of Leeds

School of Electronic and Electrical Engineering

Submitted in accordance with the requirements for the degree of

Doctor of Philosophy

March, 2022

Intellectual Property Statement

The candidate confirms that the work submitted is his own, except where the work that has formed part of jointly-authored publications has been included. The contribution of the candidate and the other authors to this work has been explicitly indicated. The candidate confirms that appropriate credit has been given within the thesis where reference has been made to the work of others.

The candidate performed the major tasks of the work presented in these published papers, such as development of the model, experimental procedures, data analysis and the results. The co-authors reviewed and guided the candidate and provide valuable feedback.

Acknowledgements

I would like to express my sincerest gratitude to my supervisor Prof. Shane Xie, who offered me this opportunity to start my PhD. I am appreciate for his encouragement, guidance, and insightful feedbacks throughout my entire PhD study. I would also like to thank my co-supervisor Prof. Abbas Dehghani for his guidance and patience. None of my work would have been possible without their kind supervision. I would like to offer my special thanks to Dr. Zhiqiang Zhang and Dr. Zhenhong Li for their invaluable advice not only in my study, but also for my daily life.

I would like to take this opportunity to thank my friends and colleges in our lab, Kun Qian, Yue Zhang, Tianzhe Bao, Chao Wang and Orla Gilson, with whom I have had many constructive discussions regarding my work

I would like to thank my parent for their love, caring and sacrifices for educating and preparing me for my future. I also express my thanks to my sister and brother for their support. I give my deepest love to my parents and all family members for their love throughout my life. Finally, I am grateful for all the volunteers who participated in this study.

Abstract

Wrist rehabilitation robots have been broadly investigated in the past decades. Robot-aided rehabilitation aims to assist patients in restoring motor functions of the wrist joint after neurological disorders, of which patients' motor intention plays an important role in the control strategy. Electromyography (EMG) signal provides a promising solution to estimate motor intention at the spinal cord level. It is challenging to adopt the EMG-based approach for control of the wrist rehabilitation robots. The implementation of the EMG-based approach with the control strategy is still at the very beginning, and current EMG-based approaches fail to capture the underlying intermediate muscular and skeletal information that aids the robot-aided wrist rehabilitation.

This thesis aims to develop real-time EMG-driven musculoskeletal models for the wrist joint as well as model-based active assistive control strategies. This first goal is to develop an EMG-driven musculoskeletal model for wrist flexion/extension motion. By interpreting the internal transformation from the muscle activity to the joint kinetic and kinematic characteristics, this model is able to identify wrist motion correctly. Secondly, a sensitivity analysis is conducted to investigate the sensitivity of the model's performance to the key parameters of the model. To facilitate the use of the EMG-driven model in the practical scenario, a direct collocation method is proposed to effectively optimize the subject-specific parameters. Thirdly, two control strategies incorporating the EMG-driven musculoskeletal model are developed, namely, adaptive cooperative control strategy and assist-as-needed control strategy. The first control strategy combines a position controller and an admittance controller to adapt the robot's

behaviour by consideration of the subject's voluntary effort and joint stiffness. The other control strategy employs the admittance controller combined with a force controller to assist the subject to accomplish the intended motion. Finally, the development of the EMG-driven model is explored for estimating the continuous multiple degree-of-freedom wrist kinematics using mirrored bilateral movement. This model also lays the substantial groundwork for future development for multiple DoF wrist robots.

The proposed EMG-driven musculoskeletal models provide insightful understandings of the underlying transformation from muscle activity to the wrist joint motion intention and achieve high estimation accuracy. This thesis first demonstrates the implementation of the model-based control strategy for improving the performance of the wrist rehabilitation robot. The model-based control strategy opens up new possibilities in the field of robot-aided wrist rehabilitation.

Contents

List of Figures

List of Tables

Abbreviations

ADL	Activity of Daily life
ANOVA	Analysis of Variance
AAN	Assist-As-Needed
DoF	Degrees of Freedom
ECRL	Extensor Carpi Radialis Longus
ECRB	Extensor Carpi Radialis Brevis
ECU	Extensor Carpi Ulnaris
EMG	Electromyography
FCR	Flexor Carpi Radialis
FCU	Flexor Carpi Ulnaris
IMU	Inertia measurement unit
MTU	Muscle-tendon units
MRI	Magnetic Resonance Imaging
NRMSE	Normalized Root-Mean-Square-Error
PID	Proportional-Integral-Derivative
PAM	Pneumatic Artificial Muscle
RoM	Range of Motion
RMSE	Root-Mean-Square-Error
sEMG	Surface Electromyography

Chapter 1

Introduction

1.1 Background

Wrist joint contributes significantly to the functions of the upper limb for performing the activities of daily lives (ADLs), experiencing multiple tasks, e.g., drinking, eating, and writing, throughout the day [19]. The wrist joint allows the hand performs the object manipulation with respect to the forearm. However, its functionalities are severely affected by the motor impairment that caused by stroke, which is a leading cause of disability and the fourth killer in the UK. It is reported that around 38000 people are died because of stroke and there are over 1.2 million stroke victims in the UK in 2016 [20].

Motor impairment is the most common and widely recognized impairment caused by stroke, with respect to the significant deviation in structure of the nervous system or a limitation in mobility [21]. The symptoms in upper limb after stroke include weakness in the arms, a lack of coordination, a change in muscle tone, swelling, pain, and spasticity. The functionalities of the wrist joint is reduced or eliminated [22]. Recovery of the impairment and the related functions are the primary goal of stroke rehabilitation [23].

Conventional wrist rehabilitation program contains the active/passive range of

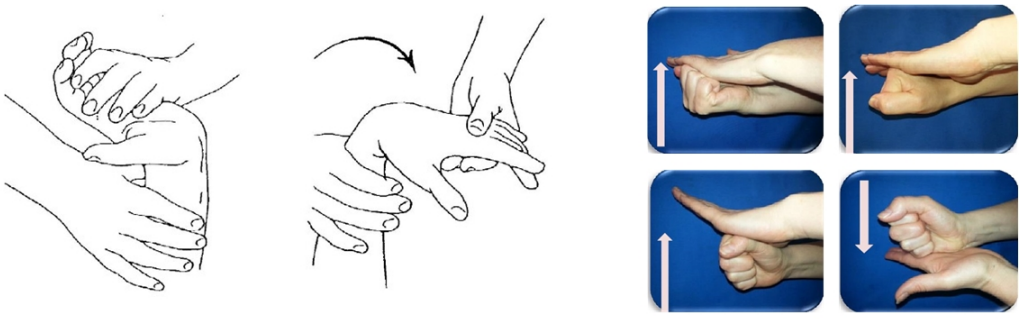

Figure 1.1: Examples of wrist joint therapy: (a) Assisted movement [1]. (b) Muscle strength training [2].

motion (RoM) training and muscle strength training protocols for post-stroke patients. Training protocols including high-intensive, repetitive and task-oriented movements that can promote motor recovery [23]. However, the long-term rehabilitation programs, throughout the patients' life, are labour-intensive and costly [24]. To tackle these issues, robot-aided therapy has grown rapidly in the last decades. Robots hold promising advantages to deliver therapy for a long time period in a high-intensive and precise manner [25–29].

Wrist rehabilitation robots are categorized into two types, end-effector and exoskeleton. The end-effector type provides prescribed motions to the patient's wrist joint, by asking patients hold the manipulator's end-effector. The exoskeleton is composed of a mechanical structure that is closely integrated with the wrist joint. Control strategies have been broadly designed and implemented for both types, delivering different rehabilitation tasks.

The control strategies are designated to restore the functionalities of wrist joint and promote the motor recovery [30]. As shown in Figure 1.2, the control strategy is divided into two categories, trajectory tracking control strategy and active assistive control strategy. The trajectory tracking control guides the wrist joint

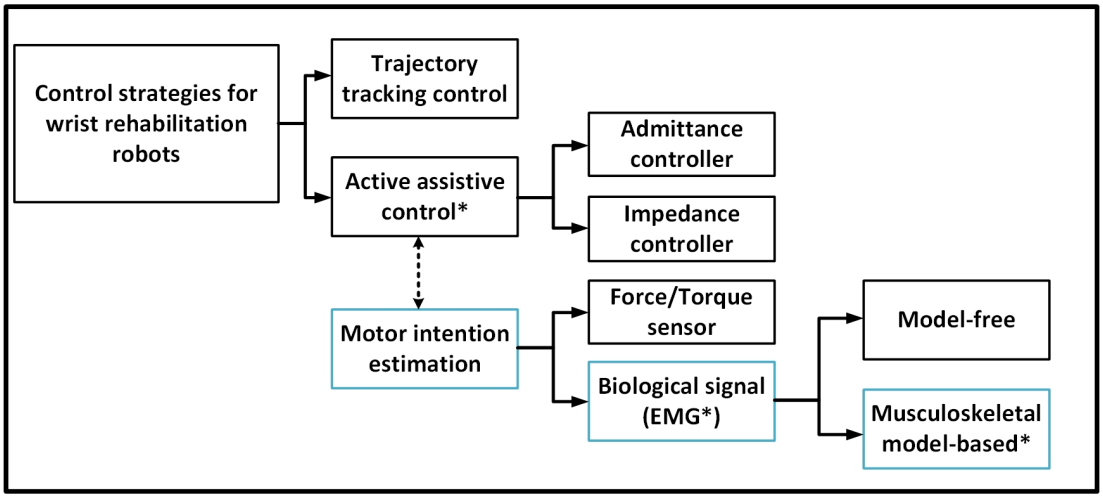

Figure 1.2: Classifications of control strategies and motion intention estimation for wrist rehabilitation robots

following a reference trajectory to stretch the muscles and restore the range of motion. The active assistive control strategies are developed to provide the robotic assistance to provoke motor recovery in rehabilitation programs [31–34]. It is crucial to understand the patient's motion intention in these control strategies. Conventional methods for intention estimation use the force/torque sensor [5], or combined with robot's dynamics [35]. Nevertheless, the measured motion intention may not represent the true voluntary effort due to the inherent noise, such as gravity, friction, and inertia. Recently, there is an increase trend in the use of biological signals for wrist rehabilitation robots, such as electroencephalogram (EEG) or electromyogram (EMG). The EMG signal is widely used as the signal is recorded from the spinal cord level and is more suitable to be integrated with the active assistive control strategies [36].

1.2 Research motivations

The state-of-the-art EMG-based motion intention estimation approaches are mostly based on the pattern recognition algorithm [37], and the model-free approach [38]. However, the pattern recognition algorithm is limited by its inherent discrete and sequential features and it can not recognize continuous kinematic variables. The model-free approaches employ the numerical transfer functions to map the EMG signal to the corresponding motion intention, but these approaches fail to interpret the underlying neuromuscular complexity. The musculoskeletal model-based approach explicitly represents the transformations between the EMG signal and musculoskeletal system to mimic the physiological human joint movement [39–41]. However, the use of EMG-driven musculoskeletal models for wrist rehabilitation robots has received less attention. The application of the model-based approach in the practical scenario is also limited by its complicated physiological parameters, resulting in a lengthy time to identify these values for each individual.

While EMG-based approaches are developed for few decades, incorporating the EMG-based approaches for the wrist robot is still at the very beginning [42, 43]. Efforts should be made into adopting the model-based approach for the control of wrist robots to realise more efficient and safe rehabilitation training environment. The main motivations of this research are to develop real-time EMG-driven wrist musculoskeletal models to provide accurate motion intention estimation while also provides the underlying intermediate effects between the muscular and skeletal systems. The musculoskeletal model-based approach then incorporates with the wrist rehabilitation robot to allow for active assistive control strategies with enhanced efficiency and safety.

1.3 Aims and objectives

1.3.1 Aims

The aim of this research is to develop real-time EMG-driven subject-specific musculoskeletal models for the wrist joint, which models are integrated with a wrist rehabilitation robot to improve its control performance as well as encourage active participation and enhance safety. In specific, the aims are:

- To develop EMG-driven musculoskeletal models for estimating the motion intention of wrist joint with high estimation performance.
- To reduce the optimization time for obtaining the subject-specific parameters in order to facilitate the clinical setup.
- To develop the musculoskeletal model-based control strategies for the wrist rehabilitation robot to enhance the training effectiveness and safety.

1.3.2 Objectives

The objectives are divided into several steps to achieve the aims described above.

- To develop and validate the EMG-driven musculoskeletal models for estimating continuous wrist flexion/extension motion.
- To evaluate the influence of the optimized parameters to the model estimation performance.
- To develop a method based on the optimal control theory to enhance the computational speed for parameter optimization.
- To incorporate the musculoskeletal model-based approach into advanced control strategies.

- To develop and evaluate the model-based approach for estimating the wrist joint in two degrees of freedom (DoFs) for the prostheses application using mirrored bilateral training strategy.

1.4 Thesis outlines

This thesis presents the work carried out in this research to achieve the aims and objectives. The first and second objective are achieved in chapter two and six with development of the EMG-driven musculoskeletal for estimating the continuous wrist flexion/extension motion. The sensitivities of the model parameters are analysed. The third objective is achieved in chapter four. A direct collocation method is proposed to optimize the physiological parameters in the wrist EMG-driven musculoskeletal model. The fourth objective is achieved in Chapter five. Two active assistive control strategies are implemented for a wrist rehabilitation robot, combined with the EMG-driven musculoskeletal model. The model is able to identify the subject's joint torque and joint stiffness in real-time. The last objective is achieved in Chapter six, in which the EMG-driven musculoskeletal model are developed to estimate the multiple DoFs of wrist joint using the mirror bilateral movement. Part of this thesis has been either published in peer reviewed conference and journal paper or submitted for possible publication.

In specific, this thesis are organized in the following:

Chapter one introduces the background of robot-aided wrist rehabilitation, along with the control strategies and motion intention estimation. The motivations, aims and objectives are presented.

Chapter two present a review of the state-of-the-art wrist rehabilitation robots and control strategies. This chapter also gives a review of the EMG-based motion

intention approaches implemented in wrist rehabilitation robots. Terminologies of the wrist anatomy used in the filed of robot-aided wrist rehabilitation are introduced. Furthermore, the gap of knowledge are defined.

Chapter three presents the development of the model-based approach that is used to estimate the continuous wrist flexion/extension movement. The underlying transmitted states from EMG signal to joint kinematics are explicitly presented. To optimize the subject-specific parameters, a genetic algorithm is designed to minimize the differences of predicted joint motion and ground truth. Furthermore, a sensitivity analysis is conducted in order to analyse the sensitivities of the model output to the optimized parameters. This chapter contains materials that have been published in [44]:

- Y. Zhao, Z. Zhang, Z. Li, Z. Yang, A. A. Dehghani-Sanij and S. Xie, "An EMG-Driven Musculoskeletal Model for Estimating Continuous Wrist Motion," in IEEE Transactions on Neural Systems and Rehabilitation Engineering, vol. 28, no. 12, pp. 3113-3120, Dec. 2020.

Chapter four presents the development of an effective parameter optimization algorithm for the model-based approach, according to the optimal control theory. A comparison of the computation speed is conducted with the use of genetic algorithm for model-based approach. Result demonstrates the proposed method require less optimization time. This chapter contains materials that have been published in:

- Yihui Zhao, Zhiqiang Zhang, Zhenhong Li, Ahmed Asker, Abbas A. Dehghani-Sanij and Sheng Q. Xie, "A Direct Collocation method for optimization of EMG-driven wrist muscle musculoskeletal model", 2021 IEEE International Conference on Robotics and Automation, Xian, China, 30 May to 5 June 2021.

Chapter five proposes the implementation of the musculoskeletal model-based approach for a pneumatic muscle driven wrist robot. two control strategies, adaptive cooperative control strategy and assist-as-needed control strategy, are developed. This first control strategy combines a position controller and a admittance controller to adapt the robot's behaviour by consideration of the subject's voluntary effort and joint stiffness. The other control strategy employs the admittance controller in combined with a force controller to assist the subject to accomplish the intended motion. In addition, the robot's compliance is adapted in response to the estimated joint stiffness through the EMG-driven model. This chapter contains materials that have been accepted for publication in:

- Yihui Zhao, Abbas A. Dehghani-Sanij and Sheng Q. Xie, "Electromyography-based Adaptive Cooperative Control for a Wrist Orthosi", IEEE 27th International Conference on Mechatronics and Machine Vision in Practice (M2VIP 2021), November 26-28, 2021, in Shanghai, China.

Chapter six investigates and validates the model-based approach that can be used for establishing the EMG-based interface for the prostheses device. A mirrored bilateral training is conducted to optimize the parameters for the missing limb. The estimation performance is evaluated on the six able-bodied subjects. This chapter contains materials that have been submitted for part of the possible publication as:

- Yihui Zhao, Zhiqiang Zhang, Member, IEEE, Zhenhong Li, Zhixin Yang, Abbas A. Dehghani-Sanij and Sheng Q. Xie, "An EMG-driven Musculoskeletal Model for Estimation of Wrist Kinematics using Mirrored Bilateral Movement", IEEE transaction on measurement and instrumentation. (under review)

Chapter seven summarizes the research work in this thesis and presents recom-

mendations for its further development.

Chapter 2

Literature Review

This chapter is organized into four sections. The first section gives an overview of the wrist anatomy and its functional range of motion. The second section investigates the wrist rehabilitation robot and the control strategy. Two types of wrist rehabilitation robots, end-effector type and exoskeleton are introduced respectively. The control strategies are categorized into trajectory tracking control and active assistive control strategy. The third section provides a review of the EMG-based motion intention estimation approaches that are used for the control of the wrist rehabilitation robot. Finally, a summary of the previous research areas is presented. The gaps of knowledge regarding EMG-based approaches for motion intention estimation and control strategies are discussed, which leads to the objectives and contributions of this research.

2.1 Wrist joint

Wrist joint represents the most complex joint system in the human body. This joint connects five metacarpal bones of the hand to the ulna and radius bones of the forearm governed by a series of small bones, muscles and ligaments [45]. As illustrated in Figure 2.1, these carpal bones are roughly organized into two rows:

the distal row and proximal row. The proximal row contains scaphoid, lunate, triquetrum and pisiform. Their movements depend on the mechanical force from surrounding articulations. The distal row is comprised of trapezium, trapezoid, capitate and hamate. The distal row bones are tightly bound to the metacarpal representing the carpometacarpal joint [46].

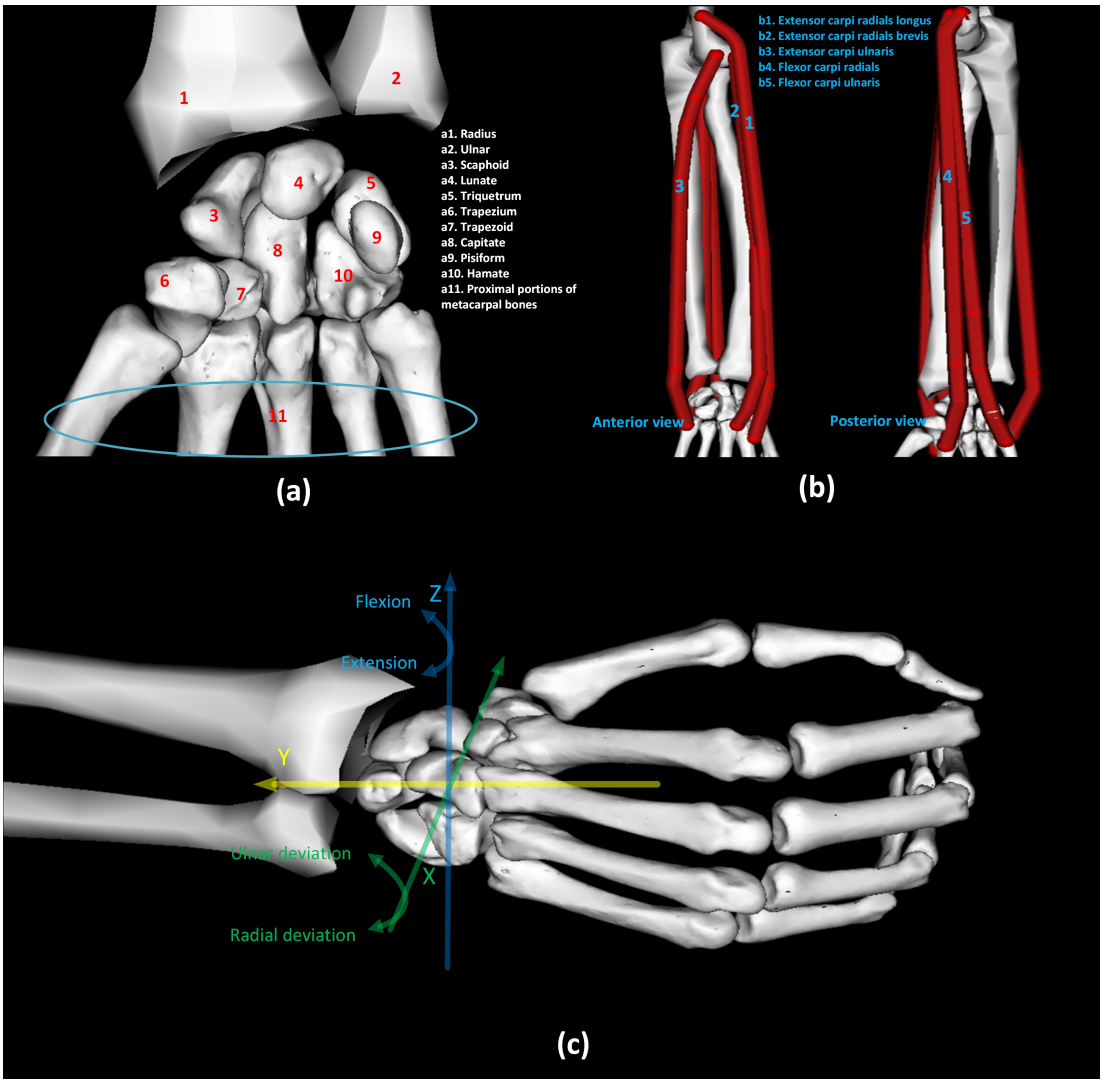

Figure 2.1: (a) Wrist anatomy. (b) Primary muscles contribute to wrist motion. (c) Wrist kinematics.

The wrist joint motion are typically recognized as two degrees of freedom (DoFs), including wrist flexion/extension, ulnar/radial deviation. These kinematic are articulated at the radiocarpal joint, the midcarpal joint, the carpometacarpal joint, and between individual carpal bones [18]. Table 2.1 gives the mean Range of Motion (RoM) of the wrist motions.

There are several muscles crossing the wrist joint and contributing to the wrist motion. These muscles can be grouped into flexors and extensors. Although all muscles are capable of rotating the wrist joint, the wrist motion is primarily articulated by the five wrist muscles, namely, flexor carpi radials (FCR), flexor carpi ulnaris (FCU), extensor carpi radials longus and brevis (ECRL, ECRB), and extensor carpi ulnaris (ECU).

In specific, the contraction of FCR and FCU are mainly contributing to the wrist flexion, with assistance from the fingers flexors, palmaris longus and abductor pollicis longus. The ECRL, ECRB, and ECU are primarily contributing to the wrist extension, with the help of the fingers extensors. The flexors and extensors also contribute wrist ulnar/radial deviation. Ulnar deviation is primarily caused by the contraction of FCU and ECU. The radial deviation is caused by the contraction of FCR, ECRL, and ECRB.

According to the International Society of Biomechanics (ISB) recommendation, the neural position of wrist joint is defined as in neutral flexion/extension and neutral ulnar/radial deviation, the third metacarpal long axis is parallel with the long axis of the radius [47]. In this thesis, the wrist flexion, ulnar deviation are defined as the positive direction while extension and radial deviation are defined as the negative direction.

It's critically considered that the forearm pronation/supination belongs to the forearm movement since this motion rotates around the forearm longitudinal axis. This is explained by the fact that the forearm pronation/supination is ar-

Table 2.1: mean RoMs for the wrist joint [18].

Motion	Range of Motions (RoMs)
Wrist flexion/extension	85°/-75°
Ulnar/radial deviation	35°/-25°

ticulated at the distal radioulnar joint and is produced by the contraction of an entirely different set of muscles. The pronator quadratus and pronate tere are the primary muscles for pronation. The supinator and biceps brachii mainly contribute to the supination. Thus, wrist flexion/extension and ulnar/radial deviation are considered as the pure wrist motion.

2.2 Wrist rehabilitation robots

2.2.1 Wrist rehabilitation

Patients after stroke or spinal cord injuries have the reduced or eliminated functionality at wrist joint that affects ADLs significantly. Physical therapies are delivered to help patients regain the motor control to perform the functional motion tasks. Several rehabilitation training strategies have been investigated, including the task-specific functional training, e.g., patients voluntarily perform the standard and repetitive tasks or strengthening training with some functional goal, [23, 48]. Other training strategies include constraint-induced movement therapy, which requires patients to use the impaired side to perform the functional tasks when patients while the unimpaired side is constrained [49–51]. Furthermore, bilateral training is another strategy to promote motor recovery, of which patients are required to perform the tasks using both arms. This is because that

the unimpaired side is able to improve the recovery of the impaired side due to the coupling effects between two arms [52].

2.2.2 End-effector type and exoskeleton

Wrist rehabilitation robots have been developed to alleviate the burden of the therapists as well as deliver the rehabilitation strategy. Wrist rehabilitation robots can be classified into two types, end-effector and exoskeleton, as elaborated in Table 2.2.

The end-effector based robots provides prescribed motions to the patient's wrist joint by asking patients to hold the robotic manipulator end-effector [53]. Some examples are illustrated in Figure 2.2. MIT-MANUS [3] is one of a typical robotic end-effector that is designed for wrist rehabilitation. This robot is capable of providing three active DoFs for wrist movements, including wrist flexion/extension, ulnar/radial deviation, and pronation/supination. Oblak *et al.,* developed an end-effector, called universal haptic drive (UHD) that provides the forearm pronation/supination in a 'wrist' mode [4]. By changing the offset position of the handle bar, UHD is designed to deliver wrist flexion/extension and ulnar/radial deviation exercise. Xu *et al.,* developed a single DoF wrist rehabilitation robot (WRed) for wrist flexion/extension[5]. The forearm is supported by an arm holder, the wrist joint is approximate to the rotation centre of WRed. Furthermore, Hesse *et al.,* developed a robotic end-effector to provide the passive and active bilateral training for forearm pronation/supination and wrist flexion/extension.

Exoskeleton has the mechanical structure that mirrors the skeletal structure of the limb. i.e., each segment of the limb associated with a joint movement is attached to the corresponding segment of the device. Martinez *et al.,* developed a wrist gimbal to enable the wrist rehabilitation for 3 DoFs [7]. Two bearings supports are

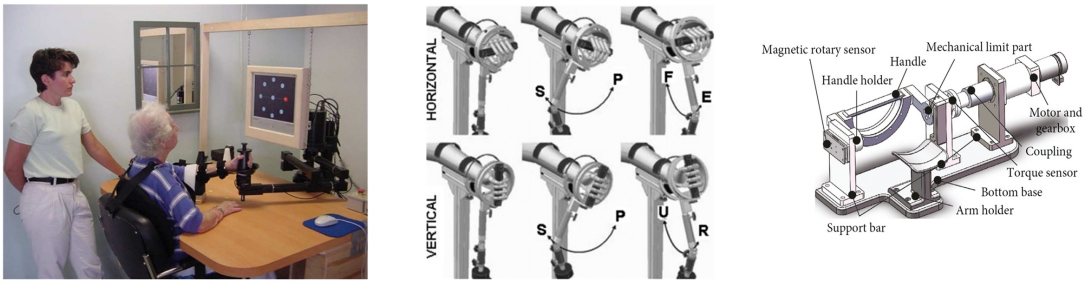

(a) (b) (c)

Figure 2.2: End-effector based wrist rehabilitation robots: (a) MIT-MUANS [3]. (b) Universal haptic drive [4]. (c) WRed [5].

implemented to ensure robustness and mechanical rigidity. An adjusted handle is used to keep the subject's wrist joint with robot's axes of pronation/supination and ulnar/radial deviation. Gupta *et al.,* developed a 4-DoF Rice-Wrist for the wrist joint [6]. a 4-DoF spherical joint is used to add the redundancy of the system and permits large rotations. Recently, Zhang *et al.,* developed a parallel wrist rehabilitation robots (PWRR), which is designed according to 2 spherical-universal-prismatic configuration [8]. It is driven by two pneumatic actuators to provide wrist flexion/extension and ulnar/radial deviation.

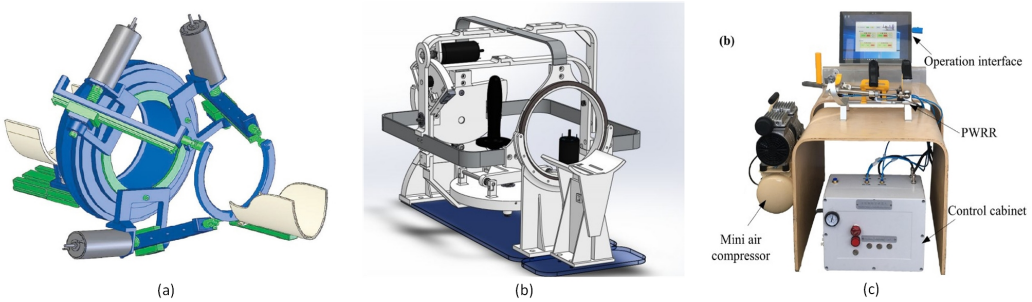

(a) (b) (c)

Figure 2.3: Wrist exoskeletons: (a)RiceWrist [6]. (b) Wrist Gambal [7]. (c)PWRR [8].

The exoskeleton also includes wearable robots that are concerned with the advantages of portability and low-weight (Figure 2.4). The wearable exoskeleton

allows the patients to easily don/doff. These exoskeletons are usually attached along the dorsal side of the forearm, covering the wrist joint and hand. Wrist flexion/extension and ulnar/radial deviation are commonly considered [54, 55]. For example, Chiaradia *et al.,* developed a cable-driven wrist exosuit to assist the wrist flexion movement [9]. A 3D-printed ergonomic plastic support is sewn in a glove to reinforce the force transferred from a dc motor to the wrist joint. The softness of wrist exosuit provides a high level of comfort for the user. Choi *et al.,* developed a soft tendon-driven wearable robots, called EXO-Wrist [10]. It provides assistance in wrist extension, in which the tension force is provided through a wire connected in series with a rotary motor. Exo-Wrist consists of a corset anchor to increase the force transmission efficiency. Higuma *et al.,* developed a low-profile wrist exoskeleton for wrist flexion/extension and ulnar/radial deviation [11]. As it is driven by two linear actuators that transform the force through two elastic elements, this device meets the requirements of compactness, low weight and flexibility. Su *et al.,* developed a 3 DoF wrist exoskeleton [56]. A lightweight and compact design is achieved by allocating three actuators in parallel with the forearm while the torque outputs for assistance are still guaranteed.

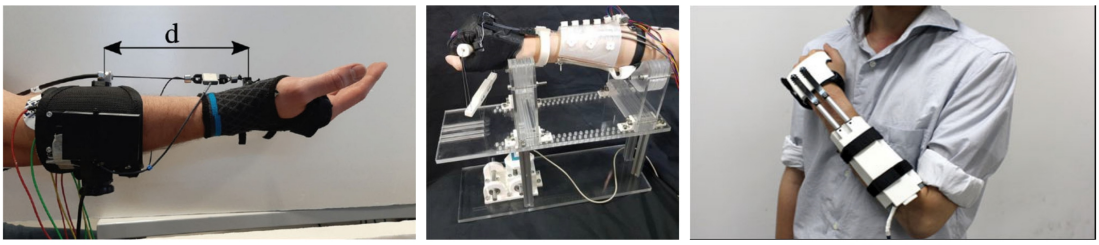

Figure 2.4: Wearable wrist exoskeletons: (a) WristExoSuit [9]. (b) Exo-Wrist [10] (c) Low profile wrist exoskeleton [11].

2.2.3 Type of actuator

Actuators are used to provide force to drive the robots to perform desired motion. Three types of actuators are commonly implemented for wrist rehabilitation robots including electric motors, series elastic actuators, and pneumatic actuators. The electric motors are commonly implemented for the wrist rehabilitation robots, in which the motors are used to actuate the robotic joint directly, such as MIT-MUANS, WRed, Wrist Gimbal. The electric motor can provide the high torque and be easily controlled, but the electric motors are heavy and have high impedance [34, 53].

To realise compliant actuators for wrist rehabilitation robots, pneumatic artificial muscle (PAM) and series elastic actuators are employed. Pneumatic artificial muscle (PAM) is a tube-like actuator that is characterized by a decrease in muscle length when pressurized. When compressed air is applied to the interior of the rubber tube, it contracts in length and expands radially. As the air exiting the tube, the inner netting acts as a spring that restores the tube to its original form. The PAM has the features of inherently compliant, lightweight, and high power-to-weight ratio so that it is commonly utilized for wearable exoskeletons. For example, Andrikopoulos *et al.,* utilized PAMs for a wrist exoskeleton. Two pairs of PAMs are placed on the dorsal and palmar side of forearm to provide two DoF by inflating/deflating corresponding pairs of PAMs [57]. Bartlett *et al.,* used the PAMs, in combination with a glove and elbow sleeve to provide a soft wrist exoskeleton [58]. The major drawback is that it is difficult to control the output force of the PAM because of the on-linearity and hysteresis [59]. Precise control of force output requires advanced modelling methods when using the proportional valves.

Series elastic actuators are employed in wrist rehabilitation robots such as UHD and the low-profile exoskeleton. Su *et al* [56] also developed a wrist rehabilita-

tion with the series elastic actuator. An elastic element is used to increase the compliance between the motor and the load, allowing for the high-performance force control and more precise interaction with patients.

Recently, the cable-driven actuators are utilized in the wrist robots, such as Wrist EXOsuit and EXO-wrist. This actuator has lightweight, lower inertia and high flexibility, as the force is transmitted through cables to actuate the joint. A smart material, shape memory alloy, is proposed as actuators for a 3 DoFs wrist robots [60]. A constitute model is used to derive the output force of the SMA actuator in response to the temperature, stress, strain and phase composition.

Table 2.2: List of state-of-the-art wrist rehabilitation robots.

Studies	DoFs	Acutation	Control strategies	Feedback signals
End-effector type				
MIT-MANUS [3, 25]	3	Motor	Impedance controller	EMG, force/torque sensor
Universal Haptive Drive [4]	2	SEA	Impedance controller	Potentiometer
CR2-Haptic [61]	1	Motor	Trajectory tracking control	Encoder
Hesse *et al.*, [62]	1	Motor	Trajectory tracking control	Force sensor; Encoder
Haptic knob [26, 63]	2	Motors	Impedance controller	Force/torque sensor; Encoder; BCI
WRed [5]	1	Motor	Admittance controller	Force/torque sensor; Encoder
H.S.Nam *et al.*, [64]	1	Motor	Not specified	Torque sensor
Exoskeleton				
Rice-Wrist [6, 65–67]	3	Motor	PD controller	Force/torque sensor; Encoder
Akdogan *et al.*, [68]	3	Motors	Impedance controller	encoder, torque sensor;
ARMin [69]	1	Motor	Impedance controller	Torque sensor; Potentiometer
PWRR [8]	2	Pneumatic actuator	Not specified	Magnetic sensor; pressure regulator
Squeri *et al.*, [28]	3	Motor	Impedance controller	Force/Torque sensor; Encoder
WRES [70]	3	SEA	Trajectory tracking control	Encoder
Su *et al* [56]	3	SEA	Impedance control	Angle encoder, force encoder
Wrist Exosuit [9]	1	Motor(Cable-driven)	Admittance controller	Force sensor;IMU
SCRIPT [71]	1	Motor	Not specified	Potentiometer
EXO-Wrist [10]	1	Motor(Cable-driven)	Not specified	Force sensor
Higuma *et al.*, [11]	2	Linear actuator	Not specified	Not specified
WEP [42]	2	Linear actuator	Force control	EMG
Andrikopoulos *et al.*, [57]	2	PMA	Trajectory tracking control	Force sensor; Flexible sensor
Bartlett *et al.*, [58]	2	PMA	Not specified	Pressure sensor
Hope *et al.*, [60]	3	SMAA	force sensor, position sensor	position control

Abbreviation: SEA = series elastic actuator; PMA = pneumatic muscle;

SMAA = Shape memory alloy actuator;

2.3 Control strategies for wrist rehabilitation robots

The goal of wrist rehabilitation robots is to provide series of training exercises for the stroke patient. These exercises should be task-specific, precise, robust and safe in order to provoke the neural plasticity [72]. These standard protocols are exerted through the control strategies, which can be categorised into trajectory tracking control strategy and active assistive control strategy.

2.3.1 Trajectory tracking control strategy

Trajectory tracking control strategy is refereed to passive training exercise. Wrist robots guiding the patient's wrist joint following a predefined trajectory. The predefined trajectory is obtained by the recommendation of the physiotherapist and depends on the healthy subject's RoM. The patient remains passive and does not offer any muscular efforts. The trajectory tracking control is also referred to as 'passive training' in the literature.

To achieve the trajectory tracking control strategy, the proportional-integral-derivative (PID) controller with feedback control signals, such as velocities, angle or torque are used [73]. For example, Rice-Wrist utilized a PD controller to minimize the trajectory tracking errors. WRES [70] also implemented the trajectory tracking control scheme while compensated for the effects of the gravity and the gear motors viscous friction.

This control strategy guides the patients' wrist joint along the predefined trajectory without taking into account the level of impairment. Patients may experience discomfort because the robot does not allow them to move their wrist joints according to their own efforts.

2.3.2 Active assistive control strategy

Active assistive control strategies not only take account of the patients' disability level but also encourage the patient's active participation in rehabilitation [72, 74]. To achieve the active assistive control strategies, impedance and admittance controllers are commonly employed in order to provide assistance in response to the patient's intention. The impedance controller asks the robots to rend particular mass, spring and damping properties to interact with the patient's generated torque. In other words, robots sense the changes in motion and provide the external force/torque to the patient. For example, an impedance controller is used to adjust the endpoint impedance of the MIT-MANUS, which allows the patient to free drive the robot [3]. UHD used the impedance controller to provide the 'patient-in-charge' mode and 'robot-in-charge' mode by setting the robot with low impedance and high impedance respectively. The patient is allowed to orient the UHD without any resistance in 'patient-in-charge' mode while the patient is passive in the 'robot-in-charge' mode. Squeri *et al.,* also proposed an impedance controller for the wrist robot [28]. The patient is asked to move the wrist robot following a desired task. The robot increases/decreases the supported torque by the robot as the patient's interactive torque decreases/increases. In this manner, the patient is encouraged to participant in the rehabilitation training exercise. Furthermore, Su *et al.,* proposed a cascaded impedance controller containing an inner loop of force control and an outer loop of position control, allowing for free movement (zero impedance) and resistance exercise by setting different stiffness and damping parameters.

The admittance controller is also utilized in the wrist rehabilitation robots, which provides the desired position in response to the patient's intention. For instance, Xu *et al.,* proposed an admittance control for the WRed, which robot modified the predefined reference trajectory based on the interaction torque measured by

the torque sensor [5]. This 'patient cooperative control strategy' can enhance the training safety and comfort as well as engage the patient's active participation in rehabilitation. The wrist exosuit also utilized the admittance controller to compute the reference motion by sensing the interaction torque generated by the user [9].

The active assistive control strategies are also achieved through other approaches. For example, a commercial wrist device, called Omega 7, is used to provide haptic feedback when the patients perform the virtual tasks in the virtual reality [75]. Furthermore, several studies utilized electromyography (EMG) signal and electroencephalogram (EEG) signal to trigger the assistance. Hu *et al.,* utilized the EMG signal to trigger a wrist robot's assistance [33]. The assistive torque is proportional to the amplitude of FCR and ECR. Ang *et al.,* utilized the EEG signal to initiate the physical therapy of the haptic knob for stroke patients [63].

Adaptation is an another important aspect of the human-robot interaction in wrist rehabilitation robots. Simple impedance and admittance controllers, however, may not be capable of dealing with the time-varying capacities of the patients and may deliver the inaccurate intervention [76]. The adaptation of the active assistive control strategy demonstrates the potential benefits of support that can be automatically adapted to the patient's changing needs [72]. The adaptation can be achieved through either the modification of the trajectory or modification of the parameters in the controller in response to the performance criteria, e.g., tracking error or completing time. Kreb *et al.,* proposed an adaptive method for the MIT-MANUS. The stiffness parameter is progressively updated based on the patient's performance, which is evaluated through four performance indexes [25]. Squeri *et al.,* developed an adaptation method that the RoM of the wrist robot is updated through a performance evaluator [28, 77]. That is, if the patient can accomplish five consecutive trial successfully, the wrist robot

increase it RoM for next trial. Pehlivan *et al.,* also proposed the adaptive law that the robot adjusts the permissible trajectory tracking errors while estimating the patient's contributed force during the repetitive task [66].

2.3.3 Motion intention estimation

Wrist rehabilitation robots interact with patients in both physical and cognitive aspects, in which the human-robot interaction plays a crucial role. The interaction between patients and robots provides vital information for design and adaptation of active assistive control strategies. Motion intention reflects the user's intended action, which could be interpreted as kinematic parameters (joint positions, velocities or accelerations) or dynamic parameters (force or joint torque). The active assistive control strategies continuously evaluate the patient's intention in order to provide the corresponding robotic assistance. The common methods applied to estimate the motion intention, including the force/torque method and sensorless method. The force/torque sensor is used to measure the torque provided by the patients directly or is combined with the robotic dynamics to estimate the intention. However, the measured signal may not truly represent the motion intention, as it also captures the uncertain noise, e.g., friction [35]. Sensorless method is developed to extract the intention from disturbance, e.g., non-linear disturbance observer [67]. However, it requires a complex algorithm which increases the computation cost. The un-modeled dynamics is another influence to identify the intention.

Recently, there are a increasing trend for using the biological signal for wrist rehabilitation robots, such as EMG [33] and EEG [63]. The biological signal could establish the direct link between the nervous system and patients' motion intention [36].

2.4 EMG-based motion intention estimation

2.4.1 Electromyography (EMG)

Skeletal muscle contains a limited number of motor units. Each motor unit is controlled by one nerve ending, which consists of a synaptic junction in the ventral root of the spinal cord, a motor axon, and a neuromuscular junction in the muscle fibres [78]. The motor unit controls from 3 muscle fibres to 2000 muscle fibres. An active potential is propagated through nerve fibres and transmitted down the motor axon. It reaches the neuromuscular junction and stimulates the contraction. Therefore, the action potentials generated in the muscle fibres of one motor unit is called a motor unit action potential (MUAP) [79]. The superposition of the MUAPs results in the EMG signal which can be detected by the electrode.

The electrode used for the EMG signal recording are mainly categorised into invasive type and non-invasive type [80]. Invasive type, such as the needle, fine-wire electrodes can provide higher precision and more specific targeting signal, which are used to detect the deeper muscle or individuals MUAPs. However, the invasive nature may hurdle the usability in developing rehabilitation robots. Non-invasive types, i.e., surface electrodes are commonly utilized in the rehabilitation field, due to their safety and ease of application.The surface electrode is used to detect the muscle activities of the superficial muscle and gives more reproducible results than invasive type [78]. The interest of surface EMG (sEMG) signal for developing the human-machine interface is popular for wrist rehabilitation robots, which is utilized to predict the joint torque or joint motion of interest [37].

There exist a time delay, namely, electromechanical delay (30 ms - 100 ms), which is the intention can be detected in advance before the actual motion happens [81]. This advantageous feature allows the robots to respond the patients' motion

intention in advance.

Table 2.3 gives the current approaches for the EMG-based intention estimation for wrist rehabilitation robots. Conventional EMG-based approaches in the wrist rehabilitation robots are using simple sequential, on/off control methods due to the robustness. On/off control is applied in a single DOF device with the adjusted threshold to trigger the robot's assistance [27, 43].

Patten recognition approach is an another approach to control the wrist rehabilitation robots [42, 65, 82, 83]. This approach extracts the features of EMG signals (feature extraction), and map to the desired motion intention (classification). Feature extraction identifies the information from the time-domain, frequency domain and other domains. The common features extracted from EMG signals include mean absolute value, autoregressive coefficients, root mean square, zero crossing or waveform length. Classification is used to map the feature vectors or combined features to the corresponding response. Common classification algorithms include support vector machine and linear discriminant analysis. For example, Mcdonald *et al.,* used the pattern recognition to decode the wrist movement when isometric contractions of the desired tasks are preformed [65]. The autoregressive coefficients and root-mean-square are used for feature extraction and LDA is used as the classifier. The pattern recognition provide high classification accuracy, but degraded performance is found when the pattern recognition is applied for patients with spinal cord injuries.

The pattern recognition approach is a discrete control method that only allows the user to control one motion class at a time. Current research interests trend to the continuous intention estimation [37]. The wrist rehabilitation robot should provide the assistance related to the motion intention more intuitively.

2.4.2 Model-free approach

The continuous motion intention estimation, which are categorised into model-free approach and musculoskeletal model-based approach. The model-free approaches utilize the regression algorithms to estimate the motion intention, such as wrist muscle forces, joint torque or joint position. The underlying numerical function or parameters are trained to map the EMG signal to the desired objectives. For instance, Liu *et al.,* proposed the NARX neural network to estimate the continuous joint motion for stroke patients. The NARX neural network contains a hidden layer with three neurons and a linear output layer with three output. The results shows the variance accounted for 98% for all joints [38]. Furthermore, they also used a linear and non-linear cascade regression algorithm for motion estimation. This regression algorithm showed the potential for the real-time application with 22 $\pm$ 0.6 ms delay, using a window length of 1024 ms and a window increment of 32 ms [84].

Two studies demonstrated that incorporating the EMG-based intention estimation into control of rehabilitation robots. Killic *et al.,* used the time-delayed neural network to estimate the wrist muscle force and implement a assistive control strategies on a wrist device [85]. Experiment result show that the muscle activations of FCR and ECR are reduced in the motion task when the wrist device is enable. Kiguchi *et al.,* proposed a neurofuzzy modifier to estimate weight matrix in order to determine the joint torque [86]. An impedance controller is implemented in a 7 DoFs exoskeleton to provide assistance in response to users intentions.

Model-free approaches for wrist rehabilitation robots have shown the ability to accurately interpret user's intentions. Studies also demonstrated that the potential of the model-free approaches in combined with active assistive control strategies. However, there are several limitations for this approach. First, a large amount

of training data sets, including EMG signals and the associated motion data are required to tune/train the numerical parameters/functions. In addition, the muscle activities vary throughout the long-term rehabilitation, re-training/tuning the model-free approaches is necessary after a certain interval. It could lead to a time-consuming task and frustrates patients' motivations for robot-aided rehabilitation.

Secondly, model-free approaches interpret user's intention by mapping the numerical functions between EMG signals and the corresponding intention. The underlying relationships between the muscular and skeletal systems are omitted. When developing assistive control strategies, the biomechanical characteristics of the wrist joint should be taken into account [53].

Thirdly, model-free approaches may not be able to respond to novel conditions that are not defined in the training data sets, e.g., different postures. This is due to the fact that differing upper-limb postures can vary the length of the muscle fibres that generate muscle force.

2.4.3 Musculoskeletal model-based approach

The musculoskeletal model-based approach consists of simulated muscular and skeleton system in order to model the movement of joints controlled by central nervous system. The musculoskeletal model-based approaches represent the underlying relationship between the EMG signal and joint kinematic and kinetic characteristics, to compute the muscle force and joint moments accordingly. In other words, the intermediate transformation from neural commands to muscular-skeletal systems are explicitly interpreted, e.g., muscle force.

There exist many noise in the EMG signals, including the inherent noise in the electronics equipment, ambient noise and motion artefact [80]. Therefore, the raw EMG signal should be filtered prior to interpret the muscle activation level.

To interpret the muscle activation level, mathematical models first take account of a time delay for the muscle activation, such as a first-order linear differential equation [40, 87] or a second-order differential equation [88, 89]. To address the non-linearity between the processed EMG signal and muscle activation, a non-linear function is used to obtain the muscle activation with respect to the EMG signal [88, 90].

Alternatively, linear envelope approach is also used to interpret the muscle activation, because it follows the trend of EMG signal and quite closely resemble the shape of tension curve [78]. It is achieved by filtering the full-wave rectified wave with a low-pass filter. In addition, this approach does not need the numerical integrations of the differential equations that could reduce the computational cost. The linear envelope approach only requires few steps of common filter configurations and could be implemented both in the digital circuit or in software [91].

The muscle-tendon force is computed regarding to the targeted muscle and the associated muscle activation level, which is established based on the Hill' muscle model. Hill proposed the Hill-type muscle model based on empirical experiments, representing the physical and mechanical properties of muscle [92]. Muscle contraction and dynamic are governed by one differential equation, making the modelling of the muscle computationally efficient. Hill's muscle model consists of a muscle fibre that is connected to a elastic tendon element. The muscle fibre includes a contractile element (CE) and a parallel elastic element (PE), which are connected in parallel. Furthermore, some models added an elastic component in parallel with CE and PE to characterise the viscous component [93]

The active force generated by CE when the tissue is stimulated by the neural command, is characterised by a force-length relationship and a force-velocity relationship [39, 88, 90, 94]. The muscle fibre produces the peak force when it at

its optimal muscle fibre length. The force-generating property is degraded to zero when the muscle fibre length decreases or increased to 0.5 and 1.5 of its optimal muscle fibre length. The force-velocity curve is relate to the muscle contraction speed to its force production, which is derived from the Hill's equation [92]. The PE generates force when the muscle is strengthened exceed the optimal muscle fibre length. The force-generating property of PE is characterised as an exponential relationship.

Tendon is modelled as an elastic element and generates force when it exceed the slack length [39, 88]. The tendon force increases as the tendon length exceeds its slack length, representing a linear relationship to the tendon strain when tendon strain is above a certain value [87]. However, it is reported that the real-time performance is significant affected by the elastic tendon [95]. Together with the explicit models of the CE, PE and tendon, the muscle-tendon force is calculated in response to the muscle activation.

Musculoskeletal modelling technique

The musculoskeletal modelling technique, which represents the geometry of skeletons and complex relationships associated with the joint of interest, is used to obtain the muscle-tendon length as well as the moment arm. Muscle-tendon length is determined through the muscle origin and insertion. Conventionally, the origin is the point that muscle is attached to a more stable bone. The insertion refers to the attachment of the muscle to a more mobile bone. Moment arm is the distance from the joint centre to the muscle's line of action, is a function of the muscle-tendon length. Besides, it is notable that the muscle-tendon length and moment arm change as a function of the joint angle.

Throughout the literature, several methods for the determination of the muscle-tendon length and moment are found. For example, Pau *et al.,* proposed a simpli-

fied musculoskeletal modelling technique for the elbow joint [91]. The elbow joint is treated as a single hinge joint with a fixed centre of rotation, actuated by two muscles. The muscle length and moment arm of triceps and biceps are obtained using the trigonometry of the geometric schematic. However, it is oversimplified to describe muscle and bones as straight lines which are connected from origin to insertion point. This is because that nearly every muscle may bend or wrap around other structures at some joints [88]. Another technique is used for the determination of the muscle-tendon length and moment arm upon using the biomechanical software, such as OpenSim [96] , SIMM [97] and AnyBody [98]. The muscle-tendon length and moment are are determined in these software with a well-established biomechanical model. For example, Lloyld *et al.,* used the SIMM to obtain the muscle-tendon length and moment arm for knee joint [94]. Ma *et al.,* obtained the muscle-tendon length and moment arm of lower limb based upon the generic biomechanical model in OpenSim. The morphological data are scaled down based on anthropometric data of the subject and kinematic data from gait analysis experiment using the motion capture system [40]. Sartori *et al.,* used the cubic B-spline interpolation method to obtain the muscle-tendon length from the OpenSim software [99].

Parameter optimization

The muscle-tendon parameters as well as the parameters for interpreting the muscle activation level should be optimized for each individual [88]. This is because these parameters representing the characteristics of the muscular properties, e.g., activity levels. Unlike the model-free approach, one set of the training data is required to optimize these parameters.

The methods for parameter optimization commonly employ the heuristic algorithms, e.g., genetic algorithm [91] and simulated annealing algorithm [90, 100].

The optimization time of the musculoskeletal model is dependent upon the number of muscles of interest and joints of interest. However, lengthy optimizations were reported in the literature, which may lead to barriers for implementing the musculoskeletal model-based approach for rehabilitation in practice. For instance, Sartori *et al* reported that 20 CPU hours are taken for 34 muscles in a lower limb model using the simulated annealing algorithm [90]. Pau *et al.,* reported an average one hour for each trial when the genetic algorithm to tune 24 muscle parameters for elbow flexion/extension [91]. Moreover, Crouch *et al.,* reported the execution time of optimization taking approximately 20 hours in their model using the simulated annealing algorithm [100].

EMG-driven models in wrist rehabilitation robots

There is a growing tendency toward using EMG-driven musculoskeletal models in rehabilitation robots for the lower limb [40, 89, 90, 94, 101]. For example, Shao *et al.,* utilized the EMG-driven musculoskeletal model to estimate the muscle force and joint during ankle flexion/extension for stroke patients [89]. The mode-based approach shows the feasibility to correctly estimate the muscle force and moment for stroke patient. Ma *et al.,* also proposed an EMG-driven musculoskeletal model for knee joint. Two muscles around the knee joint are used to computed the knee joint moments during gait cycle, in which estimation accuracy achieve mean 0.9 correlation. It shows the potential of realizing real-time computation for gait rehabilitation robot control [40]. Recently, Durandau *et al.,* demonstrated that the patients with post stroke, voluntarily control a lower-limb robotic exoskeleton [102]. Yao *et al.,* demonstrated the model-based approach to estimate the ankle dorsiflexion intention. A control strategy is then used to provide robotic assistance according to model's estimation [103].

The musculoskeletal model-based approach are also investigated to estimate the

motion intention for the prosthesis control. For instance, Crouch *et al.,* proposed a musculoskeletal model-based approach to estimate the flexion/extension motion of wrist and metacarpophalangeal (MCP) joint [100]. Furthermore, they extended their model-based approach for real-time control of a virtual cursor during the path tracking task [104]. Blana *et al.,* demonstrated the viability of real-time computation of musculoskeletal model-based approach in performing wrist and hand movement using the simulated EMG signals [105]. Sartori *et al.,* first demonstrated the real-time control a wrist-hand prothesis using the musculoskeletal model-based approach [106].

Despite that above studies demonstrated that the EMG-driven musculoskeletal models provide the accurate intentions estimation and the feasibilities for real-time application. There is a lack of studies examining the application of the musculoskeletal model-based approach for robot-aided wrist rehabilitation. One study is found in the literature [107]. However, they used the musculoskeletal model-based approach to estimate the muscle-tendon parameters under isometric conditions instead of estimating the motion intention.

Table 2.3: Review of the EMG-based intention estimation approach for wrist rehabilitation robots

Study	**Application**	**EMG channels**	**DoF**	**Approach**	**Control strategy implemented**	**Notes**
Khohar *et al.*, [42]	Wrist robot	4	2	Pattern recognition	Y	Classification accuracy reaches 88% for nineteen classes. Classification accuracy reaches 96% for thirteen classes.
Song *et al.*, [43]	Wrist robot	2	1	Proportional	Y	Stroke patients: a non-significant increase in RoM, a significant decrease in RMSE.
Zhang *et al.*, [108]	Wrist rehab	HD-EMG (89 channels)	3	Pattern recognition	N	High-average classification accuracies above 95% are achieved for most stroke patients.

Table 2.3. *(Continued)*

Study	Application	EMG channels	DoF	Approach	Control strategy implemented	Performance
McDonald *et al.*, [65]	MAHI Exo-II	8	3	Pattern recognition	N	Able-bodied subject: Single DoF = 99%, Mutilple DoF = 90%; SCI subject: Single DoF = 85%-90%; Mutliple DoF = 60%
Liu *et al.*, [38]	Exoskeleton	2	1	NARX Neural Network	N	VAF = 95% for either stroke and able-bodied subjects.
Liu *et al.*, [84]	Exoskeleton	2	1	Linear non-linear cascade regression	N	Able-bodied subject: VAF = 85%; Stroke patients: VAF =85 %

Table 2.3. *(Continued)*

Study	Application	EMG channels	DoF	Approach	Control strategy implemented	Performance
Kilic *et al.*, [85]	Wrist robots	2	1	Artificial neural network	Y	RMSE = 0.15 ; R^2 = 0.9; The muscle activation levels are reduced with the robot's assistance.
Kiguchi *et al.*, [86]	Exoskeleton	6	3	Neurofuzzy modifier	Y	The impedance properties of an impedance controller according to the posture; The muscle activation levels are reduced with robot's assistance

Table 2.3. *(Continued)*

Study	Application	EMG channels	DoF	Approach	Control strategy implemented	Performance
Crouch *et al.*, [100]	Prothesis	2	1	Model-based	N	Able-bodied subject: mean r = 0.94 in single DoF; r = 0.75 in simultaneous movement. Amputated subject: r = 0.92 in single DoF ; r = 0.75 in simultaneous movement.
Sartori *et al.*, [106]	Prothesis	8	3	Model-based	Y	They demonstrate the used of musculoskeletal model-based approach for real-time control of a prosthesis.

Table 2.3. *(Continued)*

Study	Application	EMG channels	DoF	Approach	Control strategy implemented	Performance
Blana *et al.*, [105]	Prothesis	Simulated	3	Model-based	N	Using the musculoskeletal model-based approach to simulate the American Sign Language
Colacino *et al.*, [107]	Wrist Rehab	4	1	Model-based	N	Using the musculoskeletal model to estimate the muscle-tendon parameters under isometric contractions.

Abbreviations. VAF = variance accounted for. RMSE = root-mean-square error. R^2 = correlation of determination.

2.5 Discussion

Wrist rehabilitation robots have been widely developed in the last decades. Together with the trajectory control strategies and active assistive control strategies, the robot-aided rehabilitation provide significant benefits for the patients with stroke or other spinal cord injuries. The motion intention estimation plays an crucial role in the active assistive control strategies. Current intention estimation methods are based on the force/torque sensor or sensorless method. However, the force/torque sensor may not interpret the patient's interacted torque accurately. The signal also contains noise from the uncertain dynamics of the wrist robot, such as friction. Saadatzi *et al.,* reported that utilising an inverse dynamic technique for intention estimation with appropriate wrist robot's parameters resulted in a 20% average inaccuracy [35]. To overcome this limitation, the EMG signal is applied to establish a direct link from the central nervous system or muscles to patients' intentions. Such a biological signal can intuitively estimate the intention directly from muscle activities, and it is more generalizable to a variety of wrist robots. This thesis focuses on the development of the EMG-driven musculoskeletal models for robot-aided wrist rehabilitation including the estimation of motion intentions and control of a wrist rehabilitation robot.

2.5.1 Gap of knowledge

Current EMG-based motion intention estimation for wrist rehabilitation robots are based on the pattern recognition, as shown in Table 2.3. The pattern regression only allows the user to control one motion class sequentially and it can not recognise the continuous kinematic variables, e,g., joint acceleration. Continuously evaluation of the motion intention is the key to achieve smooth control of the wrist rehabilitation robot [109]. Several studies developed model-free ap-

proaches for continuous intention estimation. However, the major drawback of these approaches is that the underlying transformations from neural signals to muscular states are omitted. These biomechanical properties provide valuable insights into wrist joint movements as well as may achieve higher estimation accuracy. The EMG-driven musculoskeletal model is a promising approach to estimate motion intentions. It consists of sub-models to explicitly recognize the wrist joint movement in accordance with neural signals and muscle contractions. It is found that the EMG-driven musculoskeletal model-based approach for robot-aided wrist rehabilitation is received less attention. Although many achievements have been already made in the lower extremities [89, 90] and prosthesis [104–106], there is a lack of studies evaluating the model-based approach for wrist joint. In addition, the real-time implementation of the EMG-driven musculoskeletal model is limited by the integration of the muscle fibre length at each iteration (numerical stiffness) [95]. We will adopt the EMG-driven musculoskeletal model for the wrist joint to achieve accurate motion intention prediction and to realize real-time computation.

Another challenge is found that the optimization procedure to identify the subject-specific parameters requires a long optimization time for each individual, as reported in the literature [90, 91, 100]. This lengthy procedure may discourage the user's participation and hurdles the implementation of the model-based approach in practical scenario. To overcome this limitation, we will develop an optimization method for the wrist musculoskeletal model in order to obtain the subject-specific parameters effectively.

Throughout the literature, incorporating the EMG-based intention estimation method for control of the wrist robot is at an early stage. Few studies implement the EMG-based intention estimation for control of wrist rehabilitation robots, based on the pattern recognition [42], proportional control [43] and model-free

approach [85, 86]. However, the former two approaches determine the robot assistance according to the discrete motion class or the simple amplitude, and the model-free approaches only interpret the extent of the muscular effort. It is suggested that the inclusion of the biomechanical characteristics, e.g., joint stiffness, for the active assistive control strategies can achieve more intuitive human-robot interaction and enhance training efficiency and safety [53, 110–112]. These methods fail to fulfil the consideration of joint stiffness for wrist rehabilitation robots. To fill the gap of knowledge, we will provide a solution to estimate the wrist joint stiffness in real-time, and we will develop the active control strategy based on the EMG-driven musculoskeletal model for a wrist exoskeleton. To the authors' best knowledge, the model-based control strategies have not been implemented for real-time control of the wrist rehabilitation robot.

2.6 Chapter summary

The chapter first introduces the wrist biomechanical characteristics and the rehabilitation for the wrist joint. In the second section, the state-of-the-art wrist rehabilitation robots are investigated, which can be classified into end-effector type and exoskeleton. The control strategies for the wrist rehabilitation robots are reported. These control strategies include the trajectory tracking control strategy and active assistive control strategy. The trajectory tracking control strategy is designed to deliver precise, repetitive tasks, while the active assistive control strategy is designed to engage the patient's active participation and provide robotic assistance. Most of the active assistive control strategies are implemented through the impedance and control controller based on the estimated user's intention. To recognize the motion intention more intuitively, the EMG signal is used in the field of wrist rehabilitation.

The last sections give a review of the current EMG-based motion estimation approach for the wrist rehabilitation robots. Most of the current approaches are using the model-free approach that mapping the EMG signal to the desired motion intention. However, the model-free approaches ignore the underlying muscular and skeleton effects. In contrast, the musculoskeletal model-based approaches take accounts into the internal transformation from neural commands to the muscular-skeleton systems, which provides the motion estimation more closer to physical wrist motion. a workflow of the EMG-driven musculoskeletal model-based approach is presented. The gaps of knowledge regarding EMG-based intention estimation and control strategies are discussed, which identify the further objectives and contributions of the development of the EMG-driven musculoskeletal models for robot-aided wrist rehabilitation.

Chapter 3

An EMG driven Musculoskeletal model for Estimating the Continuous wrist motion

This chapter presents the development of the EMG-driven musculoskeletal model for estimating the motion intention. EMG-based continuous wrist joint intention estimation has been identified as a promising technique with huge potential in assistive robots [37]. Conventional data-driven model-free methods tend to establish the relationship between the EMG signal and wrist motion using machine learning or deep learning techniques, but cannot interpret the functional relationship between neuro-commands and relevant joint motion. This model interprets the muscle activation levels from EMG signals. A muscle-tendon model is developed to compute the muscle force during the voluntary flexion/extension movement, and a joint kinematic model is established to estimate the continuous wrist motion. To optimize the subject-specific physiological parameters, a genetic algorithm is designed offline to minimize the differences of joint motion prediction from the musculoskeletal model and joint motion measurement using motion data during training. Furthermore, a sensitivity is also conduced to investigate the ef-

fects of each parameters to the model estimation performance. Results show that mean root-mean-square-errors are 10.08°, 10.33°, 13.22°, and 17.59° for flexion, extension, continuous cycle, and random motion trials, respectively. The mean coefficient of determination is over 0.9 for all the motion trials.

3.1 Introduction

Estimating human joint motion is critical for the human-machine interfaces (HMIs) that can respond to users' intentions accurately and promptly [113]. This is due to the fact that electromyogram signal (EMG)-based HMIs have prospective advantages in estimating human intention:

1) The use of non-invasive electrodes to capture EMG can interpret the muscle activities (superficial muscle) precisely;

2) EMG signal can be detected ahead of actual motion about 10 - 100 ms, which enables estimate intended action in real-time [114];

3) EMG-based HMIs allow users to control the assistive robot more intuitively and smoothly [115].

EMG-based continuous limb motion estimation approaches can be categorized into two subsets, model-free approach and model-based approach.

For model-free approaches, they involve machine learning techniques, mapping the relationship between EMG signals and the desired motion by the numerical functions. Several artificial neural network methods are applied to estimate continuous motion for the human upper limb. For example, Lei proposed a back-propagation (BP) neural network to estimate continuous elbow motion [116]. The BP neural network has three layers, of which a tansig function and a pureli function are used for the hidden layer and output layer respectively. Côté-Allard *et al.,* developed a deep learning algorithms to recognise hand gestures [117]. Never-

theless, model-free approaches have some limitations. It is a 'black box' method, employing a general map function rather than explicitly revealing the functional relationships between neuro-commands and the corresponding joint motion. A large amount of data sets containing EMG signals as well as the related motions is required to train the transfer function in order to interpret the accurate estimation with given EMG signals. In addition, model-free approaches may not be able to respond to novel motions that are not defined in the training sets.

To provide the explicit representation between the EMG signal and joint kinetic and kinematic characteristics and reduce the acquirement of training data, model-based approaches have been widely applied to estimate the users' intention. These approaches estimate the continuous limb motion through an EMG-driven musculoskeletal model. For example, Pau *et al.,* proposed a simplified geometric model together with a musculoskeletal model to estimate the continuous motion of the elbow joint [91]. A musculoskeletal model was employed to simulate the shoulder and elbow joint motion in real-time using a passive damper to avoid the numerical stiffness [118]. Blana *et al.,* proposed the implicit formulation of the musculoskeletal model in order to drive the wrist/hand motion in real-time [105]. However, their models' parameters are adapted from the existed biomechanical models and have not taken the subject-specificity into account. Crouch *et al.,* developed a musculoskeletal model using subject-specific parameters to estimate the flexion/extension motion of wrist joint and metacarpophalangeal (MCP) joint [100]. Nevertheless, using few muscles to establish the musculoskeletal model may over-estimate the physiological parameters, i.e., the parameters may exceed the physiological range when these muscles are assumed to be the only muscle groups contributing to the joint motion. In [100], the subject-specific parameters exceeded the physiological range largely, because they have only used two wrist muscles to estimate the wrist flexion/extension motion.

In this chapter, we propose a model-based approach to estimate the wrist continuous joint motion. The main contributions of this chapter include:
1) Five primary wrist muscles are grouped into flexor/extensor to avoid overestimating parameters;
2) According to the selected muscle groups, a musculoskeletal model including a muscle-tendon model and a joint kinematic model is derived to estimate the continuous wrist flexion/extension motion. Assuming the tendon is rigid, the numerical stiffness of the muscle-tendon model is alleviated.;
3) A parameter optimization algorithm is designed and implemented to tune the parameters within the physiological range by minimizing the differences of joint motion between the model's estimation and the measured data.
The remaining chapter is arranged as follows. Section 3.2 details the EMG-driven musculoskeletal model-based approach. Section 3.5 describes the data acquisition and experiment protocol. Section 3.3 discusses the method for optimization of physiological parameters and sensitivity analysis. Experiment results and discussion are presented in 3.6 and 3.7 respectively. Final section gives conclusion and future work.

3.2 Methods

In the single degree of freedom (DoF) configuration, five primary wrist muscles are grouped as wrist flexor extensor. The flexor digitorum superficialis (FDS) and extensor digitorum (ED) are excluded due to these muscles mainly contribute to the metacarpophalangeal (MCP) joint motion. Therefore, the five main wrist muscles ($i = 1, 2, \ldots, 5$) are described in following:
1) Flexor ($i = 1, 2$) includes Flexor Carpi Radialis (FCR) and Flexor Carpi Ulnaris (FCU);

2) Extensor ($i = 3, 4, 5$) includes Extensor Carpi Radialis Longus (ECRL), Extensor Carpi Radialis Brevis (ECRB) and Extensor Carpi Ulnaris (ECU).
The wrist joint motion is computed by a muscle activation interpretation method, a muscle-tendon model and a joint kinematic modelling technique. Muscle activation interpretation method computes the muscle activation levels from EMG signals. The muscle-tendon model estimates the muscle-tendon force regarding the force-length/velocity relationships and muscle activation levels, based on the Hill's muscle modelling technique. Then the joint kinematic modelling technique is developed to determine the muscle tendon length and moment arms against joint angle and computes the joint motion using forward dynamics. A parameter optimization algorithm is developed to tune the physiological parameters. In the rest of this section, we will explain how to estimate the wrist joint motion using the proposed model.

3.2.1 Muscle activation interpretation method

To interpret the muscle activation level of each muscle during the wrist motion, the EMG signals are processed through a non-linear equation. To remove the DC offset and artefact noise, the raw EMG signals are first filtered by a 4^{nd} order Butterworth band-pass filter at cut-off frequencies between 25 Hz and 450 Hz and then fully rectified. The rectified signals are low-pass filtered to obtain the characteristics of EMG to muscle force relation through a 4^{th} order Butterworth low-pass filter at a corner frequency of 4 Hz,according to [88]. Filtered signals are normalized by dividing the peak value of isometric maximum voluntary contraction (IMVC). Resultant EMG signal $u_i(t)$ has the range of 0 to 1. Furthermore, the following equation takes account of the non-linear relationship between pre-processed signal $u_i(t)$ and muscle activation $a_i(t)$

$$a_i(t) = \frac{e^{Au_i(t)} - 1}{e^A - 1} \tag{3.1}$$

where non-linear shape factor A has the range of highly non-linearity (-3) to linearity (0.01) [119].

3.2.2 Muscle-tendon model

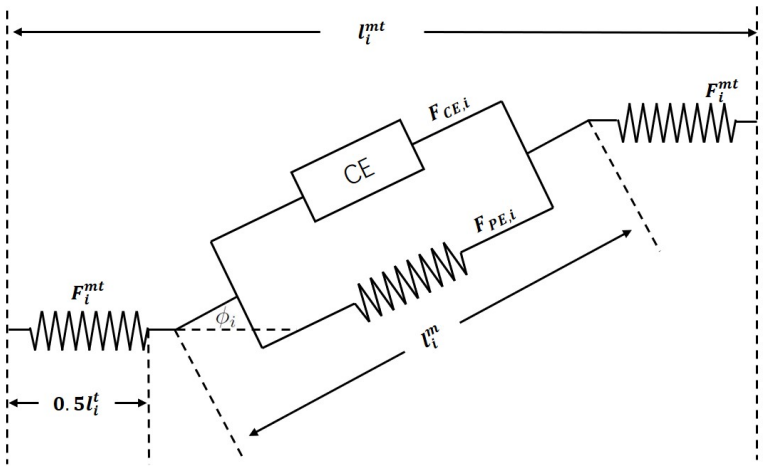

Figure 3.1: Schematic of Hill's type muscle model.

The Hill's modelling technique is used to compute the muscle-tendon force F_i^{mt}, which consists of a elastic tendon in series with a muscle fibre. The muscle fibre includes a contractile element (CE) in parallel with passive elastic element (PE). Figure 3.1 illustrates the schematic of the Hill's type muscle model, of which l_i^{mt}, l_i^m and l_i^t are the muscle-tendon length, muscle fibre length and tendon slack length respectively. Pennation angle ϕ_i is the angle between the orientation of the muscle fibre and tendon, and the pennation angle at current muscle fibre length is calculated by

$$\phi_i = \sin^{-1}\left(\frac{l_{o,i}^m \sin\phi_{o,i}}{l_i^m}\right) \tag{3.2}$$

where $l_{o,i}^m$ and $\phi_{o,i}$ represent the optimal muscle fibre length and the optimal pennation angle respectively. Besides, a scale coefficient k_i^{mt} is introduced to

account the difference of the muscle-tendon length across subjects. The muscle fibre length is then represented as

$$l_i^m = (k_i^{mt} l_i^{mt} - l_i^t)\cos^{-1}\phi_i. \tag{3.3}$$

The F_i^{mt} is the summation of the active force $F_{CE,i}$ and the passive force $F_{PE,i}$, which can be written as

$$F_i^{mt} = (F_{CE,i} + F_{PE,i})\cos\phi_i. \tag{3.4}$$

The $F_{CE,i}$ is the active force generated by CE, which can be written as

$$F_{CE,i} = F_{o,i}^m f_a(\bar{l}_{i,a}^m) f(\overline{v}_i) a_i(t) \tag{3.5}$$

where $F_{o,i}^m$ is the maximum isometric force. The function $f_a(\cdot)$ represents the active force-length relationship at different muscle fibre length and muscle activations, as illustrated as the blue curve in Figure 3.2. The mathematical form is written as

$$f_a(\bar{l}_{i,a}^m) = e^{-(\bar{l}_{i,a}^m - 1)^2 k^{-1}} \tag{3.6}$$

of which

$$\bar{l}_{i,a}^m = l_i^m / (l_{o,i}^m(\lambda(1 - a_i(t)) + 1) \tag{3.7}$$

where $l_{i,a}^m$ is the normalized muscle fibre length with respect to the corresponding activation levels. is and λ is a constant, which is set to 0.15 [94]. The k is a constant to approximate the force-length relationship, which is set to 0.45 [120]. As shown in Figure 3.3, the function $f(\overline{v}_i)$ represents the force-velocity relationship between the l_i^m and the normalized contraction velocity $\overline{v}_i$ [121]

$$f(\overline{v}_i) = \begin{cases} \frac{0.3(\overline{v}_i + 1)}{-\overline{v}_i + 0.3} & \overline{v}_i \leq 0 \\ \frac{2.34\overline{v}_i + 0.039}{1.3\overline{v}_i + 0.039} & \overline{v}_i > 0 \end{cases} \tag{3.8}$$

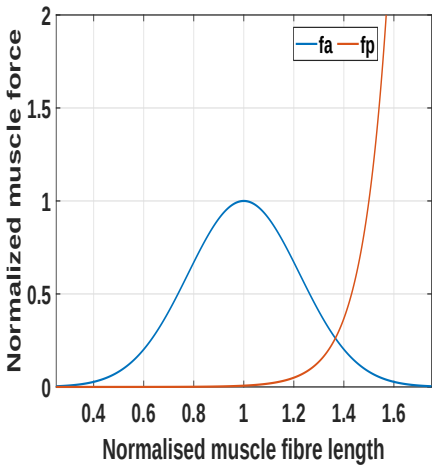

Figure 3.2: Normalised force-length relationships for the muscle fibre.

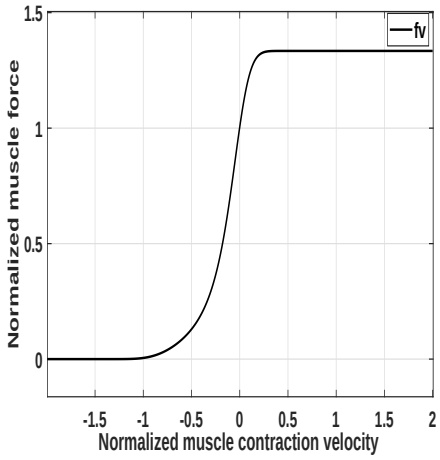

Figure 3.3: Normalised force-velocity relationship for the muscle fibre.

where $\overline{v}_i = v_i/v_{o,i}$. $v_{o,i}$ represents the maximum contraction velocity, which is set to 10 $l^m_{o,i}$/sec [87]. The v_i is computed through the time derivative of the muscle fibre length. In specific, differentiating equation (3.3) with respect to time yields

$$k^{mt}_i v_{mt} = v^t_i + v_i \cos\phi_i - \frac{d\phi_i}{dt} l^m_i \sin\phi_i \tag{3.9}$$

rewriting and differentiating the equation (3.2) gives

$$l^m_i \sin\phi_i = l^m_{o,i} \sin\phi_{o,i} \tag{3.10}$$

$$\dot{\phi}_i = -\frac{v_i \sin\phi_i}{l^m_i \cos\phi_i} \tag{3.11}$$

substituting equation (3.11) into equation (3.9) yields

$$k^{mt}_i v_{mt} = v^t_i + \frac{v_i}{\cos\phi_i} \tag{3.12}$$

where v^t_i is equal to zero as the the tendon element is assumed to be rigid enough. Therefore, the muscle fibre velocity is equal to

$$v_i = k^{mt}_i v_{mt} \cos\phi_i \tag{3.13}$$

Note that the passive force F_{PE} is the forced produced by the passive elastic element, obtained by

$$F_{PE,i} = \begin{cases} 0 & l_i^m \leq l_{o,i}^m \\ f_p(\bar{l}_i^m) F_{o,i}^m & l_i^m > l_{o,i}^m \end{cases} \tag{3.14}$$

where $\bar{l}_i^m = l_i^m / l_{o,i}^m$ indicates the normalized muscle fibre length. The $f_p(\cdot)$ is illustrated as the orange curve in Figure 3.2, in the form of

$$f_p(\bar{l}_i^m) = \frac{e^{10(\bar{l}_i^m - 1)}}{e^5}. \tag{3.15}$$

3.2.3 Joint kinematic modelling technique

The single joint configuration is used in this chapter. Therefore, the muscle-tendon length l_i^{mt} and moment arm r_i against wrist joint angle are obtained using the polynomial equation (the Fourier equations) and the scale coefficient [122]. Table 3.1 gives the coefficients for each muscle. The mean fitting accuracy is over 0.98.

$$\begin{aligned} l_i^{mt}(\theta) &= a_0 + a_1 cos(\theta\omega_1) + b_1 sin(\theta\omega_1) \\ r_i(\theta) &= c_0 + \sum_{i=1}^{2} c_i cos(i\theta\omega_2) + d_i * sin(i\theta\omega_2) \end{aligned} \tag{3.16}$$

The joint torque of each muscle can be calculated as

$$M_i = F_i^{mt} r_i. \tag{3.17}$$

Therefore, the total joint torque during wrist motion is written as

$$\tau = \sum_{i=1}^{2} M_{flexor,i} - \sum_{i=3}^{5} M_{Extensor,i} \tag{3.18}$$

where $M_{flexor,i}$ and $M_{extensor,i}$ represent the flexor torque and extensor torque, respectively.

Table 3.1: Regression coefficients for muscle-tendon length and moment arm

	Muscle-tendon length l_i^{mt}				Moment arm r_i					
	a_0	a_1	b_1	ω_1	c_0	c_1	d_1	c_2	d_2	ω_2
FCR	0.2982	0.01423	-0.03854	0.3874	0.0119	0.003831	0.001774	-0.0008396	0.0001208	1.286
FCU	0.2628	0.04982	-0.06095	0.2454	0.01463	0.0001644	0.003642	8.152e-05	-0.0007975	1.286
ECRL	-0.1317	0.4661	0.1343	0.07499	-0.01081	0.0008298	0.00358	0.0003497	-0.001045	1.286
ECRB	0.2371	0.04893	0.0622	0.2138	-0.01248	- 0.0007674	0.003978	0	0	0.597
ECU	0.2905	-0.0001401	0.005483	1.213	0.003555	- 0.01009	- 0.004209	0.0003308	0.002431	0.9968

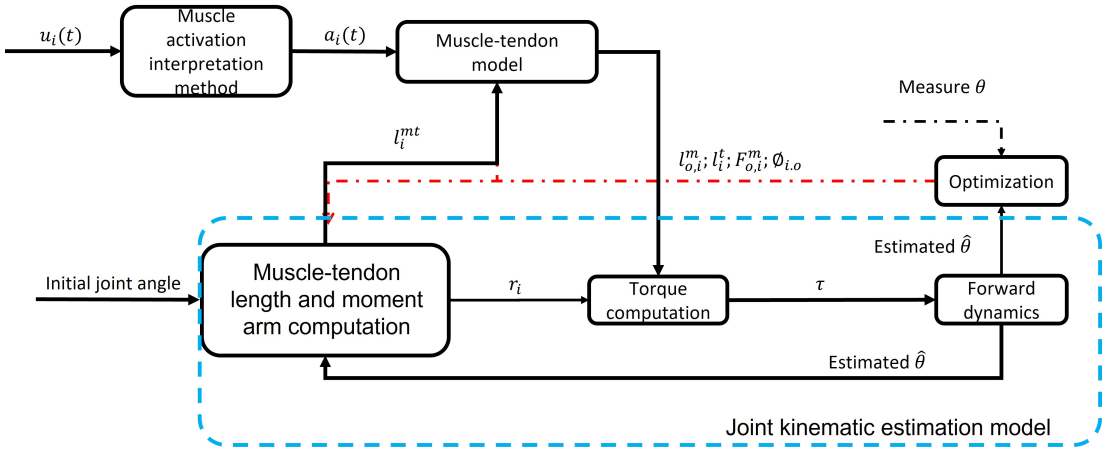

Figure 3.4: Muscle activation interpretation methods gives muscle activation levels of each muscle, muscle-tendon force is computed by a muscle-tendon model, and the joint kinematic estimation model estimates the muscle-tendon length, moment arm and the wrist joint motion θ. The physiological parameters, e.g,. optimal muscle fibre length $l_{o,i}^m$, tendon length l_i^t, maximum muscle force $F_{o,i}^m$ and optimal pennation angle ϕ_i are optimized using the GA algorithm.

The muscle activation level does not have a directly relationship with the joint motion, it is necessary to compute joint acceleration using the forward dynamics. As shown in Figure 3.4, an initial joint angle is given, the current states of muscle-tendon length and moment arm are calculated. Then the muscle length

and muscle-tendon force are obtained according to equation (3.3) and (3.4). Therefore, the joint moment is calculated, and the current state of joint acceleration is obtained and integrated to joint angle.

To obtain the joint acceleration, the wrist joint is assumed to be a single hinge joint, the palm and fingers are assumed to be a rigid segment rotating around wrist joint in the sagittal plane. Thus, the joint acceleration is computed through the forward dynamics:

$$\ddot{\theta} = \frac{\tau - mgL\sin(\theta) - C\dot{\theta}}{I} \tag{3.19}$$

where $\ddot{\theta}$ is the angular acceleration. τ is derived from equation (3.18). I is the moment of inertia of hand, which is equal to $mL^2 + I_p$. I_p is the moment of inertia at the principal axis which is parallel to the wrist flexion/extension axis [123]. m and L are the mass of hand segment and the length between rotation centre to hand's centre of mass, which are measured from subjects. θ and $\dot{\theta}$ are the wrist joint angle and angular velocity respectively. C is the damping coefficient representing the elastic and viscous effects from tendon, ligaments [124]. Therefore, the EMG-driven musculoskeletal model for the wrist joint motion estimation in discrete time can be written as

$$\begin{aligned} \dot{\theta}_{t+1} &= \dot{\theta}_t + \ddot{\theta}_t \Delta t \\ \theta_{t+1} &= \theta_t + \dot{\theta}_t \Delta t \end{aligned} \tag{3.20}$$

where Δt is the sampling time, and $\dot{\theta}_t$ and θ_t are the angular velocity and joint angle at time t.

3.3 Parameter optimization

According to the previous sections, several parameters are used to compute the muscle-tendon force and joint moment. These muscle-tendon parameters in the

proposed model, e.g., maximum isomeric muscle force, optimal fibre length, tendon length and optimal pennation angle are difficult to measure in *vivo* and varies between the age, gender. Thus, these parameters are required to be optimized for each subject. The initial guess and the physiological boundaries of the muscle-tendon parameters are chosen according to [125] and [126], which are presented in Table 3.2. The boundaries of maximum isometric force are set to ±50% of the initial guess since the variation of the physiological cross-sectional area (PCSA) are varied significantly across subjects. The parameters combined into a vector, which is represented as

$$\chi = [F^m_{o,i}, l^m_{o,i}, l^t_{o,i}, \phi_i, k^{mt}_i, A]^T \tag{3.21}$$

The estimation of χ can be written as

$$\hat{\chi} = \arg\min_{\chi}\{f(\chi)\} \tag{3.22}$$

where

$$f(\chi) = \sqrt{\frac{1}{N}\sum_{n=1}^{N}(\theta - \hat{\theta})} \tag{3.23}$$

where θ and $\hat{\theta}$ are the measured joint angle and estimated joint angle respectively, and N is the number of samples.

Genetic algorithm (GA) is used to find out the best match of the subject-specific parameters. GA is commonly implemented in the musculoskeletal model [91]. It can evaluate multiple solutions in the search space, and reduce the risk of falling into a local minima. GA mimics the nature evolutionary process by representing the muscle-tendon parameters as a 'chromosome'. This algorithm randomly generates a set of possible solutions for the joint kinematic modelling technique. The objective function evaluates the "fitness" of each possible solution at each generation and reaches the best set of parameters iteratively.

Table 3.2: Boundary conditions of the parameters

Parameters (units)	**Bounds**
Maximum isometric muscle force $F^m_{o,i}$ (N)	[initial guess±50%]
Optimal muscle fibre length $l^m_{o,i}$ (m)	[initial guess±0.010]
Tendon length l^t_i (m)	[initial guess±0.010]
Optimal pennation angle $\phi_{o,i}$ (rad)	[initial guess±5%]
Non-linear shape factor A	[-3,0.01]
Scale coefficient k^{mt}_i	[0.9,1.2]

3.4 Sensitivity analysis

After the parameter optimization, a sensitivity analysis is conducted to investigate the sensitivities of the model output to the optimized muscle-tendon parameters. The sensitivity can be calculated by [127]:

$$SI_j = \frac{(M_{j,pret} - M_{opt})/M_{opt}}{(P_{j,pret} - P_{j,opt})/P_{j,opt}} \tag{3.24}$$

where $M_{j,pret}$ and M_{opt} represent the perturbed model output and optimal model output respectively. $P_{j,pert}$ and $P_{j,opt}$ are the j^{th} perturbed parameter and the j^{th} optimized parameter in the proposed model respectively. The muscle-tendon lengths and moment arms are also included.

To evaluate the effects of each parameters to the model output, optimal muscle fibre length, tendon length and optimal pennation angle are perturbed by ±10% of the initial value. The maximum isometric forces are perturbed by ±20% due to the large variety of PCSA across subjects. The sensitivity coefficient SI_j is used for comparison between parameters.

3.5 Experiment

The experiment is approved by the MaPS and Engineering Joint Faculty Research Ethics Committee of the University of Leeds (MEEC 18-002). Eight subjects participate in this experiment (six males and two females), between the age of 25 and 31. The consent forms are signed by all subjects. The subject's weight data and the length of their hand are measured prior to experiment, in order to calculate the moment of inertia of the hand.

Figure 3.5: Experimental setup 16 reflective markers are attached on subject's right upper limb. Electrodes are placed on five primary muscles of wrist joint including FCR, FCU, ECU, ECRL and ECRB.

EMG data acquisition

Delsys Trigno^{TM} system is used to record the raw EMG signals. The sampling rate of EMG signals is 2000 Hz. Avanti electrodes are placed over five wrist muscles over right forearm, according to section 3.2. The placement of electrodes is placed following SENIAM recommendation [128] and palpation.

Motion Capture system

The trajectory data is captured through the motion capture system (VICON Motion Systems Ltd. UK) at 250 Hz. 16 reflective markers are placed on the subject's right upper limb. Markers are allocated over the spinous process of the 7^{th} and the 10^{th} thoracic vertabra, right scapula, xiphoid, acromio-clavicular joint, clavicle, lateral/medial humerus medial epicondyle, right radial/ulnar styloid, middle forearm and the right third metacarpus. The kinematic data and EMG data are synchronized using a trigger module via the VICON nexus software. The wrist joint angle is computed from VICON upper limb model [129].

Experiment setup

Subjects are asked to seat on the armchair while torso is fully straight, right shoulder is abducted at 90° and elbow is flexed at 90°, as shown in Figure 3.5. Their forearm and hand are fully relaxed and the position of hand is set as the neutral position ($\theta = 0°$). The subject's arm is shaved and skin is cleaned up using an alcohol wipe in order to minimize the artefact and impedance of the electrodes. The quality of the signal is checked visually before the experiment. The IMVCs and the static anatomical posture of each subject are also recorded. Four sets of wrist movement are performed whilst the MCP joint is keeping full extension to reduce the effects of digit muscles during the experiment. Wrist movement speed is not constrained. Furthermore, the subjects are informed to avoid the ulnar/radial deviation and the experimental data with radial/ulnar deviation are excluded.

The wrist motion trials include:

1) Flexion motion, which move the wrist towards to the palm side and then return to neutral position.

2) Extension motion, which starts from neutral position, move the wrist towards to the back-hand side and then return to neutral position.

3) Continuous cycle motion requires to perform consecutive wrist flexion/extension motion. Starting from neutral position, and then move the wrist to either flexion/extension direction, and finally return to neutral position.

4) Random motion is based on the subject's intention. They are asked to move their wrist freely in varying amplitudes and at varying speed.

The resultant motion data are low-pass filtered and set as the reference. Five repetitive trials are performed for each movement and a three minute break is given between each trial to prevent muscle fatigue. The first continuous cycle trial is selected as a training trial to optimize the parameters. The remaining four continuous cycle motion trials and all flexion/extension motion and random motion trials are used for validation. Each flexion/extension motion trial and the training trial lasts for 2-5 seconds while the continuous cycle/random motion trial lasts for about 15-20 seconds.

3.6 Results

3.6.1 Verification of EMG-driven model

The proposed model is verified by the validation sets using the root-mean-square-error (RMSE) and the coefficient of determination (R^2). RMSE and R^2 indicate the difference in terms of amplitude and correlation between the estimated joint angles/velocities and reference respectively. Table 3.3 and Fig. 3.7 summarizes the mean RMSEs and R^2 of the experimental motion trials across all subjects. The random motion trials of subject 2 and subject 3 are excluded due to the unacceptable noise captured in the experiment. In this study, the mean RMSE

and R^2 of the random motion trials are calculated using the remaining subjects' data.

Predefined motion

The results of one single flexion/extension and one continuous cycle trial of subject four are illustrated in Figure 3.8 and Figure 3.9 respectively. In each subfigure, joint angle (top panel) and joint velocity (bottom panel) denote the estimated results compared with the experimental measurement. The results of the single flexion/extension trials indicate the model can estimate the correct motion according to the measured EMG signals. Furthermore, the results of the pre-defined trials shows the proposed model with the optimized muscle-tendon parameters can estimate the wrist flexion/extension motion accurately.

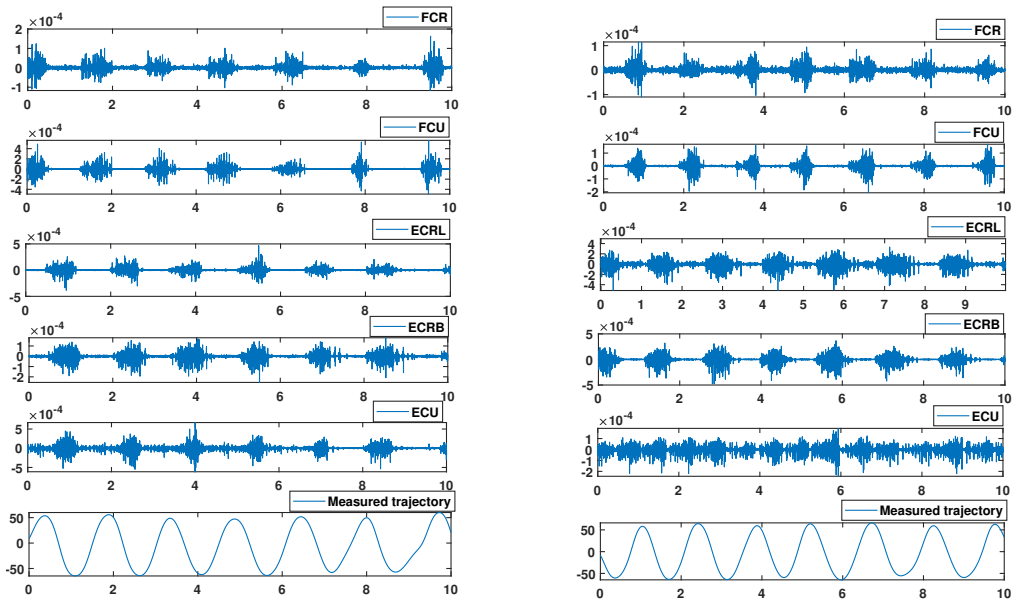

Figure 3.6: Representative examples of the recorded EMG signal. Left: female subject; right: male subject.

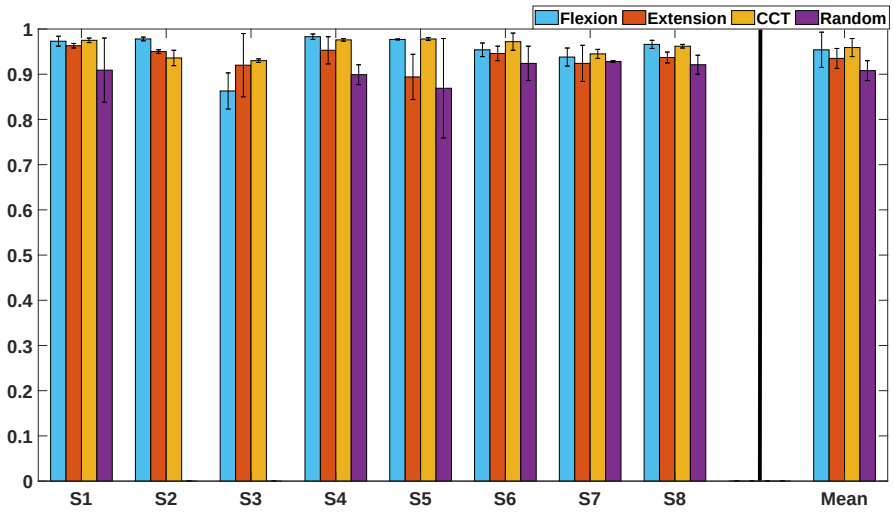

Figure 3.7: Mean R^2 across subjects in the flexion (mean $R^2 = 0.95$), extension (mean $R^2 = 0.94$), continuous cycle motion (CCT, mean $R^2 = 0.96$) and random motion (mean $R^2 = 0.91$) with the standard deviation.

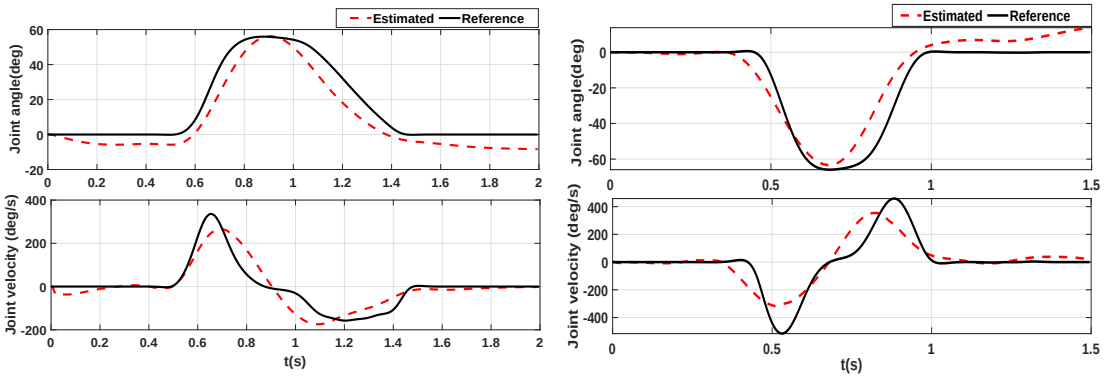

Figure 3.8: Representative example of the estimated results (red dashed line) and the reference (black line) of single flexion ($R^2 = 0.985, \mathrm{RMSE} = 7.79°$), single extension ($R^2 = 0.971, \mathrm{RMSE} = 8.49°$). In each panel, the estimated joint angle (top figure) and joint velocity (bottom figure) are presented.

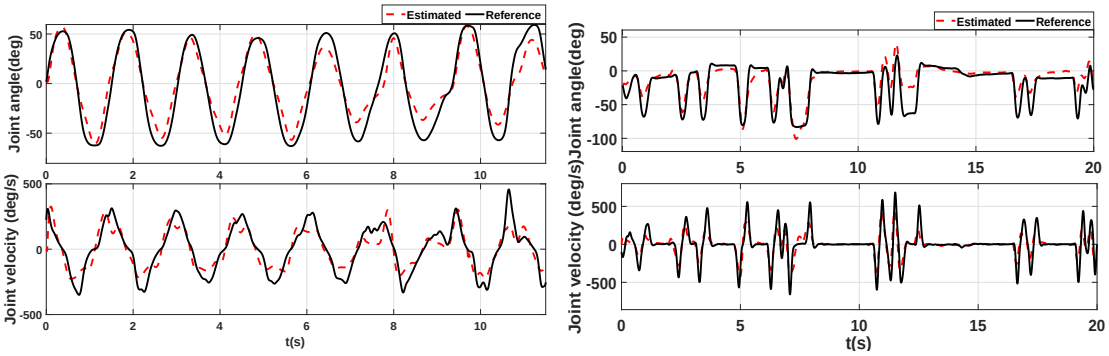

Figure 3.9: Representative example of the estimated results (red dashed line) and the reference (black line) of continuous cycle motion ($R^2 = 0.972, \text{RMSE} = 13.27°$) and random motion ($R^2 = 0.875, \text{RMSE} = 14.87°$). In each panel, the estimated joint angle (top figure) and joint velocity (bottom figure) are presented.

Random motion

The results of random motion trials denote that the proposed model can provide the accurate estimation in trend (mean $R^2 = 0.91$), but the amplitudes deviate from the reference (mean RMSE = 17.59°). Additional estimation performance of subject six and eight are illustrated in Fig. 3.10 and Fig. 3.11, respectively.

3.6.2 Parameters Identification

The subject-specific parameters are identified by GA. Table 3.4 presents the variation of the optimized parameters together with the initial guess (left column) of subject five. The deviations of the optimal fibre length, tendon length, optimal pennation angle and muscle-tendon length scaler are small from the initial guess (max 7.46% in ECRL). The maximum isometric forces deviate largely from the initial value. The optimized non-linear shape factor A is -2.716.

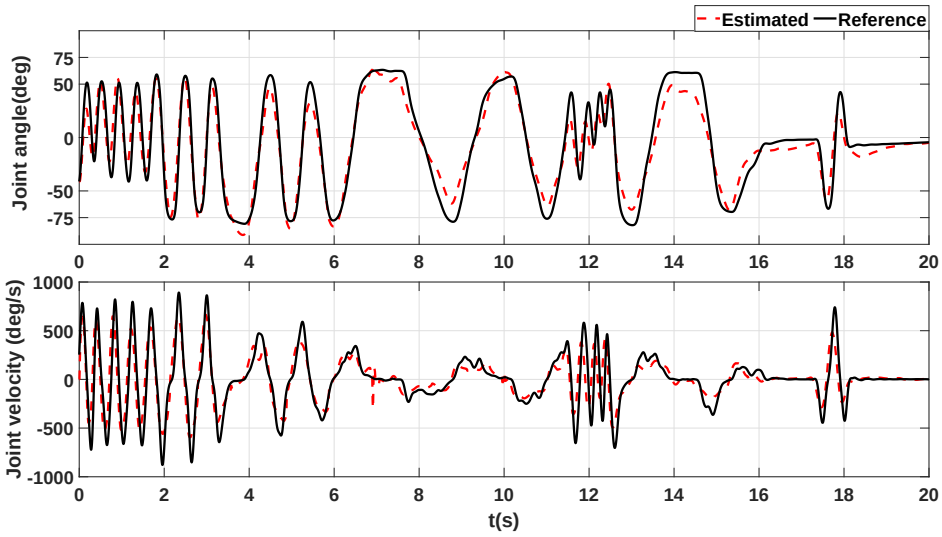

Figure 3.10: Representative example of estimation result of one random trial in subject six. The R^2 and RMSE are 0.962 and 13.5° respectively.

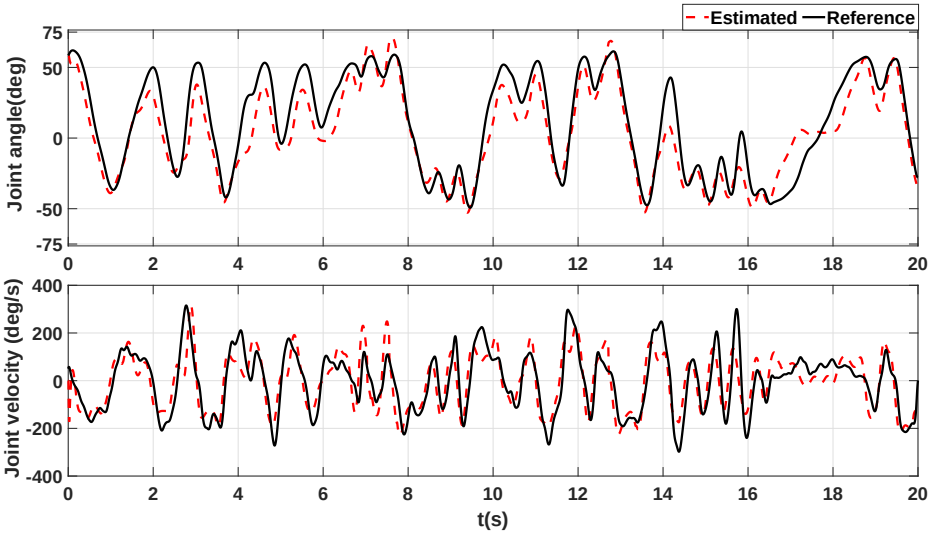

Figure 3.11: Representative example of estimation result of one random trial in subject eight. The R^2 and RMSE are 0.937 and 14.6° respectively.

Table 3.3: Mean RMSE (deg) in validation trials

		Trial			
Subject		**Flexion**	**Extension**	**Continuos cycle**	**Random**
S1	**Mean**	12.49	14.39	13.48	15.06
	Std.	1.11	6.57	1.70	1.72
S2	**Mean**	3.54	8.50	14.45	Null
	Std.	0.91	5.14	3.51	Null
S3	**Mean**	12.71	7.93	9.40	Null
	Std.	3.05	2.55	1.15	Null
S4	**Mean**	9.59	9.01	15.64	14.94
	Std.	2.66	2.00	3.61	5.38
S5	**Mean**	8.08	10.27	8.59	26.63
	Std.	2.23	1.90	1.38	8.77
S6	**Mean**	6.50	15.85	15.47	17.79
	Std.	1.48	5.49	2.97	4.85
S7	**Mean**	16.91	9.03	15.50	12.99
	Std.	2.32	0.91	2.58	0.42
S8	**Mean**	10.80	7.69	13.25	18.13
	Std.	1.66	0.75	1.88	1.00
Trials mean		10.08	10.33	13.22	17.59
Std.		4.13	3.08	2.77	4.41

Std. = standard deviation

Table 3.4: Representative example of the optimized parameters

	Parameter index									
	$l^m_{o,i}$ (m)		$F^m_{o,i}$ (N)		l^t_i (m)		$\phi_{o,i}$ (rad)		k^{mt}_i	
Muscle index	Initial	Variation	Initial	Variation	Initial	Variation	Initial	Variation	Initial	Variation
FCR	0.062	101.40%	407	68.96%	0.24	103.90%	0.05	102.38%	1	96.38%
FCU	0.051	100.78%	479	92.33%	0.26	100.85%	0.2	99.73%	1	97.87%
ECRL	0.081	98.38%	337	73.77%	0.24	104.02%	0	NaN[1]	1	96.47%
ECRB	0.058	99.73%	252	136.03%	0.22	99.47%	0.16	97.79%	1	92.54%
ECU	0.062	98.86%	192	139.28%	0.2285	96.46%	0.06	96.61%	1	94.88%

[1] The denominator is zero. The optimized pennation angle of ECRL is 0.0399 rad.

3.6.3 Sensitivity analysis

To evaluate the sensitivities of the optimized parameters, the results of the sensitivity analysis of the optimized parameters is presented. Figure 3.12 and Table 3.5 illustrate the sensitivity coefficient of each parameters, of which the SI of the non-linear shape factor A is 0.3134. The muscle-tendon length and tendon length have significant effects on the model output. The muscle fibre length, maximum isometric force and the moment arm have moderate effects on the model output. However, the optimal pennation angle show very low SI.

Table 3.5: Sensitivity coefficients (SI) of the optimized parameters

	FCR		FCU		ECRL		ECRB		ECU	
	Value	SI	Value	SI	Value	SI	Value	SI	Value	SI
$l^m_{o,i}$ (m)	0.0629	0.89	0.0514	0.55	0.080	0.12	0.058	0.33	0.0613	0.032
$F^m_{o,i}$ (N)	280.65	0.45	442.27	0.54	248.60	0.081	342.79	0.44	267.42	0.018
l^t_i (m)	0.249	11.00	0.262	20.46	0.249	5.01	0.219	19.12	0.2204	1.95
$\phi_{o,i}$	0.0511	0.00059	0.199	0.019	0.0399	0.00039	0.157	0.005	0.0580	-2.5E-05
l^{mt}_i		22.97		49.88		17.23		22.48		13.79
r_i		0.35		0.44		0.02		0.24		0.01

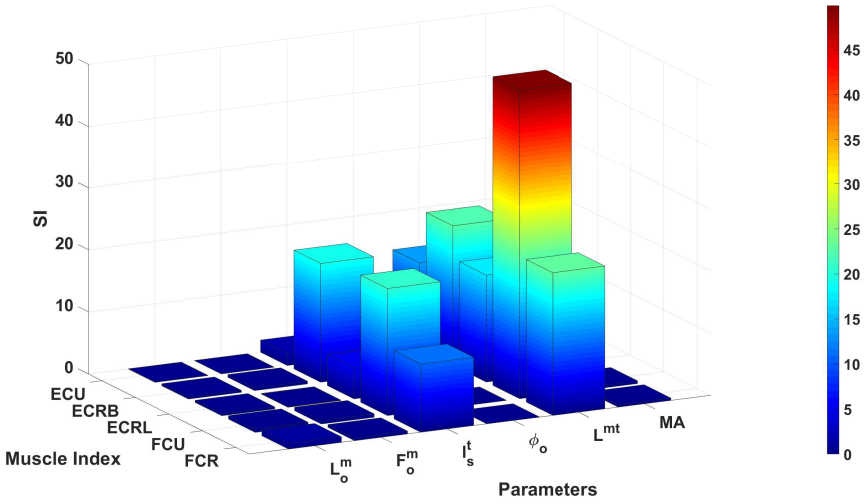

Figure 3.12: Sensitivity analysis of the muscle-tendon parameters of each muscle.

3.7 Discussion

Model's performance

In this chapter, the experiments are conducted to evaluate the accuracy and tracking performance of the proposed model for the estimation of the continuous wrist joint flexion/extension motion. The estimated joint angles of all motion trials are highly correlated to the reference elucidate that the proposed EMG-driven model can respond to the subjects' intention accurately according to the given EMG signals. The EMG-driven model shows its capability to maintaining high performance (mean $R^2 = 0.91$) in terms of the varying rotating velocities and different range of motions.

The RMSEs are similar in the single flexion/extension trials but increase in the continuous cycle motion and random motion trials. The estimation errors may be caused by the crosstalk and the muscle co-activation that generates small muscle force during the wrist flexion/extension motion. Recently, high-density surface

EMG is used to collect the high-resolution signals over the forearm. Therefore, the spatial distribution of the muscle activities can be identified and clustered to increase the fidelity of the EMG signals [130]. Furthermore, the passive tendon force is largely different in wrist flexion/extension motion which also results in estimation errors. Nevertheless, it is preferred to estimate the joint motion with greater R^2 rather than the RMSE for the application of EMG-based HMIs in assistive robots [131]. This is because the EMG-driven musculoskeletal is an open-loop estimation model. In practical, the close-loop control strategies are employed in HMIs. The estimation errors can be reduced through adding feedback signals, e.g., using a Kalman filter [132] or an error estimation model [41]. Furthermore, the proprioceptive output from the muscle spindle model or the force feedback from the Glogi tendon organ model may also have potential as the feedback signals in the EMG-driven model [133].

Comparison with literature

The proposed model is compared with the models [91] and [100], which estimate the singe degree-of-freedom joint motion through the open-loop musculoskeletal model. The proposed model shows better performance in the continuous cycle motion and random motion compared with [91], whose method has the mean RMSEs of 22° and 22.4° for continuous cycle motion and random motion respectively. The mean RMSE of single elbow flexion/extension is smaller than the proposed model. However, they have tuned each trial four times and selected the smallest RMSE. The lumped-parameter model shows the mean correlation of 0.94 for the wrist random motion trials of the able-bodied subjects [100]. However, the optimized parameters are over-estimated, e.g., the optimal muscle length and maximum isometric muscle force is their model.

Parameters of the EMG-driven model

The optimized parameters are constrained within the physiological range, as shown in Table 3.4. The proposed EMG-driven model uses five primary muscles of wrist joint [106], the effects of finger flexor/extensor are minimized by keeping the thumb and digits relaxed. The tendon length and the optimal muscle fibre length deviate slightly from the initial guess, indicating these parameters are not over-estimated.

According to the results of the sensitivity analysis, the proposed model has very low sensitivity to the pennation angle (SI $\approx 10^{-3}$), which is consistent with [134]. The model output has moderate sensitivities to optimal fibre length, maximum isometric force, moment arm and non-linear shape factor. The sensitivities of the tendon length and the muscle-tendon length are very high in the proposed model, because these parameters influence the muscle fibre length with regard to the joint angle. This suggests that the muscle-tendon force is affected by the muscle-tendon properties except for the optimal pennation angle.

Using the regression algorithms to estimate the muscle-tendon length can only represent the average value from cadaver studies. State-of-the-art methods to determine the muscle-tendon length include using the biomechanical model API, e.g., OpenSim [96], or the highly accurate estimation model [99]. Nevertheless, using the regression algorithms to compute the muscle-tendon length can ease the computational burden when the musculoskeletal model is used in real-time [133]. The exclusion of the elastic tendon can also reduce the computational cost through alleviating the numerical stiffness in the muscle-tendon model. The wrist muscles have smaller ratios of tendon length to muscle fiber length, which has less effects to the muscle-tendon force output [87]. When elastic tendon is considered, the forward integration of the muscle fibre length at each iteration are required. However, if $a(t)$ and $f(a)$ are close to zero, this equation becomes to numerically stiff.

To address this issue, other approaches have used a passive damper which is modelled in parallel with the CE to avoid computing the infinite muscle contraction velocity in the muscle-tendon model [118], or have used the implicit formulation of the musculoskeletal model to reduce the numerical stiffness [105, 133]. Nevertheless, the proposed model shows similar results in terms of R^2 compared with [133], by assuming the tendon is rigid without increasing the computational complexity.

Genetic algorithm is used for the Hill's muscle model and can avoid local minima using the physiological constraints. The average optimization time is around half an hour. The optimization time can be further reduced by reducing the number of parameters for optimization based on the sensitivity analysis, e.g., optimal pennation angle.

Offline computation time

The processing time of the proposed model is measured by executing a 20-second continuous trial [100]. The mean computation time for the muscle activation interpretation method, the muscle-tendon model and the joint kinematic modelling technique are 68 ms, 390 ms and 690 ms respectively. The program is executed on a personal PC with quad-core processing unit (4.2GHz) and 16GB of RAM memory. The overall computation time of the proposed model indicates that it is feasible for real-time implementation, according to the real-time control constraints.

Limitations and future work

The proposed EMG-driven musculoskeletal model is experimentally verified on wrist flexion/extension motion. Nevertheless, there are several limitations. Firstly, the grouped five primary muscles not only have the contributions to wrist flex-

ion/extension, but also to other DoFs, i.e., ulnar/radial deviation.

Secondly, the proposed model has been validated on healthy subjects.Patients with neurological discords, e.g., stroke patients, have abnormal EMG patterns when performing daily activities. For example, Nizamis *et al.,* demonstrated that Duchenne muscular dystrophy patients have a higher activation level than the healthy subjects when perform wrist motion [130]. Nevertheless, the EMG-driven musculoskeletal model shows the potential to estimate the motion intention for the stroke patients at the lower limb [89, 102]. Future work will carry on evaluating the performance of the proposed model for patients.

Future work includes the qualitative evaluation of real-time application of the proposed model into our wrist rehabilitation robot [12]. In addition, the model will be extended to estimate continuous wrist motion with multiple DoFs.

3.8 Chapter summary

This chapter proposes an EMG-driven musculoskeletal model to estimate the continuous wrist motion. Muscle activation levels are calculated from five superficial wrist muscles. Together with the muscle activation levels and musculoskeletal model, the muscle-tendon model computes the muscle-tendon force. The continuous wrist flexion/extension motion is obtained through the joint kinematic modelling technique. The genetic algorithm is developed and implemented to obtain the subject-specific physiological parameters. In addition, the muscle-tendon parameters are bounded within the physiological range. The proposed musculoskeletal model shows an accurate estimation in the wrist flexion/extension motion with the mean R^2 of 0.9 for all the motion trials. The mean RMSEs are 10.08°, 10.33°, 13.22° and 17.59° for single flexion/extension, continuous cycle and random motion trials, respectively.

Only calibration trial is used for each subject, which is selected from the continuous cycle trial. This indicates that the musculoskeletal model-based approach can facilitate the rehabilitation setup since only a few training data are required. To meet the real-time application requirement, the tendon element is assumed to be stiff enough. This setting can significantly reduce the computational burden by alleviating the numerical stiffness in the muscle-tendon models. Furthermore, the design of the interactive control strategies for the wrist rehabilitation robots can benefit from the use of the musculoskeletal model-based approach due to it reveals the underlying states of the muscular and skeleton states and estimates the motion intention accurately.

Chapter 4

A Direct Collocation Method for optimization of EMG-driven Wrist musculoskeletal model

This chapter presents the new method for the subject-specific parameter optimization for the EMG-driven musculoskeletal model. The EMG-driven musculoskeletal model has been broadly used to detect human intention in rehabilitation robots. This approach computes muscle-tendon force and translates it to the joint kinematics. However, the muscle-tendon parameters are difficult to measure in *vivo* and are varied across subjects. A direct collocation method is proposed to optimize the subject-specific parameters in the wrist musculoskeletal model. The resultant optimized parameters are used to estimate the wrist flexion/extension motion. The estimation accuracy is compared with the parameters optimized by the genetic algorithm. Experiment results show that the direct collocation method has a similar estimation accuracy compared with using the genetic algorithm, the mean correlations are 0.96 and 0.93 for the genetic algorithm and direct collocation method respectively. Besides, using the direction collocation method requires less optimization time (75 seconds) thus indicates the potential

use for the clinical scenario.

4.1 Introduction

Decoding the user's intention based on the electromyography (EMG) signal can provide an intuitive control strategies for rehabilitation robots. The interests in using the EMG-driven musculoskeletal (EMG-MS) model to estimate the joint motion have risen recently [39, 102]. This approach uses the muscle activation dynamics and muscle-tendon model to transfer the EMG signals to the muscle-tendon force accordingly [119]. Together with the explicit representation of the joint geometries, the joint kinematics are computed [91, 100]. Nevertheless, the output of the EMG-driven musculoskeletal model is influenced by the muscle-tendon parameters significantly, i.e., maximum isometric force, optimal muscle fibre length, tendon length and pennation angle [135, 136]. It is difficult to measure these parameters in *vivo* and these parameters are closely related to gender, age and activity levels. Thus, these parameters must be optimized in order to create a subject-specific EMG-MS model for each individual.

Several methods are proposed to optimize the muscle-tendon parameters in the musculoskeletal model-based approach [91, 100, 137, 138]. For example, a linear scaled method is proposed. The muscle-tendon parameters are linearly scaled in response to the anatomical dimension obtained from a motion capture system. A reference biomechanical model then is used to scale the musculoskeletal anthropometric properties are scaled to different subjects [137]. However, this method has scaled the subject-specific parameters from the user's anatomical data solely, which has the less accuracy in intention estimation. To date, the inverse (or forward) dynamics methods are used to optimize the subject-specific parameters, which minimize the difference between the experimental measurement and

the model estimated joint moment/motion [91, 100, 139]. The resultant parameter optimization problems are commonly solved by the heuristic algorithms, e.g., genetic algorithm, to find the best 'fitness' to minimize the targeted objective function. However, due to a large amount of muscle-tendon parameters and the corresponding large search space, the heuristic algorithms may require a long optimization time that leads to barriers for implementing the EMG-MS model in the clinical environment [140]. For instance, an average optimization time of 20 hours was reported in a lower limb EMG-MS model for estimating the multiple degrees-of-freedom joint moments [90]. Pau *et al.,* used the genetic algorithm to optimize 24 muscle parameters in an EMG-MS model, which took an average one hour for each trial [91]. Moreover, Crouch *et al.,* reported the execution time of optimization taking approximately 20 hours in a lumped-parameter EMG-MS model using the simulated annealing algorithm [100].

To alleviate the optimization time, the parameter optimization problem can be solved by formulating the EMG-MS model into an optimal control problem [141]. However, solving the optimal control problem using the indirect method is also computationally expensive [142]. Instead, the direct collocation method is a computationally efficient method in finding the solutions in the EMG-MS model related problems. Recently, the direct collocation method becomes popular to determine the muscle activities [143], internal joint contact force [144] or the optimal trajectories [145]. With a given movement and EMG signals, the direct collocation method is able to determine the muscle-tendon parameters. Falisse *et al.* applied the direct collocation method to estimate the optimal tendon slack length and the optimal muscle fibre length by minimizing the joint moment between model's estimation and measured joint moment in a lower limb musculoskeletal model [146]. However, they only optimize two kinds of muscle-tendon parameters and compared them with the linear scaled method.

This chapter proposes a direct collocation method to optimize the muscle-tendon parameters in a wrist joint musculoskeletal model, which includes maximum isometric force, optimal muscle fibre length, tendon length and pennation angle. For this purpose, a wrist joint EMG-MS model is formulated into an optimal control problem and converts it into a non-linear programming (NLP) problem. A vector including the discretized state variables, control variables and muscle-tendon parameters is generated. In order to determine the muscle-tendon parameters, the control variables are set the input EMG signals during the optimization. A gradient matrix of a objective function and a Jacobian matrix of constraints are established for the NLP solver. The optimized parameters are then applied for the wrist EMG-MS model to estimate the continuous wrist flexion/extension motion. Based on the same objective function, maximum iteration number and stop criteria, the estimation performance through the direct collocation method is compared with the genetic algorithm. Results show that the optimized parameters by the direct collocation method can estimate the wrist flexion/extension accurately. Under the same performance, the direct collocation method requires less optimization time.

The remaining sections of this chapter are organized as follows. In section 4.2, the experiment protocol are presented. Section 4.3 gives the description of parameter optimization using genetic algorithm and the direct collocation method respectively. Section 4.5 gives the results regarding the optimized muscle-tendon parameters and the comparison with the genetic algorithm, followed by a conclusion in Section 4.6.

4.2 Experimental protocol

In this chapter, the EMG and motion data are selected from the continuous wrist flexion/extension trial in **Chapter three**. The continuous motion trial lasts about 15-20 seconds and five repetitions are performed for each subject. Detailed description for the experimental protocol can be found in section 3.5 in **Chapter three**. One cycle of the continuous wrist flexion/extension motion is extracted from the first trial in order to optimize the parameters using the direct collocation method and genetic algorithm respectively. The remaining motion trials are used to validate and compare the estimation performance between the direct collocation method and genetic algorithm.

4.3 EMG-MS model

Similar to the previous chapter, the EMG-MS model in this chapter is used to estimate the flexion/extension motion of the wrist joint, which comprises the muscle activation dynamics, muscle-tendon dynamics, and joint kinematic estimation model. The dynamic equations should be differentiable in the direct collocation method. For a fair comparison, the EMG-MS model is the same for both optimization methods.

Muscle activation dynamics

The raw EMG signals are first filtered using a 2^{nd} order butterworth band-pass filter at cut-off frequencies between 25 Hz and 450 Hz to remove baseline and artefact noise, and then fully rectified. The rectified signals are then low-pass filtered using 4^{th} order butterworth low-pass filter at a corner frequency of 4 Hz. Filtered signals are normalized by dividing the peak value of isometric maximum voluntary contraction, resulting the enveloped signal $e_i(t)$. A first order differ-

ential equation is used to compute the muscle excitation $s_i(t)$, which is written as [105]:

$$\frac{ds_i(t)}{dt} = (\frac{e_i(t)}{t_{act}} + \frac{1 - e_i(t)}{t_{deact}})(e_i(t) - s_i(t)) \tag{4.1}$$

where the t_{act} and t_{deact} are the activation time and deactivation time, are set to 15 ms and 50 ms respectively [121]. A non-linear function is used to transfer the $e_i(t)$ to muscle activation $a_i(t)$, which is represented as [119]:

$$a_i(t) = \frac{e^{As_i(t)} - 1}{e^A - 1} \tag{4.2}$$

where the non-linear shape factor A has the range of -3 to 0.01.

Muscle-tendon model

The muscle-tendon force F_i^{mt} is computed by the muscle-tendon model, comprising a tendon in series with a muscle fibre. The muscle fibre includes a contractile element (CE) in parallel with passive elastic element (PE). Thus the F_i^{mt} can be derived by the the summation of the active force $F_{CE,i}$ and the passive force $F_{PE,i}$, which can be written as,

$$F_i^{mt} = (F_{CE,i} + F_{PE,i}) \cos \phi_i. \tag{4.3}$$

where the $F_{CE,i}$ and $F_{PE,i}$ are

$$F_{CE,i} = F_{o,i}^m f_a(\frac{l_i^m}{l_{o,i}^m(\lambda(1 - a_i(t)) + 1)}) f(\overline{v}_i) a_i(t) \tag{4.4}$$

$$F_{PE,i} = F_{o,i}^m f_p(\frac{l_i^m}{l_{o,i}}) \tag{4.5}$$

where ϕ_i is the pennation angele in response to current muscle contraction state. $F_{o,i}^m$ indicates the maximum isometric force. l_i^m and $l_{o,i}^m$ are the muscle fibre length and optimal muscle fibre length respectively. λ is set to 0.15 in this study. The equations of pennation angle and active/passive force-length relationships are the same in the previous chapter. Additionally, two simplification are made in this

study for calculation of the derivatives for the direct collocation method. First, the $f(\overline{v}_i)$ is set to 1 in this study. Second, the muscle tendon force F_i^{mt} is fully derived by the variation of the l_i^m, in which the tendon length is assumed to be constant in this study. Therefore, the muscle fibre length l_i^m is computed through

$$l_i^m = (l_i^{mt} - l_i^t)\cos^{-1}\phi_i \tag{4.6}$$

where l_i^{mt} are l_i^t are the muscle-tendon length, tendon length respectively.

Joint kinematic estimation

In this study, the joint kinematics is computed by the coordinate relative to the wrist joint, where is located at the mid of the radial and ulnar bones. It is assumed that the hand is a rigid segment and is rotated around the joint centre in the sagittal plane. Thus, the equation of motion is written as

$$I\ddot{\theta} + mgLsin\theta + C\dot{v} = \tau \tag{4.7}$$

where I is the moment of inertia of hand. $\ddot{\theta}$ is the angular acceleration. m and L represent the mass of subject's hand and the length of the hand. θ and $\dot{v}$ represent the wrist joint angle and angular velocity respectively. C is the damping coefficient representing the elastic and viscous effects from tendon, ligaments. τ is the joint torque, which is calculated by ($i = 1 \ldots 5$):

$$\tau = \sum_{i=1}^{2} M_{flexor,i} - \sum_{i=3}^{5} M_{extensor,i} \tag{4.8}$$

where $M_{flexor,i}$ and $M_{extensor,i}$ represent joint torque computed by the wrist flexor and extensor respectively.

$$M_i = F_i^{mt} r_i. \tag{4.9}$$

The l^{mt} and r_i are obtained using the Fourier equations, which are differentiable.

$$l_i^{mt} = b0 + b_n cos(nw\theta) \tag{4.10}$$
$$r_i = d0 + \sum_{n=1}^{2} d_n cos(nw\theta) + h_n sin(nw\theta)$$

where the coefficient b_i, d_i and h_i are the regression coefficients. Then, the wrist joint motion can be estimated through the EMG-MS model through the forward dynamics.

4.4 Parameters optimization

To establish the subject-specific EMG-MS model, the muscle-tendon parameters including the optimal muscle fibre length, tendon slack length, maximum isometric force, and pennation angle are optimized for each subject. The non-shape factor A is also included. For the direct collocation method and genetic algorithm, the parameters can be represented in a form of

$$p = [F_{o,i}^{m^T}, l_{o,i}^{m^T}, l_{o,i}^{t^T}, \phi_{o,i}^{T}, A] \tag{4.11}$$

where p is a parameter vector used in both optimization methods. This parameter optimization problem is solved by an objective function. The objective function is written as

$$\Psi = \int_{t_1}^{t_f} (\theta_{measured} - \theta_{estimated})^2 dt \tag{4.12}$$

where $\theta_{measured}$ and $\theta_{estimated}$ represent the measured joint angle and estimated joint angle respectively. The t_1 and t_f represent the initial time and end time respectively. Furthermore, the boundary conditions of parameters for both op-

timization method are set as

$$\begin{aligned} 10 \leq F_{o,i}^{m}(\mathrm{N}) \leq 1000; \\ 0.06 \leq l_{o,i}^{m}(\mathrm{m}) \leq 0.1; \\ 0.2 \leq l_{i}^{t}(\mathrm{m}) \leq 0.4; \\ 0 \leq \phi_{o,i}(\mathrm{rad}) \leq \frac{\pi}{2}; \\ -3 \leq A \leq 0.01. \end{aligned} \tag{4.13}$$

4.4.1 Genetic algorithm

In the previous chapter, the genetic algorithm is applied for parameter optimization. Results suggest that, together with the parameters optimized through the genetic algorithm, the EMG-MS model can provide the precise wrist flexion/extension motion estimation. The genetic algorithm mimics the natural

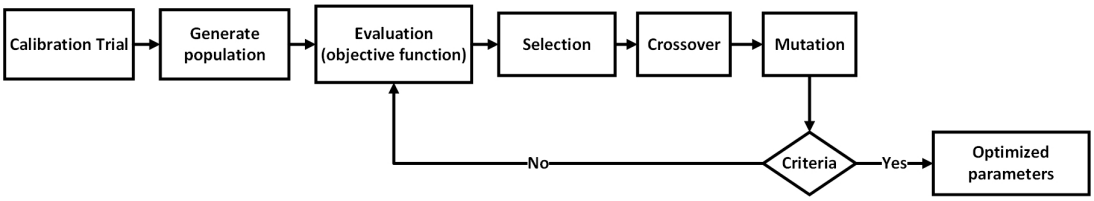

Figure 4.1: Flowchart of the genetic algorithm for parameter optimization.

evolutionary process by representing the parameters as a 'chromosome'. The algorithm randomly generates a set of possible solutions (population) for this parameter optimization problem. The best fitness (selection) at each generation to generate the "offspring" (crossover and mutation). The best set of parameters can be reached iteratively. It can evaluate multiple solutions in the search space, and reduced the risk of falling into local minima. Thus, to determine the best match of the subject-specific parameters, the objective function can be rewritten

as

$$\hat{p} = \arg\min_{p}\{\Psi(p)\} \tag{4.14}$$

where $\hat{p}$ is the optimized parameters. In this study, the MATLAB GLOBAL optimization toolbox is used to solve this optimization problem. The tolerance is set to $1 \times e^{-4}$ and the maximum iteration number is set to 1000, other settings are set to the default value.

4.4.2 Direct Collocation Method

In this section, a transcription method is introduced to convert the the optimal control problem into the finite-dimension NLP problem, which treats the controls, states and static parameter p as an unknown vector [141]. Thus, the direct collocation is used to optimize the parameters.

In specific, the wrist EMG-MS model has the enveloped EMG signals $e_i(t)$ as the control variables

$$u(t) = [e_i(t)]. \tag{4.15}$$

The state variables contain the joint angle θ, velocity v and muscle excitation $s_i(t)$, which can be represented by

$$x(t) = [\theta, v, s_i(t)]. \tag{4.16}$$

The static parameter is

$$p = [F_{o,i}^{m^T}, l_{o,i}^{m^T}, l_{o,i}^{t^T}, \phi_{o,i}^{T}, A]. \tag{4.17}$$

Therefore, the objective function can be rewritten as

$$\Psi = \int_{t_1}^{t_f} (\theta_{measured} - \theta_{estimated}(x(t), u(t), p))^2 dt \tag{4.18}$$

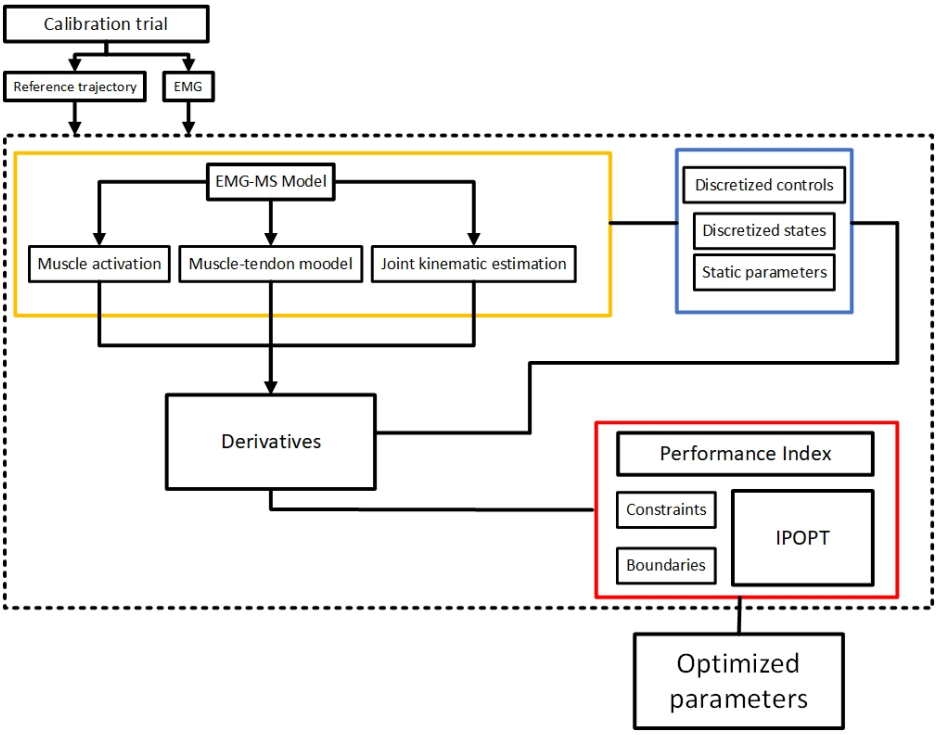

Figure 4.2: Flowchart illustrates the processes for the parameters optimization using the direct collocation method. The controls, states are discretized for the IPOPT solver. The optimal solution is solved that the objective function is minimized.

The control variables and state variables are discretized simultaneously into number of grid points N with respect to the time history. We use a vector Y to combine the discretized controls, discretized states,

$$Y = [x_1^T, u_1^T, x_2^T, u_2^T, x_1^T, u_1^T, \ldots, x_N^T, u_N^T, p],$$
$$0 = t_1 < t_2 < t_3 < \cdots < t_N = t_f \tag{4.19}$$

where N is the number of grid points. We add the the parameter vector p the end of Y for optimization.

Constraints and boundary conditions

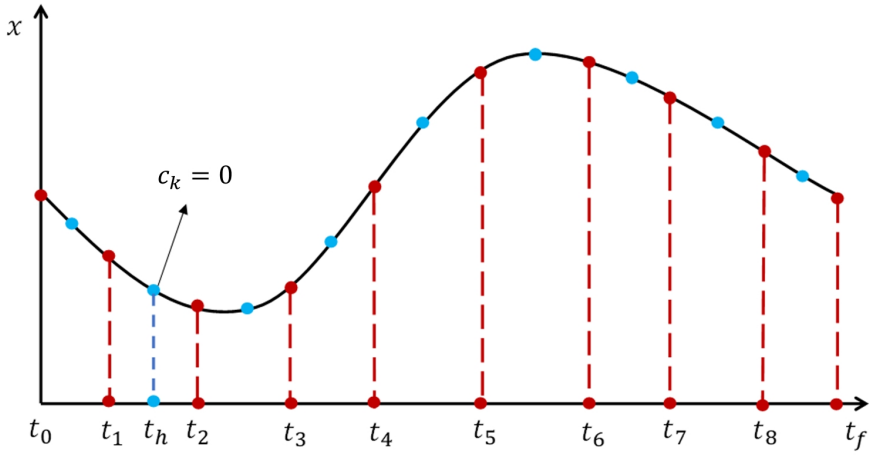

Figure 4.3: Transcription method for the wrist EMG-MS model. At each grid, the system dynamics should satisfy constraints.

The wrist EMG-MS mode can be rewritten as the system dynamics, including the muscle activation dynamics, muscle-tendon mode and joint kinematic model

$$f(x, \dot{x}, u, p) = \begin{cases} \dot{\theta} - v \\ I\dot{v} + mgl\sin(\theta) + Cv - \tau \\ \dot{s}_i - (e_i - s_i)(\frac{e_i}{t_{act}} + \frac{1-e_i}{t_{deact}}) \end{cases} \tag{4.20}$$

where $\dot{\theta}_k$, $\dot{v}_k$ and $\dot{s}_{i,k}$ represent the derivatives of the state variables.
The states, control and static parameters at each grid should satisfy the constraints that are imposed by the system dynamics [147]. Thus, the system dynamics are converted into the equality constraints using the finite differential approximation. The mid-point rule is used this study.

$$c_k = f(\frac{x_{k+1} + x_k}{2}, \frac{x_{k+1} - x_k}{t_{k+1} - t_k}, \frac{u_{k+1} + u_k}{2}, p) = 0 \tag{4.21}$$
$$k = 1, 2, 3 \ldots N - 1;$$

where c_k represents the equality constraints at each grid. Furthermore, task constraints are also used to restrict that the motion is consistent with measured data at the initial and end condition.

$$\begin{aligned} s_i(t_0) &= 0; \\ \theta(t_0) = \theta(t_f) &= 0; \\ v(t_0) = v(t_f) &= 0; \end{aligned} \tag{4.22}$$

In addition to equation (4.13), we introduce two additional boundary conditions for the controls and states,

$$\begin{aligned} 0 \leq e_i, s_i &\leq 1; \\ -70^\circ \leq \theta &\leq 70^\circ; \end{aligned} \tag{4.23}$$

The boundary conditions for the direct collocation method are reformulated as

$$\begin{aligned} UB &= \{x_U(t1), u_U(t1), x_U(t2), u_U(t2), \ldots, p_U\} \\ LB &= \{x_L(t1), u_L(t1), x_L(t2), u_L(t2), \ldots, p_L\} \end{aligned} \tag{4.24}$$

Where the UB and LB represent the upper bound and lower bound respectively. Note that the length of boundary conditions should be the same as the discretized parameter vector Y.

Implementation

After the transcription, this parameter optimization problem contains 7 states variable (2 joint kinematics and 5 muscle activations), 5 controls variables (5 enveloped EMG signals) and 21 static parameters. The optimization trial is discretized into 101 equal interval ($N = 101$), which results $12 \times 101 + 21 = 1233$ variables in vector Y and $7 \times (101 - 1) + 10 = 710$ equality constraints.

To enhance the computational efficiency, the gradient matrix G of the objective function and the Jacobian matrix J of the constraints are calculated, which are written as

$$G = \frac{\partial \Psi}{\partial Y} = \begin{bmatrix} \frac{\partial \Psi}{\partial Y_1} \\ \frac{\partial \Psi}{\partial Y_2} \\ \vdots \\ \frac{\partial \Psi}{\partial Y_{N-1}} \\ \frac{\partial \Psi}{\partial Y_N} \end{bmatrix} \tag{4.25}$$

$$J = \begin{bmatrix} \frac{\partial c_1}{\partial Y_1} & \frac{\partial c_1}{\partial Y_2} & \cdots & \cdots & \frac{\partial c_1}{\partial Y_N} \\ \frac{\partial c_2}{\partial Y_1} & \ddots & \ddots & \ddots & \frac{\partial c_2}{\partial Y_N} \\ \vdots & \ddots & \ddots & \ddots & \vdots \\ \frac{\partial c_k}{\partial Y_1} & \frac{\partial c_k}{\partial c_k} & \cdots & \cdots & \frac{\partial c_k}{\partial Y_N} \end{bmatrix} \tag{4.26}$$

In addition, the partial derivatives of the constraint functions with respect to the static parameters are written as

$$[-\frac{\partial \tau}{\partial F_{o,i}^m}^T, -\frac{\partial \tau}{\partial l_{o,i}^m}^T, -\frac{\partial \tau}{\partial l_{o,i}^t}^T, -\frac{\partial \tau}{\partial \phi_{o,i}}^T] \tag{4.27}$$

This NLP problem can be solved by the standard solver. In this study, an IPOPT is chosen as it is insensitive to the initial guess. The IPOPT solver is set with the Hessian matrix approximation, and the tolerance is also set to $1 \times e^{-4}$ and the maximum iteration number is set to 1000. Other settings are remaining default. The genetic algorithm and the direct collocation method are executed using the MATLAB R2020a on the PC with quad-core (4.2 GHz) and 32 G RAM.

4.4.3 Jacobian matrix of the constraints

The Jacobian of the constraints with respect to the variables results in a large sparse matrix In this sparse matrix, the constraints ware the function of two adjacent grids, as the controls, states are obtained through the mid-point rule.

As illustrated in Figure 4.4, the sparse matrix include $700 \times 1233 = 863100$ elements, but only 5910 are non-zeros elements. The dense blocks indicate the partial derivatives of constraints with respect to the controls, states and static parameters.

In detail, the black circle presents a 7-by-12 matrix that describes the non-zero elements of the Jacobian matrix at a single grid. The first row indicates the partial derivatives of motion dynamics with respect to the kinematic state variables, θ and v. The second row contains the partial derivatives of the muscle-tendon model (equation (4.3) – (4.9)) with respect to the state variable v. The last 5 rows are the piratical derivatives of muscle activation levels (equation (4.1)) with respect to the muscle excitation $s_i(t)$ and the enveloped EMG signals $e_i(t)$. Besides, the last 10 rows (circled in yellow) represent the task constraints at the beginning and end of the optimization trial. The last 21 columns (circled in red) are also non-zero elements which represent the partial derivatives of the constraint functions with respect to the static parameters.

The Jacobian matrix can be easily solved in the NLP solver, the sparse structure can improve the computation performance.

4.5 Results and discussion

4.5.1 Verification of the optimized parameters

The optimized parameters through the direct collocation method and the genetic algorithm are verified using the remaining wrist continuous flexion/extension trials. Root-mean-square-error (RMSE) and coefficient of determination (R^2) are used to evaluate the estimation performance compared with the measured joint trajectories. Hereinafter, the optimized parameters through the genetic algorithm and direct collocation method are referred as GA-based parameters and DC-based

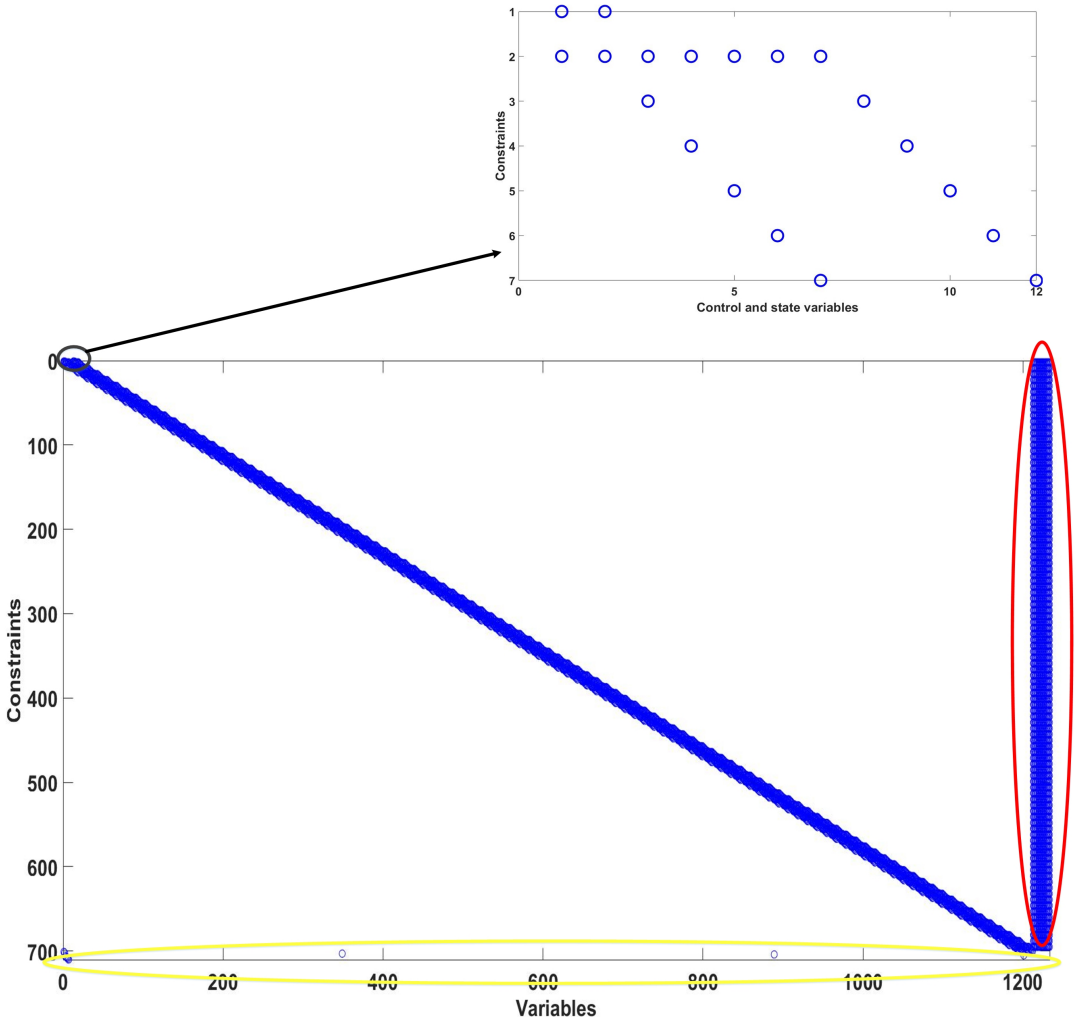

Figure 4.4: The Jacobian matrix is computed for the direct collocation method, comprising 5190 non-zero elements for $N = 101$. The row and column represents the constraints and discretized parameter Y respectively. The top figure indicates the Jacobian matrix at a single grid, which comprising 19 non-zeros elements. Each non-zero elements correspond to the derivatives of the constraints to the controls and states. In addition, the non-zero elements related to the task constraints and static parameters are circled in yellow and red respectively.

parameters in the following sections.

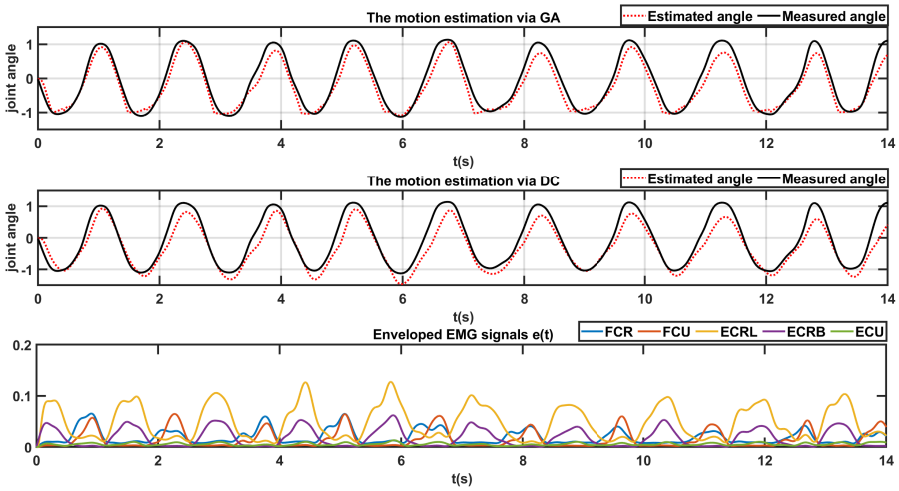

Figure 4.5: Comparison of estimation performance using two different optimization methods in one representative subject. Correlations are 0.98 and 0.96 respectively.

Figure 4.5 and Figure 4.6 illustrate the estimation accuracy with the optimized parameters using two different methods in two subjects. In each figure, the first panel is the estimation when the genetic algorithm is applied. The second panel is the estimation when the direct collocation method is applied. The bottom figure corresponds to the enveloped EMG signals (bottom figure) $e_i(t)$. The R^2 ($R^2 > 0.9$) are similar in both subjects, but RMSE increases from 0.25 rad to 0.32 rad in the Figure 4.5 and from 0.17 rad to 0.23 rad in the Figure 4.6, respectively, when the DC-based parameters are applied.

Figure 4.7 illustrates the mean R^2 across all subjects. The mean R^2 are 0.93 and 0.96 for the DC-based parameters and GA-based parameters, respectively. The correlation of the DC-based parameters is slightly less than the genetic algorithm based but overall R^2 is high ($R^2 > 0.9$). Fig 4.8 presents mean RMSE across subjects, which are 0.27 rad and 0.38 rad for the GA-based parameters and DC-

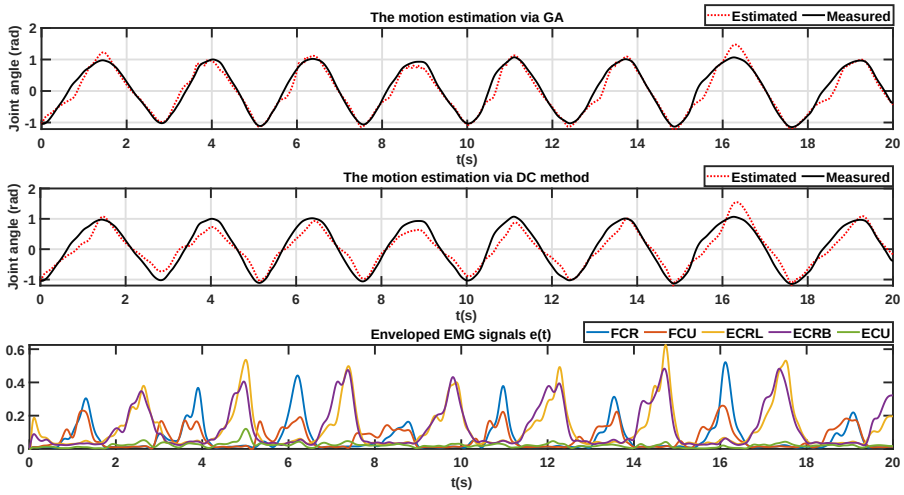

Figure 4.6: Comparison of estimation performance using two different optimization methods in one representative subject. Correlations are 0.97 and 0.95 respectively.

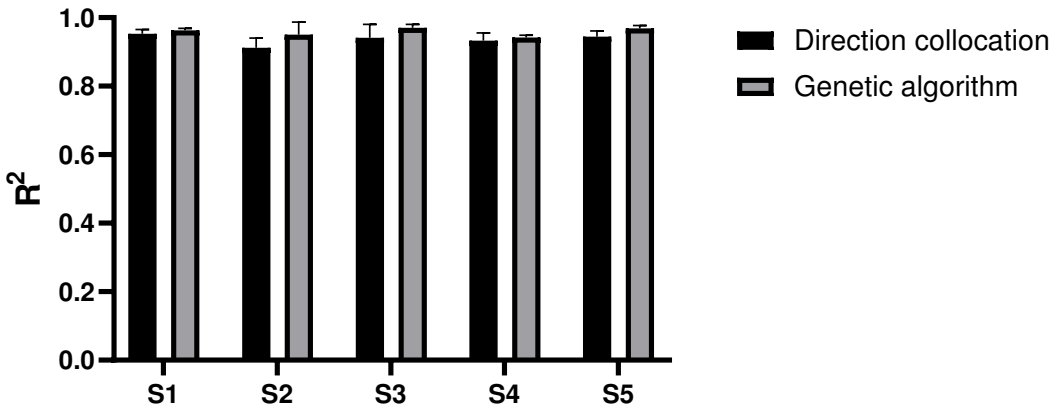

Figure 4.7: The mean R^2 across all subjects are 0.93 and 0.96 for DC-based parameters and GA-based parameters respectively.

based parameters respectively.

Both methods can offer the EMG-MS model with optimal parameters that accurately estimate continuous wrist flexion/extension motion. However, the mean

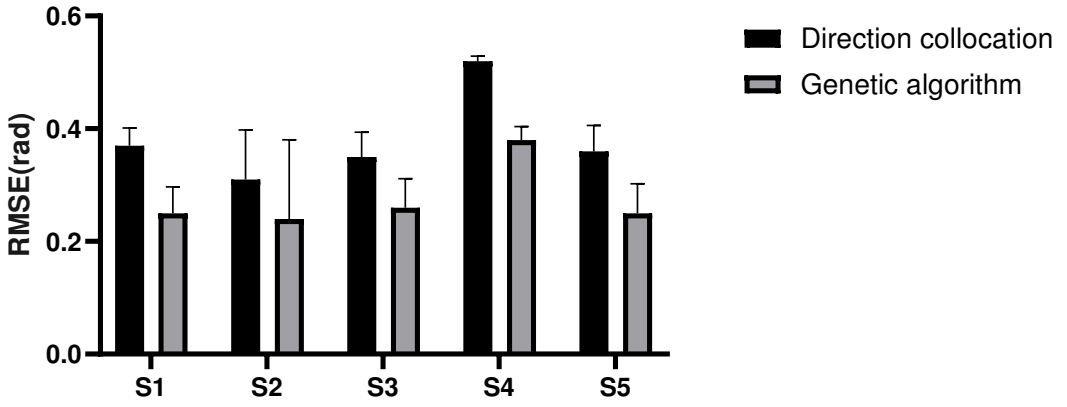

Figure 4.8: The mean RMSE across all subjects are 0.38 rad and 0.27 rad for direct collocation method and genetic algorithm, respectively.

RMSE of the genetic algorithm is less than the DC-based parameters, which indicates using the genetic algorithm can provide a better motion estimation in terms of the amplitude of wrist flexion/extension motion. The differences in RMSE between two methods may be caused by the difference of the optimized parameters. Both methods cannot determine the unique optimized parameters due to a large search space that is presented in equation (4.13). This indicates that the proposed method may be trapped in the local minimal, whereas the genetic algorithm shows the capability to reduce the risk to be trapped in local minima. This leads to different optimized parameters. For instance, the muscle-tendon force is sensitive to these parameters, which results in different joint kinematics accordingly. To prevent the proposed method is trapped in the local minimal, future work can apply different initial guesses for the optimization to reduce the risk to be trapped in local minima [142]. Nevertheless, it is worthy to note that the high RMSE is commonly occurred in most of the EMG-MS models, even using the genetic algorithm. This is because the EMG-driven model is an 'open-loop' estimation model. Moreover, the EMG signal are an non-stationary signal and

the subject cannot perform the same muscle activation level in one trial, e.g., the muscle activation levels in Figure 4.5.

Table 4.1: Comparison of the optimized parameters of one representative subject using two different optimization methods.

	$F^m_{o,i}$**(N)**		$l^m_{o,i}$ **(m)**		$l^t_{o,i}$ **(m)**		ϕ_i **(rad)**	
Muscles	Var.(GA)	Var.(DC)	Var.(GA)	Var.(DC)	Var.(GA)	Var.(DC)	Var.(GA)	Var. (DC)
FCR	135.72%	117.90%	149.75%	138.48%	104.20%	123.73%	60.51%	213.86%
FCU	59.28%	98.42%	100.06%	131.07%	132.41%	140.37%	166.97%	132.24%
ECRL	49.32%	111.44%	130.01%	153.34%	111.55%	113.95%	2051.60 %	1796.20%
ECRB	27.82 %	164.67 %	121.74%	150.53%	106.42%	126.64%	146.58%	10.14%
ECU	247.95%	261.04%	129.25%	135.87%	167.47%	133.10%	225.18%	243.52%

Var. = variation. GA = genetic algorithm. DC = direct collocation method.
$F^m_{o,i}$ = maximum isometric force. $l^m_{o,i}$ = optimal muscle fibre length.
$l^t_{o,i}$ = tendon length. $\phi_{o,i}$ = optimal pennation angle.

The variations of the optimized parameters of one representative subjects with respect to the initial value are listed in Table 4.1. The variations of the non-linear shape factor A are 67.825% and 4.21% for GA-based parameters and DC-based parameters respectively. The optimized optimal muscle length, tendon length and pennation angle increase in both approaches, compared with the initial value. The most deviations occur at the pennation angle. However, due to the sensitivity analysis in the previous chapter, the optimal pennation angle has less effects on the muscle-tendon force output. In addition, the muscle-tendon length and optimal muscle fibre length are increased after optimization for both methods, which affect the muscle-tendon force output significantly [135, 136]. The most difference between the two parameter sets is the optimized maximum isometric force of the FCR, FCU and ECRB. In GA-based parameters, these parameters decreased significantly while they are increased when direct collocation method

is used.

4.5.2 Computational performances

Table 4.2: Computation performances (mean) of two difference methods

	time (*second*)	R^2	RMSE(rad)
Genetic algorithm	1697	0.96	0.27
Direct collocation	75	0.93	0.38

Both optimization methods are run several times within the limited maximum number of iterations (iterations = 1000) to calculate the mean optimization time. The best value of the objective function are selected using the same stop criteria (tolerance = $1 \times e^{-4}$). Table 4.2 presents the mean computation time for the genetic algorithm and the direct collocation method. The most prominent difference between the genetic algorithm and the direct collocation method is the computation time, which are 1697 s and 75 s respectively. The optimization time using the direct collocation method is significantly reduced. This is because that the proposed method simultaneously estimates the solution at all node points. Furthermore, the large sparse constraint Jacobian matrix is used, which can be easily computed in the NLP problem [147].

This studies has several limitations: 1) only one optimization technique is compared in this study. We will include more heuristic algorithms for this parameter optimization problem in future. 2) the static parameters are non-zero elements allocated at the end of each row in Jacobian matrix. Further improvement in computational speed may be obtained by treating the muscle-tendon parameters as controls, then these controls are adding into each block. A special constraint is then used to ensure that the control remains constant through the iterations.

4.6 Chapter summary

In this chapter, the direct collocation method is proposed to optimize the subject-specific parameters in the wrist EMG-MS model. After formulating the wrist EMG-MS model into an optimal control problem, a transcription method is used to transcribe it to a non-linear programming problem by discretizing the control variables and state variables into discretized grid. By adding the parameters into the unknown vectors, the subject-specific parameters can be optimized through the IPOPT solver.

The optimized parameters using the direct collocation collocation method are verified through the wrist EMG-MS model and compared to the optimized parameters using the genetic algorithm. Experimental results indicate both methods can estimate the wrist flexion/extension motion with high correlations, but the RMSE is higher when the DC-based parameters are used.

The aim of this chapter is to use the direct collocation method for the reduction of the optimization time for the wrist EMG-MS model. The computational speed is significantly greater than the genetic algorithm, which the optimization time are 1697 s and 75 s for the direct collocation method and the genetic algorithm respectively. This suggests that the direct collocation method has the potential to be utilized in the clinical setting.

Chapter 5

EMG-driven Model-based Control for a Wrist Exoskeleton

This chapter presents the use of the EMG-driven musculoskeletal model to incorporate with the active assistive control strategies. The EMG-driven musculoskeletal model not only estimates the motion intention but also provides the assessment of the joint in real-time that aids the control strategies. Two control strategies are implemented on a wrist exoskeleton that is actuated by pneumatic muscles. It is a wearable exoskeleton to assist the wrist flexion/extension motion. The capability of the EMG-driven musculoskeletal model for joint stiffness estimation is experimentally evaluated with the mean passive and active joint stiffness were 0.78 Nm/rad (Std = 0.55) and 10.53 Nm/rad (std = 3.22) respectively. Both estimated joint stiffnesses are within the range of measurements reported in the literature.

The adaptive cooperative control strategy is first proposed. This control strategy consists of an admittance controller and a position controller in order to modify the reference trajectory based on the joint torque. The admittance parameters are adapted by the estimated joint stiffness. In this manner, the wrist robot is capable to change its compliance and adapt its behaviour to the subject's muscular effort.

Experimental work was conducted on the 12 healthy subjects including three training protocols: Trajectory tracking control (TTC), fixed cooperative control (FCC) with two cooperative ratios, and adaptive cooperative control (ACC) with two cooperative ratios. Results reveal the mean root-mean-square are 0.264 rad, 0.172 rad, and 0.2 rad for TTC, FCC and ACC. It is found that ACC changes the robot's compliance in accordance with the wrist joint impedance, which shows that the proposed control strategy has the potential to enhance the training efficacy and safety of robot-aided wrist rehabilitation.

This chapter also proposes an active assistive control strategy, namely, the assist-as-needed control strategy. In contrast to the ACC, this control strategy does not rely on the reference trajectory. It is an active training strategy that encourages the subjects to actively trace a trajectory. An admittance controller is combined with a low-level force controller to assist the subjects to accomplish the intended movement. The robot's assistance is determined through the kinematic errors and is adapted by the joint impedance property. Experimental evaluation is conducted on ten healthy subjects. Results show that the proposed control strategy could provide assistance by the consideration of the subjects' muscular efforts and wrist joint impedance.

5.1 Introduction

Rehabilitation robots has grown rapidly in the last two decades [34, 53]. Robots hold promising advantages that deliver high-intensive and precise training for stroke patients [23]. It is proven that the active participation can improve the muscle function and neural-motor skills during robot-aided rehabilitation [32]. Estimation of the patient's intention and related control strategies played the important role in interactive training scheme.

Incorporating the EMG signal to estimate the patient's intention has been widely extended into rehabilitation robots [76]. The EMG signal is used to trigger the robot's assistance for the patient when exceeding a certain 'threshold'. For example, Kreb *et al.,* proposed the performance-based impedance control strategy to modulate the robot's assistance according to speed, time and EMG. The EMG signal is used to initiate the game when EMG activation above the threshold [25]. Song *et al.,* used the EMG signal to trigger the assisted torque for the wrist flexion/extension that is proportional to the EMG amplitude [33]. The pattern recognition method is also applied to control a wrist exoskeleton. Khokhar *et al.,* demonstrated the the support vector machine (SVM) classification technique to control a wrist exoskeleton in real-time. However, the pattern recognition only recognize the motion class sequentially. To achieve the smooth control of the rehabilitation robots, it is important to estimate the continuous motion variables [109].

Major attentions of current EMG-based continuous approaches are concerned with regression methods [37]. Regression methods map the EMG signal to the desired intention through the numerical functions, which cannot describe the neural musculoskeletal states during motion tasks [39, 148]. In contrast, the musculoskeletal model is an alternative approach for intension estimation. It explicitly interprets the relationships from the EMG signal to intention by imitating the interactive effects between muscular and skeletal systems [149]. Estimating the underlying musculoskeletal states, i.e., muscle force and joint stiffness, are also available through the model-based approach. These musculoskeletal states benefit the design of control strategies for interactive training.

The impedance control and admittance control are commonly utilized in the wrist rehabilitation robots. The impedance control asks the robots to rend particular mass, spring and damping properties to interact with user's muscular

effort. That is, the inputs of the impedance controller is the motion changes and robot outputs the force/torque [73]. For example, Squeri*et al.,* proposed an impedance controller for a wrist robot [28]. The impedance control scheme increases/decreases the supported torque by the robot as the patient's interactive torque decreases/increases. In this manner, the patient is encouraged to participate in the rehabilitation training. The admittance controller is also utilized in several robots, which outputs the desired position with respect to the interaction force/torque inputs. For instance, Xu *et al.,* proposed the admittance control for a wrist device, which reacquires the desired position during the pre-defined trajectory [5]. It can enhance the training safety and comfort as well as engage the patient's active participation.

The constant parameters impedance/admittance controller may fail to incorporate the variability of the patient, e.g., the joint impedance properties changes across individuals and muscle activities. To overcome this limitations, adaptive methods have been designed in order to continuously challenge and engage the patients to exert their own effort in the robot-aided therapy [150]. It is reported that regulating the controller parameters in response to the stiffness property of the joint can improve the performance of human-robot interaction [110, 151–153]. In specific, the human's limb impedance is continuously modified by the central nervous system according to the task requirement. Although the torque contributions of different muscles may counteract each other, impedance contributions of muscles always add to the joint impedance.

It is a challenging task to estimate the joint stiffness property in real-time [154], as the joint impedance property increased with muscle contraction. Joint impedance property is commonly evaluated through experimental measurements. For example, the passive joint stiffness is estimated by the torque-wrist motion relationship with robot manipulator in a certain RoM [16, 17]. The active stiffness

is measured through keeping wrist stable when the subject holds an end-effector under an external position or torque perturbation [155]. The model-based approach, however, is able to estimate the joint stiffness directly by differentiating the model dynamic equations [156].

The aims of this chapter is to incorporate the EMG-drive musculoskeletal model for the control of a wrist exoskeleton, while the real-time evaluated biomechanical characteristics of wrist joint is utilized to design the adaptation law. Two EMG-driven model-based control strategies, adaptive cooperative control (ACC) strategy and assist-as-needed control (AAN) strategy, are proposed. To the author's best knowledge, the model-based control strategies have not been implemented for real-time control of wrist rehabilitation robots. This chapter is divided into four sections, which are organized in the following. Section 5.2 introduces the wrist exoskeleton, which has one DoF and is actuated by the pneumatic muscles. The mechanical design and sensory system are also discussed. Section 5.3 gives the evaluations of the EMG-driven musculoskeletal model for wrist joint estimation. Section 5.4 details the design of the adaptive cooperative control strategy. Experimental results are discussed accordingly. Section 5.5 discusses the assist-as-needed control strategy with experimental evaluation. The final section gives the chapter summary.

5.2 Wrist exoskeleton

The proposed EMG-driven musculoskeletal model-based control strategies are incorporated with the wrist exoskeleton that is designed to assist wrist flexion/extension. As illustrated in the Figure 5.1, the wrist exoskeleton consists of a customized frame, two Festo pneumatic muscles and sensory system. The Festo Fluidic muscles are used as the antagonistic actuators. Each muscle has the

effective length of 9 cm and the maximum contraction length of 1.8 cm and is connected to a mechanical hinge by a steel wire. Besides, the hinge is secured coaxial with the biological wrist joint to prevent the undesired torque. The steel wires are guided around the cylindrical hinges in the clock/counter-clockwise setup, in which ball bearings are used to reduce the friction in the hinge.

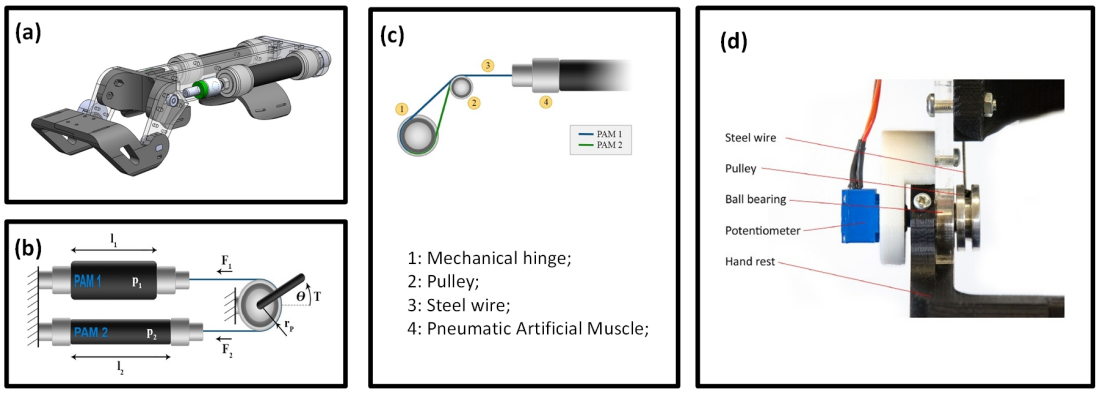

Figure 5.1: Mechanical configuration of the wrist exoskeleton [12]. PAM is the abbreviation of pneumatic artificial muscle. (a) The CAD of the wrist exoskeleton. (b) Force distribution of the pneumatic muscles. (c) The configuration of steel wires enables flexion/extension movement. (d) Placement of the angle sensor.

To set the wrist robot at the neutral position, the wires are under certain tension by pressurizing both muscles. The length of two pneumatic muscle should retain

$$l_1 + l_2 = const \tag{5.1}$$

where l_1 and l_2 represent the length of two pneumatic muscles respectively.
The sensory system is illustrated in Figure 5.2. Two load cells are connected in line with the pneumatic muscles respectively. A potentiometer is utilized as a angle sensor, which is also aligned with rotation centre. Two proportional pressure regulators are used for pressure control of two muscles.

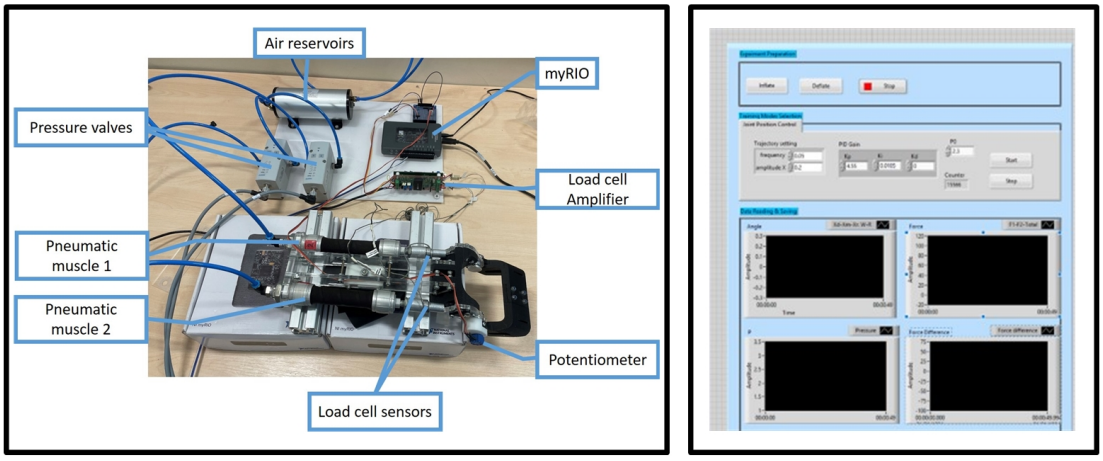

Figure 5.2: (a) The sensory system of the wrist exoskeleton. (b) Control interface in LabView software.

All sensors are communicated with the NI-myRIO contoller. A custom LabVIEW program is designed to process the sensing information and provide the control strategies discussed in the following sections.

5.3 EMG-driven musculoskeletal model-based approach

To incorporate the model-based approach with the active assistive control strategy, the EMG-driven musculoskeletal model is developed to estimate the joint torque and joint stiffness in the wrist flexion/extension motion. The optimized model of each subject is utilized for the proposed control strategies.

5.3.1 Estimation of wrist joint torque

In this section, the EMG-driven musculoskeletal model is utilized to compute the joint torque during the wrist flexion/extension motion, and the physiological parameters are optimized offline using the genetic algorithm. Detailed equations and parameter optimization can be found in section 3.2 and section 3.3 in **Chapter three**, respectively.

5.3.2 Estimation of joint stiffness

The EMG-driven musculoskeletal model is also capable of estimating the joint impedance property, i.e., either passive joint stiffness and active stiffness, in real-time. As the wrist joint stiffness varies upon the passive element of the muscle tissues as well as active muscle activities during motion tasks [13], it is important for control strategies to take account of the joint impedance property. To obtain the joint stiffness K_{joint}, the stiffness of each muscle is first calculated by

$$K_i^{mt} = \frac{(K_i^{CE} + K_i^{PE})K_i^t}{K_i^{CE} + K_i^{PE} + K_i^t} \tag{5.2}$$

where K_i^{mt} indicates the muscle-tendon stiffness. The K_i^{CE}, K_i^{PE} and K_i^t are the stiffness of the contractile element, passive element and tendon element. Similar to the Hill's muscle model, the K_i^{CE} is in parallel with K_i^{PE}, and the K_i^t is connected in series with K_i^{CE} and K_i^{PE}. Inclusion of the elastic tendon (the numerical stiff equation increases the computation burden of the muscle-tendon model, which hurdles the implementation of the EMG-driven model in real-time. The tendon is assumed as the rigid element in this study, due to the ratio of tendon slack length to muscle-fibre length is small in wrist muscles [87]. Therefore, the muscle-tendon stiffness can be re-written as

$$K_i^{mt} = K_i^{CE} + K_i^{PE} \tag{5.3}$$

where

$$K_i^{CE} = \frac{\gamma a_i(t) F_{o,i}^m f_a(\bar{l}_{i,a}^m)}{l_{o,i}^m} \tag{5.4}$$

where γ is set to 23.4 [157]. The K_i^{PE} is calculated by the slope of the passive force-length relationship to account for the muscle fibre stiffness in absence of the muscle activation $a_i(t)$ [156]. In specific, the K_i^{PE} is obtained through

$$K_i^{PE} = \begin{cases} 0.0751 F_{o,i}^m & \bar{l}_i^m < 1 \\ 6.32 F_{o,i}^m & \bar{l}_i^m \geq 1 \end{cases} \tag{5.5}$$

Thus, the wrist joint stiffness K_{joint} is obtained by [156]

$$K_{joint} = \sum_{i=1}^{5} (r_i^2 K_i^{mt} + \frac{\partial r_i}{\partial \theta} F_i^{mt}) \tag{5.6}$$

5.3.3 Data collection for joint stiffness estimation

The date collection section is conduced to optimize the physiological parameters for each subject. Although the estimation performance is already proved by the previous chapters, The joint stiffness estimation is not yet evaluated. The feasibility of the model-based joint is also evaluated, which is compared with the measurements from the literature.

Twelve healthy subjects (age between 27 and 30) are participated into this data collection section. Prior to the experiment, participation consent forms are signed by all subjects. This experiment is approved by the MaPS and Engineering Joint Faculty Research Ethics Committee of the University of Leeds (MEEC 18-002). To measure the EMG signal, electrodes (Delsys quattor sensor) are attached over four wrist muscles, including Flexor Carpi Radialis (FCR), Flexor Carpi Ulnaris (FCU), Extensor Carpi Radialis(ECR), Extensor Carpi Ulnaris (ECU). The raw EMG signal of ECR is assigned to the Extensor Carpi Radialis longus (ECRL) and Extensor Carpi Radialis Brevis (ECRB), as these two muscles are closely

adjacent [106]. The placement of electrodes are first based on the palpation. The qualities of signal are then evaluated through the Delsys data acquisition software. The sample frequency is 2000 Hz.

To record the motion data, two inertia measure units (IMUs) are attached at the third metacarpal bones and back of the forearm respectively. The sample frequency is 256 Hz. A Kalman filter is used to computed the wrist flexion/extension angle.

Before the experiment, subject are asked to perform the maximum voluntary contractions (MVCs) for muscle activation normalization. Then subject are asked to perform the continuous wrist flexion/extension motion for parameter optimization. Each motion trial lasts 15 seconds and 3 trials are recorded. 5 minutes interval are given between trials to avoid the muscle fatigue. Since IMUs are sampled at 256 Hz, all sensors are resampled and synchronized at 1000 Hz for data processing.

5.3.4 Evaluation of joint stiffness

The estimation performance of the EMG-driven musculoskeletal model has been previous evaluated. After the optimization, the R^2 across all subjects is range from 0.75 to 0.9. All optimized parameters and MVCs are stored for further implementation in active assistive control strategies. One representative example is illustrated in Figure 5.3.

After optimization, the joint stiffness is calculated based on equation (5.6). The passive and active stiffness are evaluated by comparing with measurements in the literature respectively. The passive joint stiffness is simulated at the zero muscle activation level ($a_i(t) = 0$) and neutral position ($\theta_m = 0$). The active joint stiffness is emulated at the neutral position ($\theta_m = 0$) while the flexor are activated around 15% MVC ($a_{1,2}(t) = 0.15$), as reported in [155, 158]

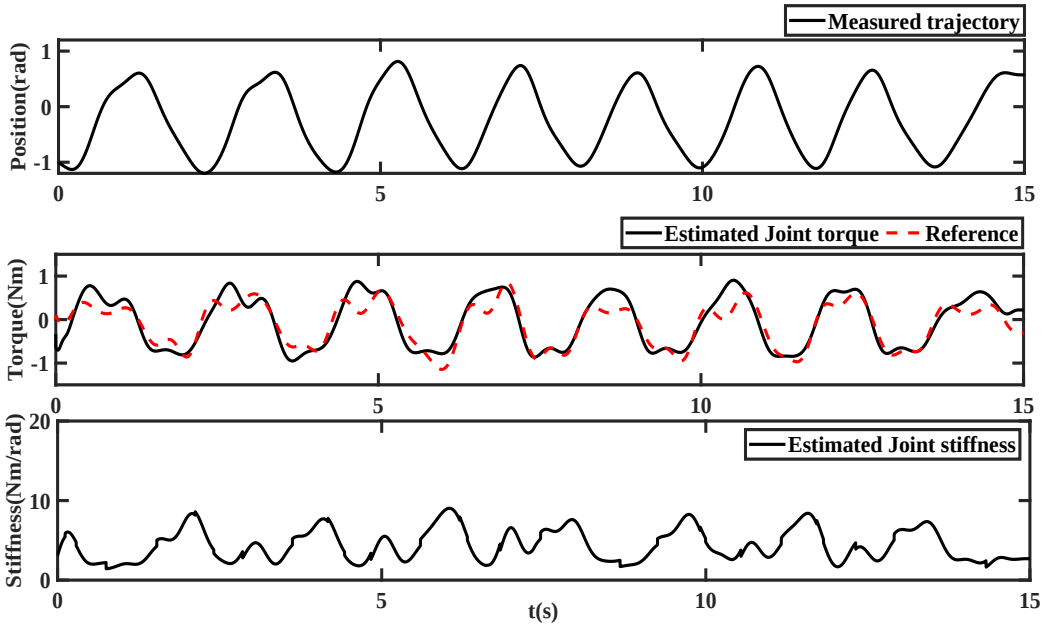

Figure 5.3: Representative subject of estimated joint torque and joint stiffness using the optimized muscle-tendon parameters.

The results of the estimated passive and active joint stiffness across all subjects are presented in Table 5.1. The passive joint stiffness has a range from 0.21 Nm/rad to 2.22 Nm/rad, while the active joint stiffness has a range from 7.45 Nm/rad to 16.48 Nm/rad. The mean passive and active joint stiffness are 0.78 Nm/rad (Std = 0.55) and 10.53 Nm/rad (std = 3.22) respectively. Figure 5.4 elucidates the comparison of the passive joint stiffness with measurements in the literature. Table 5.2 gives the comparison between the model estimation and reported mean value under the same condition which wrist joint is at neutral position and flexors are activated around 15% MVC. Results yield that the model estimation has the similar value compared with [158], but slightly larger than [155].

Table 5.1: Results of joint stiffness estimation across all subjects.

	Subject Index							
	S1	S2	S3	S4	S5	S6		
Passive stiffness (Nm/rad)	0.81	0.43	0.41	0.19	0.21	0.55		
Active stiffness (Nm/rad)	14.31	7.27	11.44	7.45	10.07	9.14		
	Subject Index							
	S7	S8	S9	S10	S11	S12	Mean	Std.
Passive stiffness (Nm/rad)	1.17	2.22	0.83	0.64	0.83	1.06	0.78	0.55
Active stiffness (Nm/rad)	9.56	16.48	6.30	10.51	8.86	14.94	10.53	3.22

* Active stiffness is calculated at neutral position with flexor activation of 15% MVC.

* Std. = standard deviation.

Table 5.2: Comparison of active joint stiffness with literature

Study	Contraction	Position	Active stiffness (Nm/rad)	Model estimation (Nm/rad)
Halaki *et al.*, [158]	Flexor (15%MVC)	Neutral	10.5 ± 0.4	10.53 ± 3.22
Milner *et al.*, [155]	Flexor (15%MVC)	Neutral	9.22± 6.60	10.53 ± 3.22

5.3.5 Discussion

Wrist joint stiffness play an important role in motion and postural control [159]. In this section, the passive and active joint stiffness are derived through the EMG-driven musculoskeletal model. To evaluate the estimated joint stiffness, the joint stiffness found in the literature are used for comparison, which are measured experimentally with the aid of rigid manipulators. In specific, the passive joint

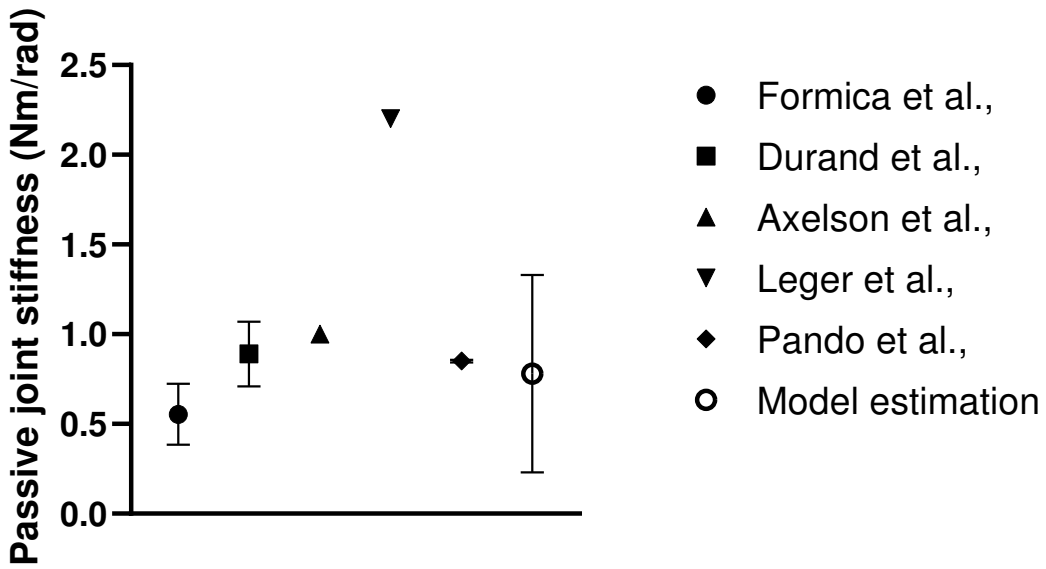

Figure 5.4: Comparison of the estimated passive stiffness with measurements in the literature. Prior measurements has the range from 0.554 Nm/rad in [13], 0.89 Nm/rad (Std. = 0.18) in [14], 0.554 Nm/rad in [15], 2.2 Nm/rad in [16] and 0.85 Nm/rad (Std. = 0.007) in [17].

stiffness is determined by the passive torque-angle curve, i.e., the wrist joint is passively driven from neutral position to the certain RoMs. Likewise, the active joint stiffness is determined by the external perturbation, i.e., the position perturbations are applied to wrist joint while the subject maintains a constant level of torque or EMG Level [160]. The regression algorithms are used to obtain either passive or active joint stiffness.

For the passive stiffness, the model estimated has the mean value of 0.78 Nm/rad (Std. = 0.55). Prior studies reported the passive stiffness in wrist flexion/extension range from 0.554 Nm/rad (toward flexion) and 1.021 Nm/rad (toward extension) in [13], 0.89 Nm/rad (Std. = 0.18) in [14], 0.554 Nm/rad in [15], 2.2 Nm/rad in [16] and 0.85 Nm/rad (Std. = 0.007) in [17]. The model estimated passive

joint stiffness in this study is within the middle range of reported value from prior measurement.

Likewise, the active stiffness is compared with two studies. In [155, 158], the EMG signal are measured during the perturbation, while subjects sustain 15% MVC of flexors. The mean estimated active joint stiffness is 10.53 Nm/rad (Std. = 3.22), which falls into the middle range of the experimental measurements from the literature(10.53 Nm/rad (Std. = 0.4) and 9.22 Nm/rad (Std. = 6.6) respectively). The age group reported in the literature, either passive or active, covers the age group tested in this study. The results reveal that the EMG-driven musculoskeletal model has the capability to interpret the wrist joint stiffness property after optimization. In addition, the use of the EMG-driven musculoskeletal model allows for the real-time computation of the joint stiffness.

It is worthy to notice that the optimized trial for each subject does not exceed the limits of the wrist's RoMs, in which passive stiffness is mainly charactered by the stretch of muscle tissues. The passive stiffness has a distinctive difference if encounters the limits of the wrist's RoMs, which increases significantly due to the stretch of ligaments [155]. The active joint stiffness is dominated by the muscle contraction. This study emulates the active stiffness at the neutral position. The active stiffness varies over the wrist's RoM, as show in Figure 5.3. This can be explained by the active force-length curve in response to the variability of the muscle fibre length during motion tasks. The muscle activation levels also contribute to the active joint stiffness, which is caused by the increases/decreases in the number of cross bridges [161].

The joint stiffness varies across the subjects, range from 0.21 Nm/rad to 2.22 Nm/rad and 7.45 Nm/rad to 16.48 Nm/rad for passive stiffness and active stiffness respectively. The variabilities may caused by muscle conditions that affect the muscle-tendon force generating properties, such as the physiological cross-sectional area.

In the EMG-driven musculoskeletal model, these properties are represented by the optimized parameters, such as the maximum isometric force.

The joint stiffness is a significant factor for the assessment of the patients after stroke. One of the most prevalent symptoms and a key source of impairment is the increased joint stiffness [13]. This is may due to the alteration of the intrinsic muscle properties, resulting in the abnormal joint stiffness [162]. The methods used to evaluate subject's joint stiffness provide vital information during robot-aided therapy. In other word, the estimated joint stiffness not only can be used to facilitate the clinical assessment of impairment and the evaluation of therapeutic efficacy, but also can be conducive to design of the active assistive control strategy. For example, the robot's behaviour can be modified in response to the wrist joint stiffness during rehabilitation. The regression algorithms used in the prior studies are difficult for real-time implementation. Additional efforts are needed to establish the relationship between the stiffness, joint position, and muscle activation level. In contrast, the joint stiffness can be estimated in real-time without additional computational cost.

This section presents the parameters optimization of each subject as the preparation for the control strategy. The use of the EMG-driven musculoskeletal model for wrist joint stiffness estimation is also evaluated and discussed. Therefore, the following sections implement the EMG-driven musculoskeletal model into the design of the active assistive control strategies, with respect to the participant's voluntary effort and the real-time assessment of the joint stiffness.

5.4 Adaptive cooperative control strategy

One of the active assistive control strategies, namely, adaptive cooperative control strategy (ACC) is proposed in this section, which aims to improve the training

effectiveness and safety [112, 163]. In the proposed control strategy, the robot is capable to adapt its behaviour through accommodating the subject's voluntary effort. The wrist exoskeleton re-acquires the trajectory during the rehabilitation training exercise. The controller parameters are adapted according to the joint stiffness property in order to improve the performance of human-robot interaction [152].

5.4.1 Control strategy

This control strategy consists of a PID-based position controller and an admittance controller. The position controller is used to ensure the tracking performance when tracking a reference trajectory. The admittance controller is implemented to modify the reference trajectory based on the subject's muscular effort. To guarantee the patient's safety during rehabilitation exercise, the wrist exoskeleton should provide adjustable compliance by changing the parameters of the admittance controller [112]. This is achieved by regulating the admittance parameter is response to the variation of the joint stiffness K_{joint} (equation (5.6)). The estimated joint torque and joint stiffness property are accessed through EMG-driven musculoskeletal model-based approach in real-time.

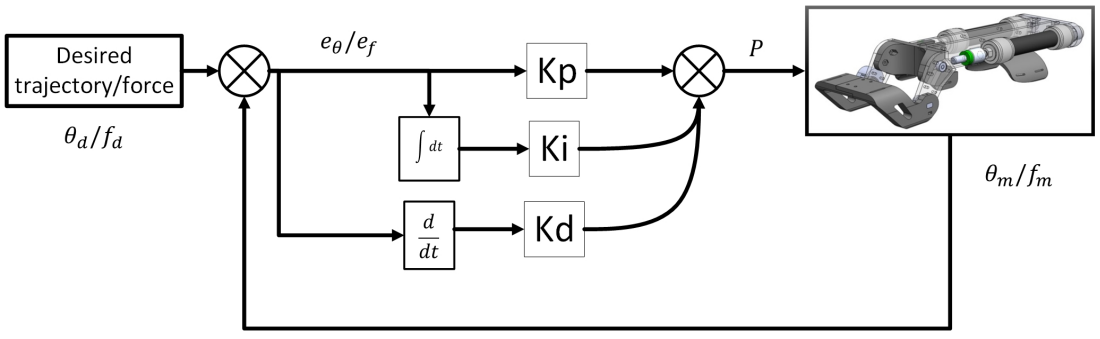

Figure 5.5: The block diagram of the PID controllers for trajectory tracking control and force control.

Trajectory tracking control is commonly implemented to delivery the passive training for the stroke patients, which guides the patient's wrist following the reference trajectory [61, 70, 164]. The reference trajectory can be determined from the RoMs of the healthy subject.

As illustrated in Figure 5.5, the trajectory tracking control is achieved through a PID controller, which is utilized to control the pressure of each pneumatic muscle. The mathematical form is written as

$$e_\theta(t) = \theta_d(t) - \theta_m(t) \tag{5.7}$$

$$P_{2\times1}(t) = K_{tp}e_\theta(t) + K_{ti}\int_0^t e_\theta(t)dt + K_{te}\frac{de_\theta(t)}{dt} \tag{5.8}$$

where θ_d and θ_m are the desired angle and measured angle respectively. The parameters K_{tp}, K_{ti} and K_{td} are well-tuned to minimize the tracking errors (K_{tp} = 4.65; K_{ti} = 0.0075; K_{td} = 0.00225). $P_{2\times1}$ is the desired pressures for two PAMs respectively. The result of the trajectory tracking control is shown in Figure 5.6. The reference trajectory is set with the amplitude of 0.25 rad and frequency of 0.05 Hz. The max error is 10% and root-mean-square error is 0.0129 rad.

To achieve the cooperative control strategy, an admittance controller is utilized to determine the deviation of the trajectory in response to estimated joint torque $\hat{\tau}$. The wrist exoskeleton deviates the reference trajectory whenever the motion intention is detected, otherwise it continue to follow the reference trajectory. In this study, the joint position and joint torque is defined as positive when wrist is flexed. The transfer function of the admittance controller is written as

$$\theta_d(s) = \theta_r(s) + \frac{C_r\hat{T}(s)}{Ms^2 + Bs + K} \tag{5.9}$$

where θ_d and θ_r are the desired trajectory and reference trajectory respectively. C_r is the cooperative ratio. $T(s)$ is the joint torque obtained from the EMG-driven musculoskeletal model. The M, B and K are the mass, damping and stiffness

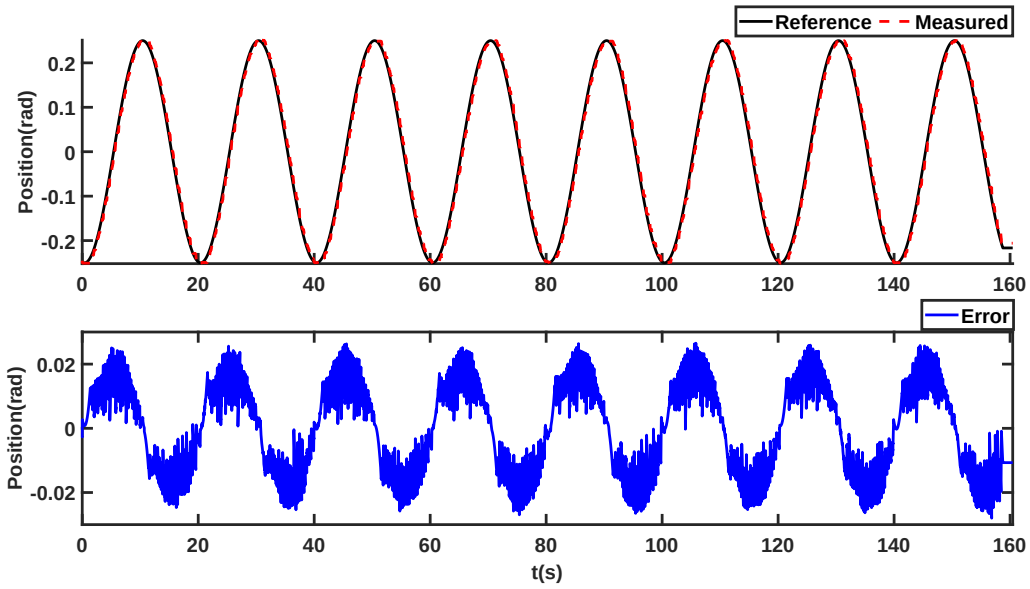

Figure 5.6: Tracking performance of the trajectory tracing control. The predefined trajectory is set as an amplitude of 0.25 rad with the frequency 0.05 Hz.

parameters of the admittance controller. In this manner, the estimated joint torque by the EMG-driven musculoskeletal model is the input to the admittance controller, the admittance controller outputs the deviation of the trajectory which is added to the reference trajectory. The estimated joint stiffness is used to modify the damping and stiffness parameters of the admittance controller. During the training protocols, the PID controller is used to minimize the tracking errors. Figure 5.7 gives the block diagram of the proposed control strategies.

To adjust the compliance of the wrist exoskeleton, an adaptation method is derived based on the estimated joint stiffness K_{joint} (equation 5.6). The stiffness parameter K of the admittance filter is linearly adapted by

$$K = K^{max} - (K^{max} - K^{min})\frac{K_{joint} - K_{joint}^{min}}{K_{joint}^{max} - K_{joint}^{min}} \tag{5.10}$$

The damping parameter B is a function of stiffness parameter, which is determ-

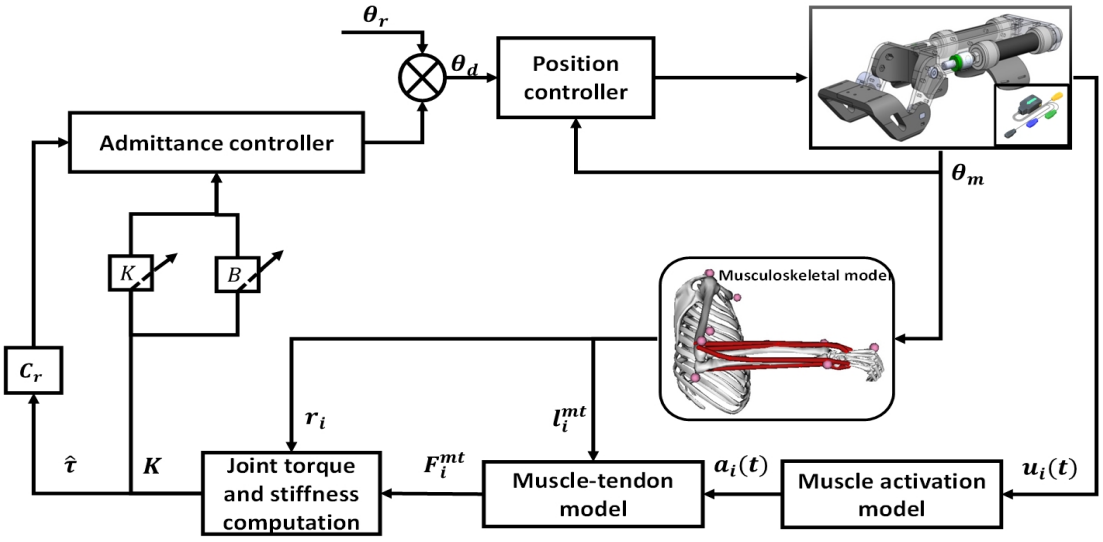

Figure 5.7: The block diagram of the control system in the wrist exoskeleton.

ined by [153]

$$B = 0.2\sqrt{K} \tag{5.11}$$

The K^{max} and K^{min} are determined by trial and errors. To limit the stiffness parameter and avoid the instability of the control system and enhance safety, a saturation function is implemented in the LabView program.

5.4.2 Experiment protocol

Twelve subjects (S1-S12) (same subjects in the 5.3.3) are participated in this test in the lab environment. All subjects have no reported wrist muscular disorders and can perform the wrist flexion/extension in full RoMs. Before the experiment, the subject is guided to set on the chair and wear the wrist exoskeleton comfortably. The arm is supported by two customized arm holders to minimize the gravitational effect.

The placement of the electrode is the same in section 5.3.3, as shown in Figure 5.8.

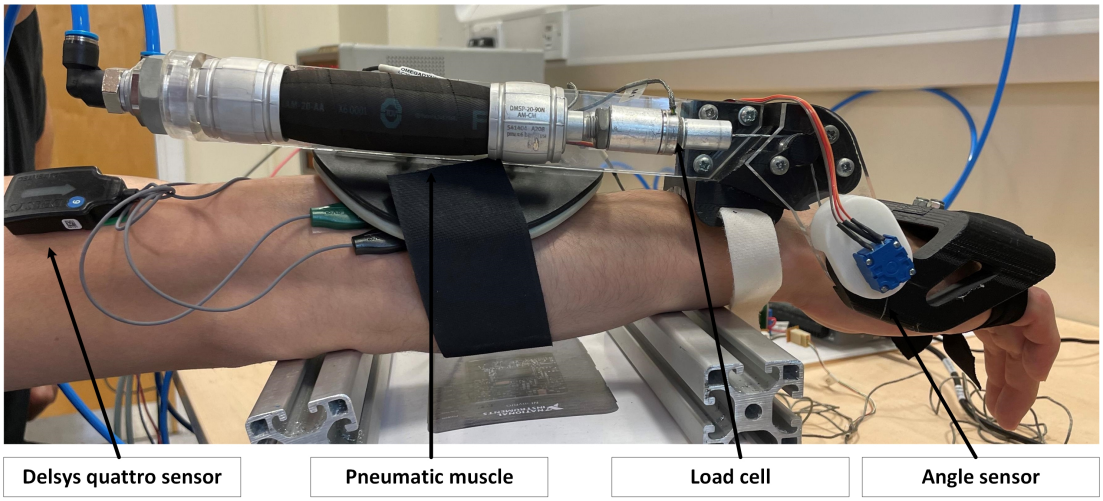

Figure 5.8: Experiment setup. The wrist exoskeleton guides the subject's wrist following the predefined trajectory. The sEMG signal is recorded from the primary wrist muscles.

The quality of the EMG signals is evaluated using the customized LabView program. Besides, all sensor data are synchronized at 200 Hz and stored in the customized LabVIEW program for offline analysis.
In this study, three training protocols, namely, trajectory tracking control (TTC), fixed cooperative control (FCC), and adaptive cooperative control (ACC) are implemented. For FCC and ACC, two different cooperative ratios are utilized to evaluate the performance. In specific, each training protocol is defined as,

1) The first training protocol (TTC) is conducted without the cooperative control strategy ($C_r = 0$). T the parameters of the PID controller are same as in section 5.4.1. The joint torque $\hat{\tau}$ and muscle activation levels $a_i(t)$ are monitored at the same time.

2) The second protocol (FCC) is conducted with the fixed admittance parameters, of which the M, K and B are set to 0.15, 10 and 0.63. Two cooperative ratio ($C_r = 0.3, 0.6$) are used in FCC. In this experiment, the desired traject-

ory is determined by the estimated joint torque solely.

3) The third protocol (ACC) is conduced with the proposed adaptive control strategy. Two cooperative ratio ($C_r = 0.3, 0.6$) are also utilized in the ACC. In this experiment, reference trajectory and wrist robot's compliance are regulated according to the estimated joint torque and joint stiffness.

During experiments, subjects are not required to be passive during experiment. Instead, subjects are encouraged the involve their voluntary effort. The reference trajectory for all experiment is set as a sine-wave with the amplitude of of 0.25 rad and frequency of 0.05 Hz. In addition, the deviation is limited between ± 0.45 rad, which is close to the maximum ROM of wrist robot exoskeleton. Each protocol contains three trials and each trial lasts 60s. Five-minute break are given between trials to prevent muscle fatigue.

5.4.3 Statistical analysis

Three performance indexes are utilized to evaluate the performance of three training protocols including root-mean-square-error (RMSE), root-mean-square of estimated joint torque (RMS_τ), and root-mean-square of the deviation ($\mathrm{RMS}_{\mathrm{dev}}$). The RMSE between the desired trajectory (reference trajectory for TTC) and measured trajectory is calculated to evaluate the tracking performance.
To evaluate the performance of the proposed adaptive cooperative control strategies, the ratio of the RMS_τ and $\mathrm{RMS}_{\mathrm{dev}}$ is computed.

$$r_{td} = \mathrm{RMS}_\tau / \mathrm{RMS}_{\mathrm{dev}} \tag{5.12}$$

where the large value indicates the wrist exoskeleton modifies the trajectory slightly in response to muscular efforts. The small value means the wrist exoskel-

eton gives more RoMs when the subject's muscular effort is detected.

$$\mathrm{RMSE} = \sqrt{\sum_{n=1}^{N}(\theta_d - \theta_m)} \tag{5.13}$$

$$\mathrm{RMS}_\tau = \sqrt{\sum_{n=1}^{N}\hat{\tau}} \tag{5.14}$$

$$\mathrm{RMS}_{\mathrm{dev}} = \sqrt{\sum_{n=1}^{N}(\theta_d - \theta_r)} \tag{5.15}$$

Separate one-way analysis of variance (ANOVAs) are for each experiment. RMSE is used as the response variable. Furthermore, a *post-hoc* analysis using Tukey's Honest Significant Difference test is applied when there is a significant difference between control strategies. The significance level is set at $p < 0.05$.

5.4.4 Results

Figure 5.9 gives a representative example of TTC, along with the estimated joint torque and muscle activation. The black solid line indicates the reference trajectory and the red dotted line is the measured trajectory, of which the RMSE is 0.0209 rad and RMS_τ is 0.552 Nm. The result shows that the measured trajectory deviates significantly when the subject's intention is presented, e.g., at 10 second.

The representative examples of tracking response for the second experiment (FCC) are shown in Figure 5.10 and Figure 5.11. The green line represents the desired trajectory which is generated according to the estimated joint torque. For the FCC with 0.3 C_r, the RMSE between the desired trajectory and measured trajectory is 0.016 rad. The RMS_τ and $\mathrm{RMS}_{\mathrm{dev}}$ are 0.401 Nm and 0.012 rad, respectively. For the FCC with 0.6 C_r, the RMSE, RMS_τ and RMSdev are 0.0146 rad, 0.319 Nm, and 0.0191 rad.

In FCC, the deviation of the reference trajectory is in line with the estimated joint

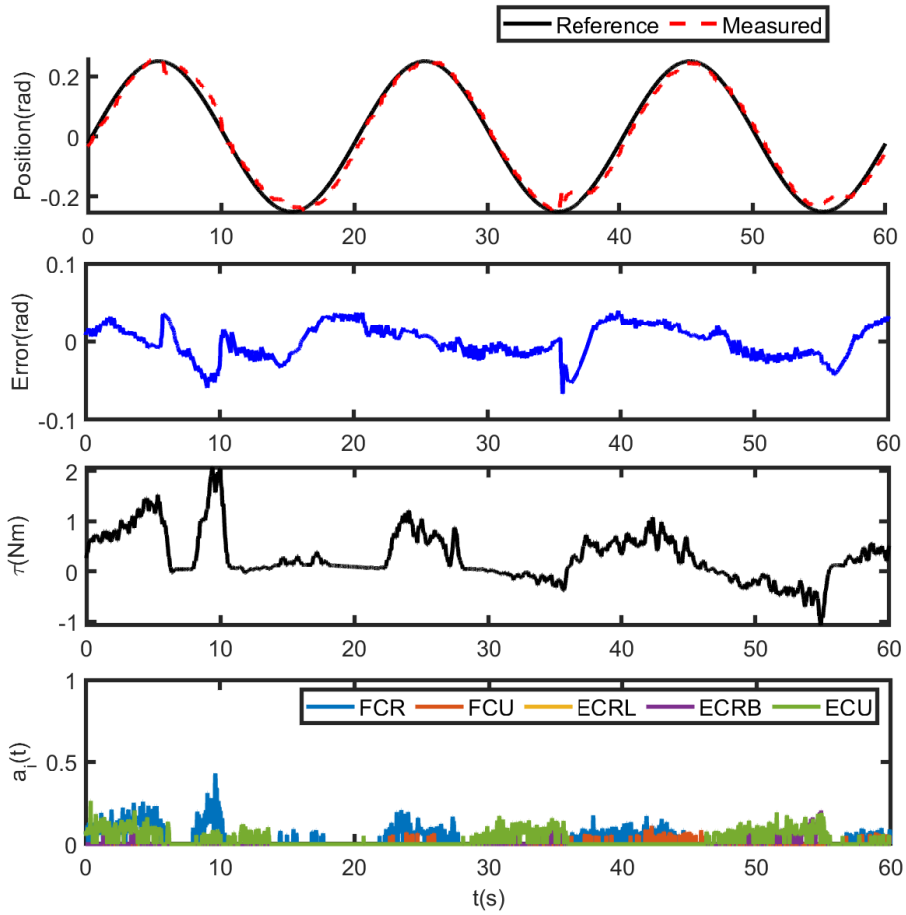

Figure 5.9: Representative example of the first training protocol (TTC) with consideration of subject's participation. The RMSE and RMS_τ are 0.0209 rad and 0.552 Nm respectively.

torque. For instance, in Figure 5.10, in the span of 20 seconds and 30 seconds, the wrist exoskeleton gives more RoM toward wrist flexion when the joint torque is positive. The robot reduces the RoM in the extension as the joint torque is positive between 10 seconds and 20 seconds. A larger deviation is found when the larger cooperative ratio is applied.

Figure 5.12 and Figure 5.13 illustrate the tracking performance of the ACC with two different cooperative ratios in a representative subject. The RMSE

are 0.0174 rad and 0.0268 rad when the cooperative ratio is set to 0.3 and 0.6 respectively. The real-time adaptation of admittance parameters is also presented in figures. In the third training protocol, stiffness and damping parameters increase as muscular efforts decrease while parameters decrease as muscular efforts increase. These parameters are also affected by the joint position. As such, the robot becomes more compliant and allows the subject to change the trajectory significantly. For instance, at 10 seconds of Figure 5.12, the reference trajectory deviates more in flexion when the admittance parameters are small. In Figure 5.13, the wrist exoskeleton reaches the limited deviation when the stiffness and damping parameters are small while large muscular efforts are detected, during 20 to 30 seconds.

Statistical results

Each experiment contains 36 trials ($n = 36$) for statistical analysis. Two-way ANOVAs analysis results that both factors has significant effects ($p = 0.014$), of which adaptation has more significant effect than the cooperative ratio ($p < 0.001$ versus $p = 0.019$).

Figure 5.14 illustrates the results of each experiment. The mean RMSE of TTC is 0.0264 rad (std = 0.008). The *post-hoc* tests show that TTC is significantly different from other experiments($p < 0.001$).

The mean RMSE are 0.0172 rad (std = 0.002) and 0.0171 rad (std = 0.002) for FCC with 0.3 C_r and 0.6 C_r respectively. The mean RMSE are 0.0186 rad (std = 0.002) and 0.214 rad (std = 0.006) for ACC with 0.3 C_r and 0.6 C_r respectively. The mean RMSE significantly decreases when the cooperative control strategies are applied. Small RMSEs are found in FCC with two different cooperative ratios are applied. However, no significant difference is found between FCC with two different cooperative ratios ($p = 1$). The ACC with 0.3 C_r is not significant

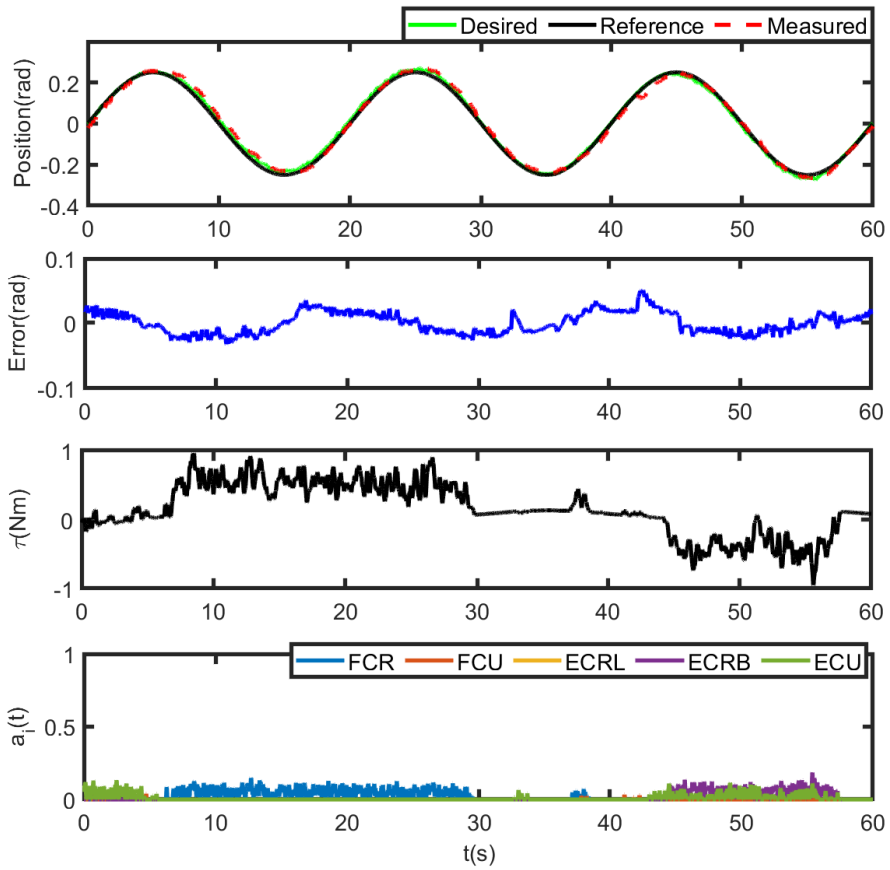

Figure 5.10: Tracking performance of one representative example of FCC (0.3 C_r). The RMSE is 0.016 rad. RMS_τ and RMS_{dev} are 0.401 Nm and 0.012 rad respectively.

different to ACC with 0.6 C_r ($p = 0.104$), and is not significant different to the FCC with 0.3 C_r ($p = 0.718$). However, there is a significant difference between ACC with 0.6 C_r and FCC with 0.6 C_r ($p = 0.002$).

The ratio of the RMS_τ and RMS_{dev} is calculated for fixed cooperative control and adaptive cooperative control respectively. The FCC with 0.3 C_r has the largest r_{td} among all protocols (32.87). The ACC with 0.3 C_r also have a large r_{td} (25.093), but smaller than the FCC with 0.3 C_r. In addition, the smallest r_{td}

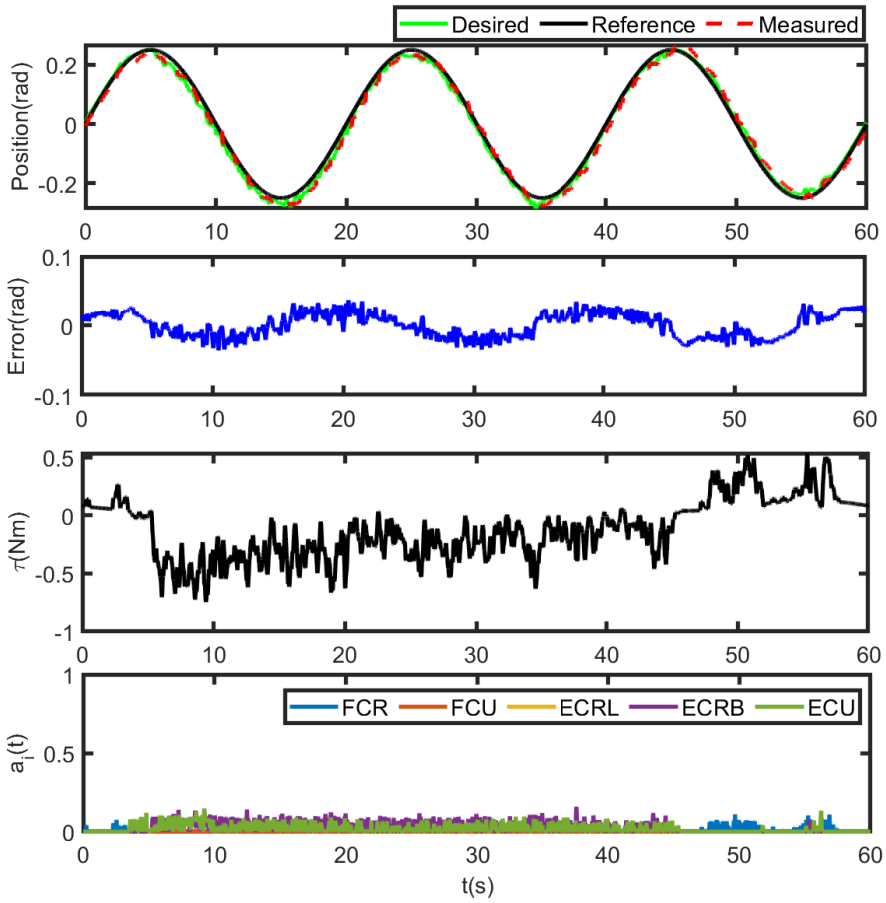

Figure 5.11: Tracking performance of one representative example of FCC (0.6 C_r). The RMSE, RMS_τ and RMS_{dev} are 0.0146 rad, 0.319 Nm, and 0.0191 rad.

is found in ACC with 0.6 C_r (11.59), compared with FCC with 0.6 C_r (16.435). This indicates the wrist exoskeleton become more compliant for subjects by the consideration of the wrist joint impedance.

5.4.5 Discussion

This section proposed the adaptive model-based control strategy to improve training effectiveness and safety. During the repetitive motion exercise, the EMG-

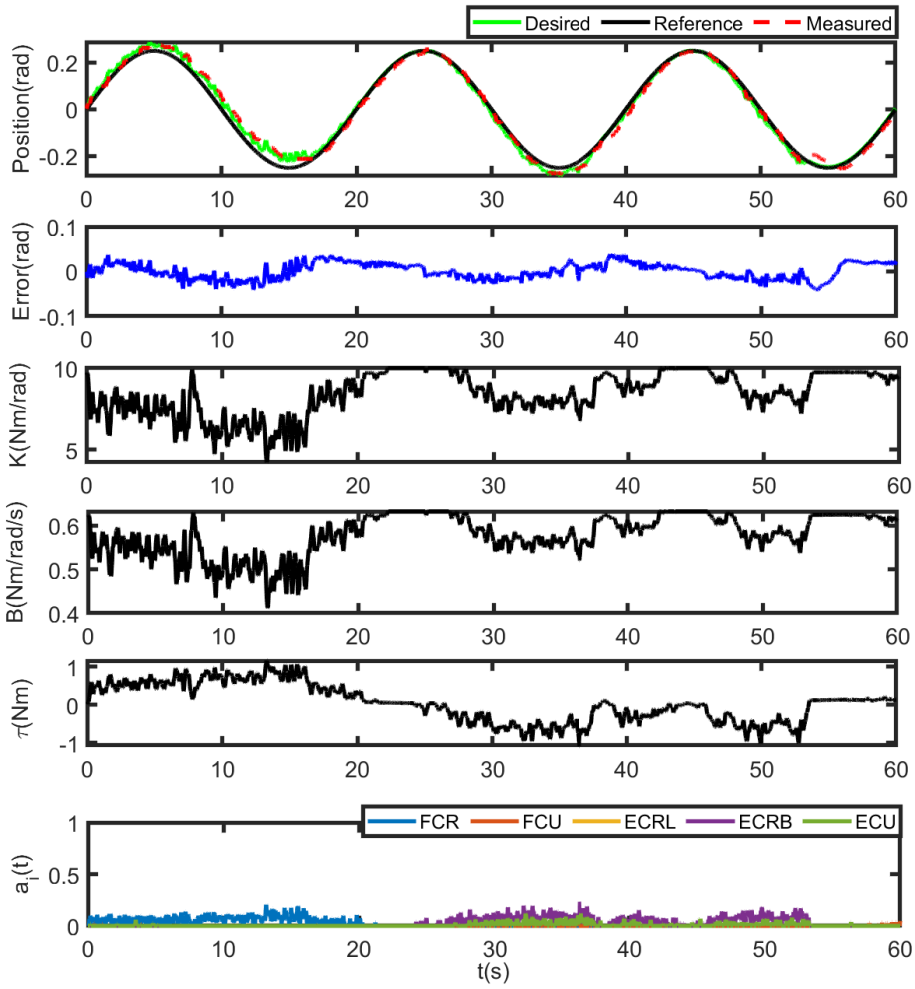

Figure 5.12: Tracking performance of one representative example of ACC (0.3 C_r). The RMSE is 0.0174 rad. RMS_τ and RMS_{dev} are 0.494 Nm and 0.022 rad respectively.

driven musculoskeletal model is used to continuously evaluate the subject's motion intention as well as the wrist joint biomechanical characteristics. The wrist exoskeleton is under a passive mode if there is no active torque and switch to ACC when the muscular effort is detected. Results reveal that the robot is capable of modifying the trajectory to accommodate the subject's intention. An adaptation

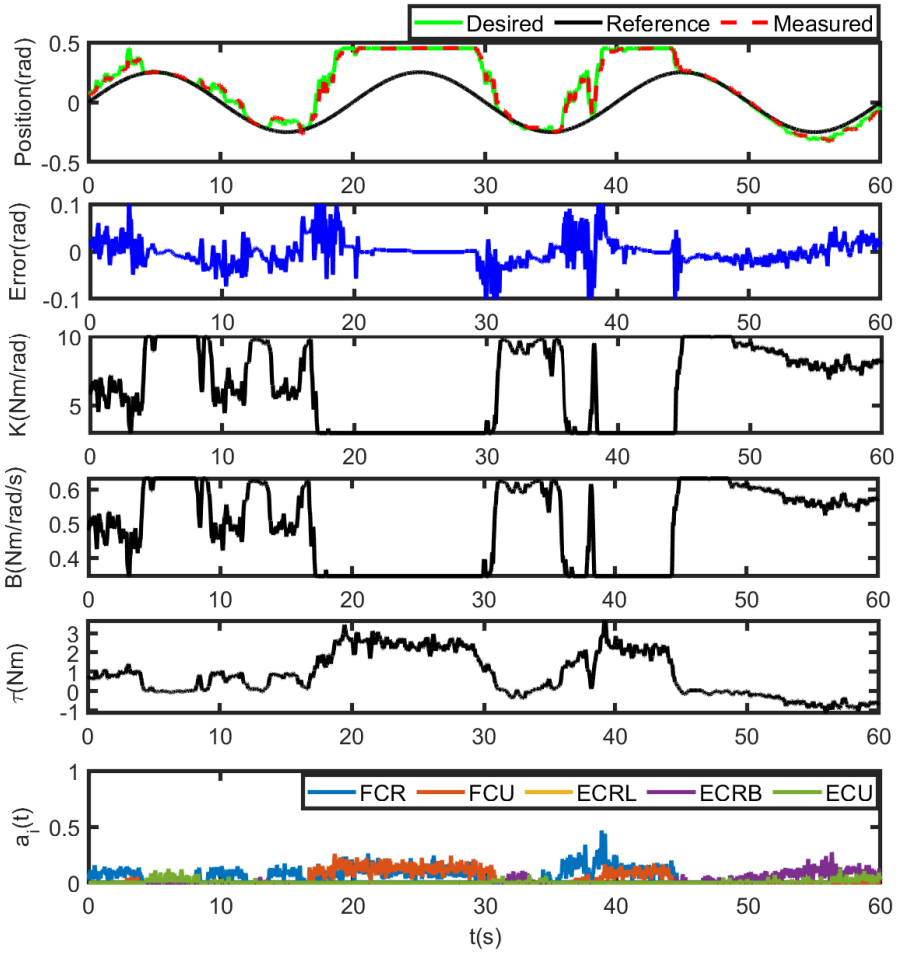

Figure 5.13: Tracking performance of one representative example of ACC (0.6 C_r). The RMSE is 0.0268 rad. RMS_τ and RMS_{dev} are 1.404 Nm and 0.2 rad respectively. In this trial, RoM's limitation is reached to ensure the training safety.

law is proposed to change the robot's compliance to ensure training safety. Experimental work is conducted with three different training protocols and different cooperative ratios. The performance of the proposed adaptive cooperative control strategy is evaluated and compared with TTC and FCC through the RMSE and the ratio of RMS_τ and RMS_{dev}.

Table 5.3: Results of TTC across subjects.

	Subject Index							
	S1	S2	S3	S4	S5	S6		
RMSE(rad)	0.0225	0.0355	0.0264	0.0327	0.0282	0.02		
rms_τ (Nm)	0.505	0.515	0.382	0.274	0.145	0.137		
	Subject Index							
	S7	S8	S9	S10	S11	S12	Mean	Std.
RMSE(rad)	0.0254	0.0245	0.021	0.020	0.0328	0.0263	0.0264	0.008
rms_τ(Nm)	0.165	0.429	0.368	0.312	0.355	0.278	0.317	0.18

Std. = standard deviation.

Table 5.4: Results of FCC ($C_r = 0.3$) across subjects.

	Subject Index							
	S1	S2	S3	S4	S5	S6		
RMSE(rad)	0.0162	0.0146	0.0204	0.0163	0.0164	0.0162		
rms_τ(Nm)	0.375	0.527	0.1524	0.169	0.34	0.278		
rms_{dev}(rad)	0.0112	0.0157	0.0046	0.005	0.0102	0.0083		
	Subject Index							
	S7	S8	S9	S10	S11	S12	Mean	Std.
RMSE(rad)	0.0195	0.0186	0.0189	0.016	0.0155	0.0178	0.0172	0.002
rms_τ (Nm)	0.144	0.5441	0.5693	0.379	0.235	0.7883	0.3828	0.2
rms_{dev} (rad)	0.0043	0.0167	0.017	0.011	0.0071	0.028	0.0119	0.007

Std. = standard deviation.

Figure 5.14 (a) gives the mean RMSE of each protocol. The mean RMSE of TTC is significantly greater than other experiments when the subject actively

Table 5.5: Results of FCC ($C_r = 0.6$) across subjects.

	Subject Index							
	S1	S2	S3	S4	S5	S6		
RMSE(rad)	0.0172	0.0167	0.0207	0.0173	0.0163	0.0159		
rms_{τ}(Nm)	0.4	0.4345	0.223	0.302	0.247	0.287		
rms_{dev}(rad)	0.024	0.026	0.013	0.018	0.015	0.0172		
	Subject Index							
	S7	S8	S9	S10	S11	S12	Mean	Std.
RMSE(rad)	0.0198	0.018	0.0159	0.0144	0.0158	0.0178	0.0171	0.002
rms_{τ} (Nm)	0.207	0.43	0.423	0.33	0.232	0.721	0.353	0.15
rms_{dev} (rad)	0.0124	0.0259	0.0253	0.02	0.014	0.052	0.0219	0.011

Std. = standard deviation.

Table 5.6: Results of ACC ($C_r = 0.3$) across subjects.

	Subject Index							
	S1	S2	S3	S4	S5	S6		
RMSE(rad)	0.016	0.0169	0.0211	0.0178	0.0204	0.02		
rms_{τ}(Nm)	0.538	0.323	0.308	0.167	0.406	0.37		
rms_{dev}(rad)	0.021	0.0138	0.0106	0.005	0.0144	0.0216		
	Subject Index							
	S7	S8	S9	S10	S11	S12	Mean	Std.
RMSE(rad)	0.0229	0.0204	0.0155	0.0174	0.0199	0.0156	0.0186	0.003
rms_{τ} (Nm)	0.326	0.6225	0.446	0.451	0.2703	0.5566	0.3923	0.15
rms_{dev} (rad)	0.0131	0.023	0.015	0.026	0.016	0.026	0.0168	0.008

Std. = standard deviation.

Table 5.7: Results of ACC ($C_r = 0.6$) across subjects.

	Subject Index							
	S1	S2	S3	S4	S5	S6		
RMSE(rad)	0.022	0.018	0.0196	0.0196	0.0208	0.023		
rms_{τ}(Nm)	0.604	0.420	0.295	0.323	0.475	0.285		
rms_{dev}(rad)	0.063	0.036	0.02	0.027	0.035	0.032		
	Subject Index							
	S7	S8	S9	S10	S11	S12	Mean	Std.
RMSE(rad)	0.030	0.024	0.015	0.030	0.022	0.014	0.0214	0.006
rms_{τ} (Nm)	0.392	0.66	0.357	0.652	0.317	0.39	0.431	0.16
rms_{dev} (rad)	0.031	0.052	0.025	0.11	0.028	0.038	0.0415	0.028

Std. = standard deviation.

participants in the experiment. This may be explained by the backdrivability of the pneumatic actuated wrist exoskeleton, which ensures safety in rehabilitation but leads to large tracking errors [165]. Moreover, it may cause discomfort or injury to the wrist joint if the robot still follows the reference trajectory or has a rigid actuator.

To evaluate the performance of the proposed ACC, the effects of FCC and ACC are compared with the different C_r. Statistical results also reveal no significant differences are found between ACC with 0.3 C_r and FCC with 0.3 C_r. When the cooperative ratio is set to 0.6, a significant difference between the ACC and FCC is found. This reveals that the proposed ACC mainly takes account of the minimization of the tracking errors under a small cooperative ratio. In contrast, the wrist exoskeleton becomes more compliant to ensure the safety when cooperative ratio is set to a large value. The r_{TD} yields that the wrist exoskeleton becomes

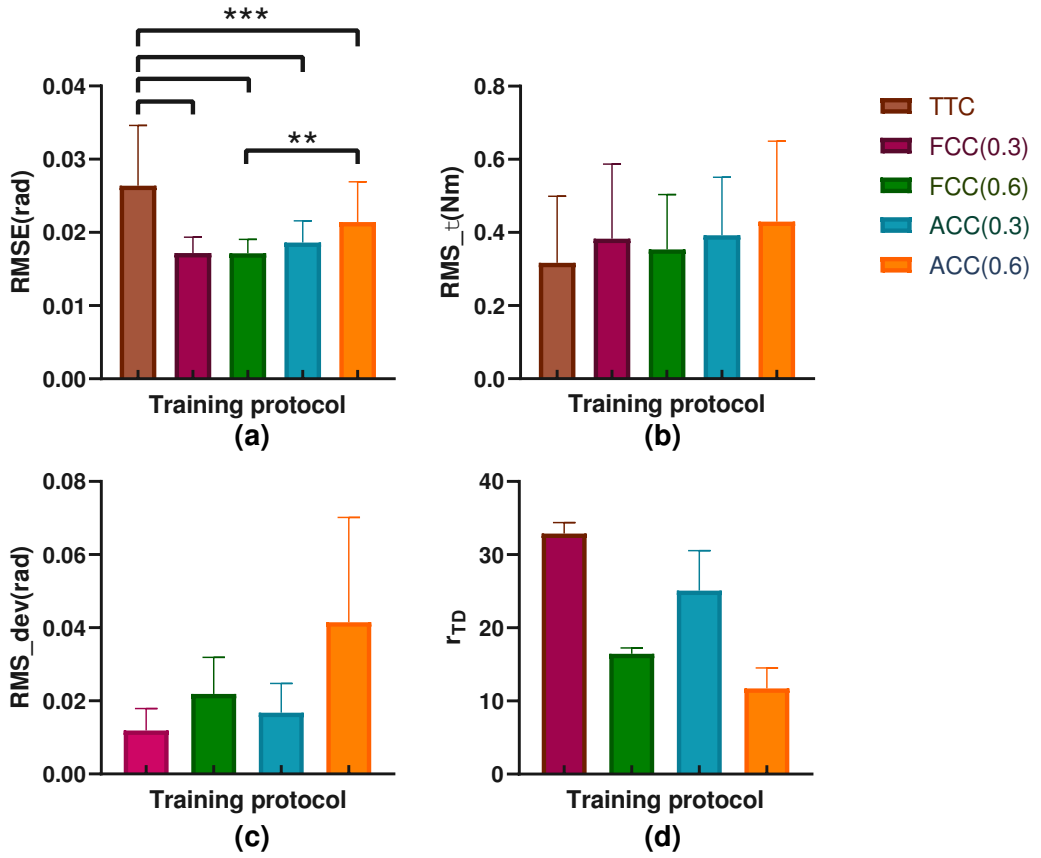

Figure 5.14: Results of the each training protocol. (a) RMSE; (b) RMS_{τ}; (c) RMS_{dev}; (d) The ratio of RMS_{τ} and RMS_{dev};

more compliant in ACC when compared with FCC.

The results of FCC show that the mean RMSEs are similar with two C_rs (0.0172 rad versus 0.0172 rad), but FCC with 0.6 C_r has less r_{td}, which means the wrist exoskeleton gives more ROMs based on the estimated joint torque when a higher ratio is applied. It is found that ACC has increased RMSE compared with FCC. This is may be caused by the selection of the stiffness parameters, which leads to larger compliance at the minimum stiffness parameter (Figure 5.13). This is consistent with results that the wrist exoskeleton provides the largest RoMs when

the cooperative ratio is set to 0.6 in ACC. It is worthy noticed that the selection of boundaries of stiffness parameter is determined by the trial and error in this study. Nevertheless, the performance of the ACC is significantly better than TTC. In this experiment, FCCs have less RMSEs than the ACCs with the corresponding C_rs. The ACC, however, presents advantages compared to that with FCC based on a fact that the robot is capable of adapting the compliance according to wrist joint stiffness. This would increase the robot's backdrivability while maintaining the adequate tracking performance. It is suggested that robot-assisted training with real-time assessment of the wrist joint will likely make therapy safer and more efficient [53, 112].

The EMG-driven musculoskeletal model provides accurate intention estimation performance, as demonstrated in previous chapters. Other methods for intention estimation include mechanical force/torque sensor, sensorless method and EMG-based model-free approaches. The force/torque sensor is commonly installed at the robot's joint of interest to measure the voluntary efforts directly. However, the measured signal is contaminated by the other components, e.g., friction, which influence the intention estimation accuracy significantly [35]. A complicated system identification is required to identify the subject's voluntary efforts from the sensor's measurement. Sensorless method does not need the force/torque sensor. However, a complex algorithm is utilized to extract the intention, which increases the computation cost. The other unknown input, such as un-modelled dynamics, is another hurdle to estimate the intention [67]. The use of EMG signal provides the direct estimation of the subject's motion intention. However, the model-free approaches only estimate the intention according to the training data. To access the wrist biomechanical characteristics in real-time, exhaustive efforts are required the establish the relationship from the EMG signal, motion data to joint stiffness [166]. The model-based approach shows a promising solution

in this study. After optimization, the musculoskeletal model is able to estimate the wrist joint stiffness in accordance with the measured EMG signal, joint motion and muscle contraction conditions without additional computational cost. The estimated joint stiffness is evaluated and compared with the literature, as demonstrated in the previous section.

There are several limitations in the current studies. The proposed EMG-driven model-based approach is tested on 12 healthy subjects. More subjects will be recruited, including patients with neurological diseases to validate the performance of the proposed control strategy. In addition, the selection of admittance parameters is based on the trial and error. Future studies will be carried out to determine the optimized admittance parameters in order to apply the proposed approach for patients.

5.5 Assist-as-needed Control

In this section, an assist-as-needed (AAN) control strategy is proposed. This control strategy includes an admittance controller combined with a PID-based force controller to provide the assistance to help the patient accomplish the intended movement. In the proposed AAN, a virtual trajectory is provide to encourage the the subject actively participant the training exercise. The proposed control strategy determines the desired trajectory based on the subject's motion intention and the assistance is obtained by the kinematic errors between the measured trajectory and desired trajectory. Similar to ACC, robot's assistance is also adapted in response to the wrist joint impedance property.

5.5.1 Control strategy

To achieve the proposed AAN, a force controller is implemented to enable the assisted torque provided by wrist exoskeleton. According to the mechanical design (section 5.2), the torque is computed by the force difference of the antagonistic PAM, which is written as

$$\frac{\tau_m}{r_p} = F_1 - F_2 \tag{5.16}$$

where τ_m is the torque measured by the wrist device and r_p is the radius of the hinge ($r_p = 0.86\,\text{cm}$). F_1 and F_2 represent the the force measured in each muscle respectively. Therefore, the output torque is transformed to the force output of each PAM. The force controller is based on the PID controller (Figure 5.5). The mathematical form is written as

$$e_f(t) = f_d(t) - f_m(t); \tag{5.17}$$

$$P_{2\times1}(t) = K_{fp}e_f(t) + K_{fp}\int_0^t e_f(t)dt + K_{fe}\frac{de_f(t)}{dt} \tag{5.18}$$

where $e_f(t)$ is the error between the desired force $f_d(t)$ and measured force $f_m(t)$. K_{tp}, K_{ti} and K_{td} are set to 0.025, 0.001 and 0.00025. Result of the force control is illustrated in Figure 5.15, in which the desired torque is set as a sine wave with 0.1 Nm amplitude and 0.025 Hz frequency. The max force error of the first PAM is 1.3889 N. The max force error of the second PAM is 1.6284 N.

The block diagram of the AAN control strategy is illustrated in Figure 5.16 (a). In contract to the ACC (section 5.4), the reference trajectory is not specified to a sine wave. θ_r is set to a initial neutral position prior to the experiment. In this scenario, active training exercise is conducted, as the patient is encouraged to participant the training exercise. A virtual trajectory is shown on a monitor. The admittance controller is utilized to generate the desired trajectory in response to the subject's intention, which is estimated by the EMG-driven musculoskeletal

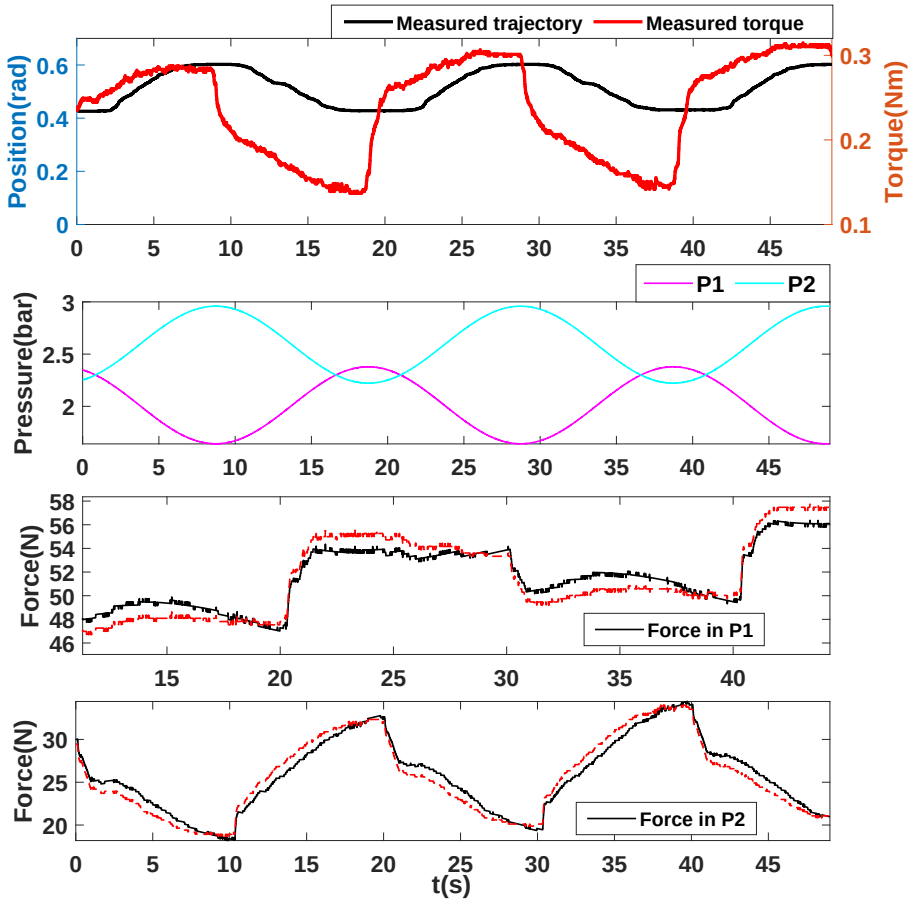

Figure 5.15: Force control of the wrist exoskeleton.

model. The transfer function of admittance controller is written as:

$$\theta_d(s) = \frac{\hat{T}(s)}{Ms^2 + Bs + K}. \tag{5.19}$$

The stiffness K and damping parameter B are set to 5 and 0.1 in this study, respectively. The M is set to zero due to the small acceleration of the wrist exoskeleton. In this study, the stiffness and dampling parameters are determined through the trial and error method. Therefore, the admittance controller outputs the intended motion with the inputs of the user's estimated joint torque. If the subject fails to track the trajectory by his/her own effort, the robot provides the

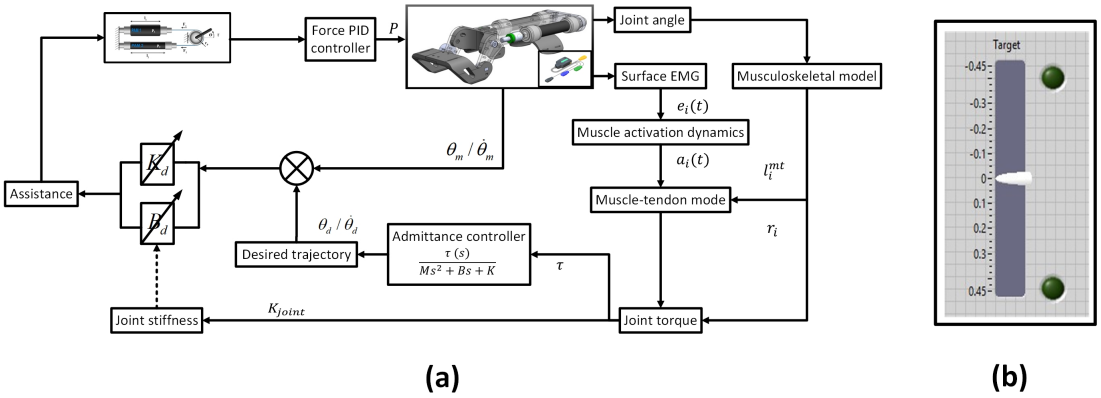

Figure 5.16: (a) The block diagram of the adaptive EMG model-based control strategy. (b) Subjects are asked to track the virtual trajectory shown on the screen.

assistance based on the kinematic errors. The assisted torque is determined by position errors and velocity errors between the desired trajectory and measure trajectory [167], which is written as

$$\tau_a = K_d(\theta_d - \theta_m) + B_d(\dot{\theta}_d - \dot{\theta}_m) \tag{5.20}$$

where τ_a is the assisted torque. K_d and B_d are the parameters. The assisted torque also takes the wrist impedance property into account [153], as the wrist joint stiffness changes as the function of the joint position and muscle activities (equation (5.3)). Therefore, the adaptation of K_d is proposed with the consideration of the real-time assessment of the wrist joint stiffness K_{joint}. Additionally, to guarantee the stability of the proposed control strategy, a boundary is set for the stiffness parameter, which is obtained by

$$K_d = (K_d^{max} - K_d^{min})\frac{K_{joint} - K_{joint}^{min}}{K_{joint}^{max} - K_{joint}^{min}} + K^{min} \tag{5.21}$$

where K_d^{max} and K_d^{min} are the boundaries of the stiffness parameter, where are determined experimentally. The K_{joint}^{max} and K_{joint}^{min} are maximum and minimum

wrist joint stiffness through the equation (5.3). The parameter B_d is a function of the K_d, which is obtained by

$$B_d = 0.02\sqrt{K_d} \tag{5.22}$$

The assisted torque is then transformed to the distributed force as the desired force in each PAM that allows the wrist exoskeleton to control force through the PID force controller.

5.5.2 Experiment protocol

Ten healthy subjects participated in this experiment in the lab environment. All subjects have no reported wrist muscular disorder and can perform the wrist flexion/extension in full (RoM). The raw EMG signal are processed and downsampled to 100 Hz. All sensing data are synchronized and stored via the customized LabVIEW program at 100 Hz.

The subjects are asked to wear the wrist exoskeleton, as shown in Figure 5.8. Electrodes are attached over four wrist muscles, including Flexor Carpi Radialis (FCR), Flexor Carpi Ulnaris (FCU), Extensor Carpi Radialis Longus (ECR). The placement of the electrode is the same as in the previous section. The quality of the EMG signals is evaluated prior to the experiment. The maximum voluntary contraction and dynamic flexion/extension trials are also recorded for normalization and muscle-tendon parameter optimization. During the experiment, the subjects are asked to track a marker on the screen. The trajectory of the marker is set to 0.45 rad.

In this study, different K_d are utilized, including:

- K_d is set to constant (K_d = 2, 4, and 6).
- K_d and B_d are obtained according to equation (5.22) and (5.21) (Adaptive).

Three trials are performed in each experiment and five-minute interval is given to prevent muscle fatigue.

5.5.3 Performance criteria

The rmse of position error (same as equation (5.13)), joint torque and assistance torque are calculated.

$$\text{RMSE} = \sqrt{\sum_{n=1}^{N}(\theta_d - \theta_m)} \tag{5.23}$$

$$\text{RMS}_{\tau} = \sqrt{\sum_{n=1}^{N}\tau} \tag{5.24}$$

$$\text{RMS}_{\tau_\text{a}} = \sqrt{\sum_{n=1}^{N}\tau_a} \tag{5.25}$$

where the θ_d in the AAN is the desired trajectory generated by subjects when tracking the marker's trajectory.

5.5.4 Results

Figure 5.17 presents tracking response of the proposed AAN when K_d is set to 2 and 4 respectively. The desired trajectory (black solid line) is generated through the admittance controller when the subject is asked to track the virtual marker. The red dotted line indicates the measured trajectory. When K_d is set to 2, the RMSE, RMS_{τ} and $\text{RMS}_{\tau_\text{a}}$ are 0.083 rad, 0.335 Nm and 0.163 Nm. The RMSE, RMS_{τ} and $\text{RMS}_{\tau_\text{a}}$ for $K_d = 4$ are 0.076 rad, 0.307 Nm and 0.294 Nm.

The tracking responses of $K_d = 6$ and $K_d = \textit{adaptive}$ are illustrated in Figure 5.18. For $K_d = 6$, the RMSE, RMS_{τ} and $\text{RMS}_{\tau_\text{a}}$ are 0.086 rad, 0.277 Nm and 0.495 Nm. When K_d is set to be adaptive, the RMSE, RMS_{τ} and $\text{RMS}_{\tau_\text{a}}$ are 0.101 rad, 0.315 Nm and 0.153 Nm.

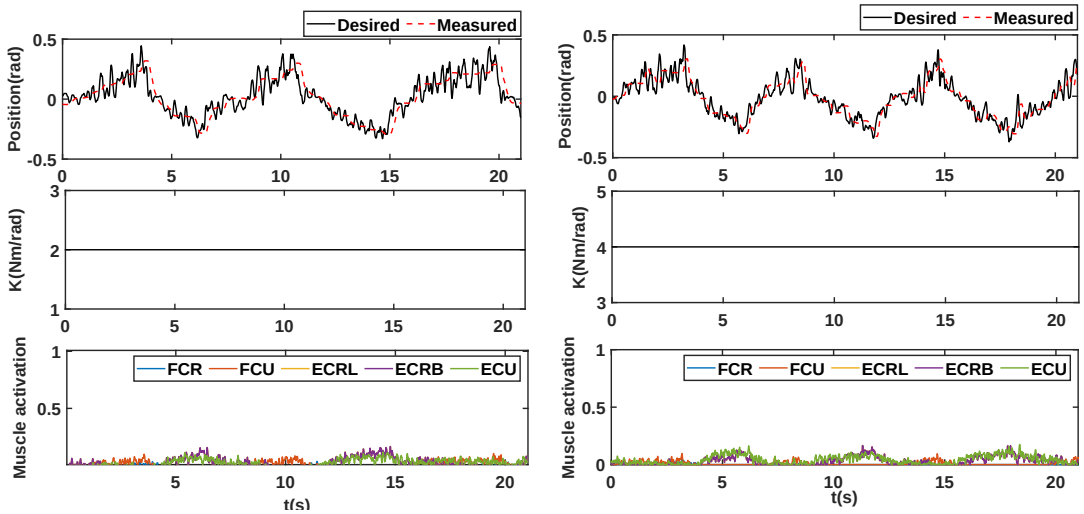

Figure 5.17: Representative examples of tracking performance when K_d is set to 2 (left figure) and 4 (right figure) respectively.

Table 5.8 gives mean RMSE, RMS_τ, and $\text{RMS}_{\tau_\text{a}}$ with different value of K_d. The results show that the proposed control strategy with different level assistance has the similar tracking accuracy. When $K_d = 2$ and $K_d = 4$ are applied, the mean RMS_τ is slightly larger than the mean RMS_τ when $K_d = 6$ and adaptive K_d. The robot assistance, $\text{RMS}_{\tau_\text{a}}$, increases as the value of K_d increases. The smallest assistance is found when the K_d is in response to the joint stiffness.

The results yield that the wrist exoskeleton is able to respond to the subjects' muscular effort and provide the robot assistance accordingly. The mean RMSE is larger than the adaptive cooperative control strategy (section 5.4.1). This is because that the proposed AAN utilizes the low-level PID controller to control the force output of the pneumatic muscles, whereas the torque control of the wrist exoskeleton is an 'open-loop' control. To improve the tracking performance, future work will take account of the wrist exoskeleton's assembly precision to

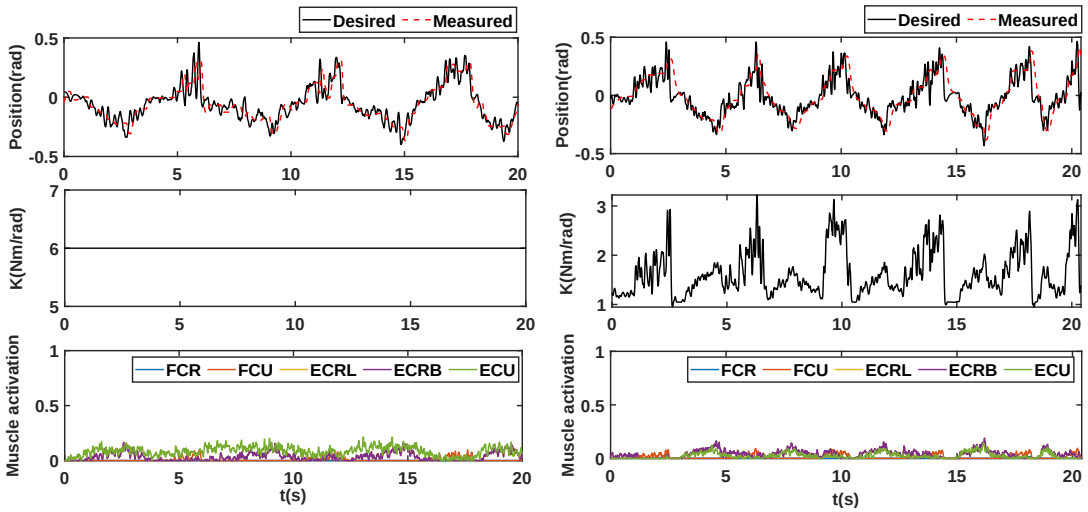

Figure 5.18: Representative examples of tracking performance when $K_d = 6$ (left figure) and adaptive K_d (right figure) respectively.

develop a 'close-loop' torque control. Moreover, the pneumatic muscle has the non-linearity and hysteresis properties, the precise force control will be achieved by the applying advanced modelling techniques and the flow control valve.

The RMS_τ indicates the subject's muscular effort, which are similar across different value of K_d. This is due to the fact that the desired trajectory is solely obtained by the admittance filter. To track the virtual trajectory, the subjects perform similar muscular efforts in each trial. The major advantage of the EMG signal, the electromechanical delay, is not observed in this experiment. Future work will implement the proposed control strategy in a microcontroller with a high sample frequency to capture this characteristic.

The RMS_τ is generated with respect to the kinematics errors and is in consistent with the values of K_d. The smallest assistance is found when the adaptive K_d is used. This can be explained by the fact that the healthy subjects perform

the voluntary wrist flexion/extension resulting in a small variation of K_d. For example, as shown in Figure 5.18 (a), the max k_d occurs at maximum flexion position. When the kinematic errors are same, the robot assistance with constant K_d might be larger than the assistance when adaptive K_d is applied. The $K_d = 4$ and $K_d = 6$ may provide too much assistance and may have negative effects for patients, e.g., slacking [72]. The use of the adaptive K_d provide the compliant assistance in response to the subject's own effort and joint stiffness. For example, at low joint impedance, same assistance is required to drive the wrist joint. At high active stiffness, the robot needs large assistance to guide the wrist joint to the intended motion. In this experiment, it is not demonstrated that the significant differences between each value of K_d through the performance criteria. In addition, It is not able to be measure the interaction torque during the experiment. This is because the force sensor is used to the control the force output of the PAMs. The force difference can not truly represent the interaction force.

To conclude, this section presents an active assistive control strategy in order to assist the subject to accomplish the virtual motion task. Experiment results show that the wrist exoskeleton is able to drive the wrist joint to the desired position in response to the subject's motion intention. Similar to the ACC, the adaption law is used to determine the robot's assistance based on the subject's stiffness. However, current study has several limitations. The performance criteria is significantly affected by the configuration of the wrist exoskeleton. Future work will carry out improvements to the wrist exoskeleton including precise torque controller and PAM force controller. The qualitative and quantitative analysis of the AAN with different values of K_d will be re-evaluated. Future work will also recruit more subjects including patients with muscular disorders to validate the proposed control strategy.

Table 5.8: The mean (standard deviation) RMSE, RMS_{τ}, and RMS_{τ_a} of AAN with different K_d across ten subjects.

	Performance criteria		
	RMSE(rad)	RMS_{τ}(Nm)	RMS_{τ_a}(Nm)
$K_d = 2$	0.117 (0.032)	0.418 (0.069)	0.233 (0.065)
$K_d = 4$	0.104 (0.036)	0.410 (0.074)	0.413 (0.144)
$K_d = 6$	0.106 (0.031)	0.385 (0.063)	0.625 (0.187)
Adaptive K_d	0.122 (0.0278)	0.377 (0.046)	0.207 (0.052)

5.6 Chapter summary

This chapter presents the EMG-driven musculoskeletal model-based active assistive control strategy for the wrist rehabilitation robot. The wrist exoskeleton used in this research is first introduced. The exoskeleton actuated by two pneumatic muscles provides antagonistic force for wrist flexion/extension motion. The second section gives the evaluation and validation of the EMG-driven musculoskeletal model for estimation of the wrist joint stiffness. The passive and active joint stiffness are emulated according to the literature. Results yielded the passive joint stiffness has the range from 0.21 Nm/rad to 2.22 Nm/rad, and the active joint stiffness has the range from 7.45 Nm/rad to 16.48 Nm/rad. Both estimated joint stiffnesses fall into the middle range of measurements reported in the literature.

In the third section, the adaptive cooperative control strategy is proposed to improve the training efficiency and ensure safety. This control strategy consists of the PID-based position control and the admittance controller. The admittance parameters are adapted with the aid of the real-time assessment of the wrist joint stiffness. The wrist exoskeleton is under the passive model to guide the

wrist joint following the reference trajectory. If the subject's voluntary effort is detected, the wrist exoskeleton is able to modify the reference trajectory and robot's compliance in accordance with the motion intention and joint impedance. Experimental results show that the tracking performance of the proposed control strategy (ACC) is significantly better than TTC, but the RMSE is larger than FCC. ACC is capable of modifying the robot's compliance in accordance with joint stiffness. The proposed adaptive cooperative control strategy shows the potential to enhance the training efficacy and safety for robot-aided wrist rehabilitation.

The assist-as-needed control strategy is proposed in this chapter, which assists the subject to accomplish the intended motion. The force controller is utilized to provide the desired torque, and the admittance controller is used to generate the desired position based on the user's intention. In the AAN, the subject is encouraged to track the trajectory by his/her own efforts. Robot's assistance is calculated by the position and velocity errors. Furthermore, the assistance is adapted based on the estimated joint stiffness. Experiment results show that the wrist exoskeleton is able to assist the wrist joint to the intended motion, and the assistance torque with adaptive K_d is smaller than the torque with constant K_d. Improvements to wrist exoskeleton will be carried out in order to provide more qualitative and quantitative results when different value of K_d are applied.

To conclude, the EMG-driven musculoskeletal model benefits the control of the wrist rehabilitation robot. The model estimates the intention more intuitively and provides a promising solution to access the wrist joint impedance property in real-time without additional cost. The proposed EMG-driven model-based control strategies provide a new solution to control the wrist rehabilitation robots with improved effectiveness and safety.

Chapter 6

An EMG-driven Musculoskeletal model For Estimating of Wrist Kinematics using Mirrored Bilateral Movement

Myoelectric control has been broadly studied for amputees in the last decades. The major challenge for myoelectric control is that the demand for training data to be recorded from the amputated side, which is impossible for the amputee. This chapter presents a musculoskeletal model-based approach to estimate the wrist joint kinematics of contralateral side using electromyogram (EMG) signals from ipsilateral side using the mirrored bilateral training strategy. The proposed approach computes the internal force/joint torque and integrates the wrist kinematics using the forward dynamics, based on the recorded wrist muscle activities. The experiments are conducted on six able-bodied subjects, involving symmetric movements of both limbs with single degree-of-freedom and combined movements of wrist flexion/extension and radial/ulnar deviation. For the contralateral case, results show that the proposed approach can provide accurate wrist movements estimation, in which the mean coefficient of determination and mean normalized root-mean-square-errors are 0.84 and 0.15 respectively, across all movement tri-

als and subjects. The proposed approach and setup give feasible meaning for the simultaneous and proportional control of wrist kinematics. Furthermore, the development of the multiple degrees of freedom wrist EMG-driven musculoskeletal model can be used on the wrist rehabilitation robots.

6.1 Introduction

The loss of upper limbs impairs physical functionality and mobility that degrades the quality of life significantly.The myoelectric control methods, using the surface electromyogram (EMG) from the residual limb, strive to restore the functionality for the amputee to perform the activities of daily life [168].

To estimate the joint kinematics using the EMG signal, a conventional approach is concerned with the pattern recognition algorithm[65]. This algorithm is limited by its inherent sequential control strategy, which recognises the desired motion classes at a time [169]. To realize the natural movements of the wrist joint that involve the combined activation of the multiple degrees-of-freedom (DoFs) [170, 171], the proportional control needs to be achieved. That is, continuous motion kinematic variables are derived from the EMG signal, instead of desired motion classes [84]. Furthermore, myoelectric control methods should provide the proportional control of multiple DoFs simultaneously [172].

The techniques for the simultaneous and proportional wrist kinematics estimation are categorized into two approaches, model-free and musculoskeletal model-based. The model-free approaches are broadly used for the myoelectric control [173–178]. These approaches establish the relationships between EMG signals and the desired movements using numerical functions. Nevertheless, the model-free approaches are limited by the demand for the abundant data to train the relevant transfer functions. Moreover, the trained functions underlying one specific

condition, may not be able to respond to one novel condition, i.e., different postures [39].

The musculoskeletal model-based approach comprises muscle physiology (i.e., Hill's muscle model) and musculoskeletal geometry to mimic the physiological human movement. This approach entails the underlying muscular transformation from neuro-commands to the corresponding limb motion. Recently, the model-based approach is emerging for the proportional estimation about the single DoF. For instance, Pau *et al.,* proposed a simplified musculoskeletal model to predict the elbow movements [91]. Han *et al.,* also utilized the model-based approach in conjunction with EMG features to estimate the elbow flexion/extension movements[132]. To provide the myoelectric control simultaneously, Blana *et al.,* proposed the musculoskeletal model for myoelectric control of hand movements to perform the American sign language [105]. Nevertheless, this model is based on the simulated EMG signals. Crouch *et al.,* proposed a lumped-parameter musculoskeletal model to compute the wrist and metacarpophalangeal (MCP) joint flexion/extension [100]. However, only wrist flexion/extension motion are concerned in their model. The wrist primary muscles also contribute to ulnar/radial deviation.

The physiological parameters in the model-based approach should be optimized to each individual to preserve the estimation accuracy. However, the training data, which requires the recording of the EMG signal and the corresponding wrist motion from the same side, is not possible in amputees. Studies addressed this problem by the mirrored bilateral movement training strategy because the amputees are able to generate the virtual movements voluntarily with their amputated side[173–175, 179]. The similar neural muscular contractions have been observed during the mirrored bilateral movement [180]. In [100], the musculoskeletal model was developed for amputees through the mirrored bilateral move-

ment. However, only two wrist muscles are included and the optimized parameters exceeded the physiological range, e.g., the muscle fibre length is much larger than the measurement in *vivo* [125].

In this chapter, we propose an EMG-driven musculoskeletal model to estimate the wrist flexion/extension and radial/ulnar deviation using the mirrored bilateral movement training strategy. Contributions of this paper are two-fold, which are 1) the explicit computation of the underlying neural-mechanical process with respect to five primary muscles, comprising the muscle activation dynamics, the muscle-tendon model, and the joint kinematics estimation model, improves the reliability for simultaneous and proportional estimation of wrist multiple kinematics. 2) the mirrored bilateral movement training strategy improves the model's feasibility that the internal physiological parameters are optimized according to the EMG signal recorded from one limb (ipsilateral) and the wrist kinematic data are recorded from the contralateral limb. Experimental work is conducted on six able-bodied subjects through a series of wrist mirrored bilateral movements in free space. Results demonstrate the proposed model-based approach provides high estimation accuracy in the contralateral case with mean R^2 of 0.86 and 0.82 for wrist flexion/extension and radial/ulnar deviation, respectively.

The remaining sections are structured as follows. Section 6.2 presents the experiment protocol and the musculoskeletal model-based approach. Section 6.3 describes the results and section 6.4 gives discussion regarding the estimation performance of the ipsilateral and contralateral cases respectively. The final section gives a conclusion.

6.2 Methods

6.2.1 Experimental protocol

Six able-bodied subjects participant in the experiments (referenced as S1-S6, the ages between 25 and 31). The experimental information sheets are given to all subjects and the consent forms are signed prior to the experiment. The experimental protocol is approved by Maths and Physical Science and Engineering Joint Faculty Research Ethics Committee of the University of Leeds (MEEC 18-002).

At the start of the experiments, the subjects are asked to sit on an armchair with the torso fully straight, the shoulders are abducted around 30° and the elbows are flexed about 90°. The elbows are supported by two customized armrests and the forearms and MCP joints are kept relaxed. The symmetric position of the upper limbs is checked carefully before each experiment. The neutral position of the wrist joint is defined as the palm facing inwards [47]. Surface EMG signals from the right forearm and the motion data from both forearms are recorded during the experiments. A period of time is given for the subject to familiarize with the experimental protocol before the experiment. and the maximum voluntary contractions (MVC) are recorded.

Subjects are instructed to perform a series of mirrored bilateral movements, involving the combination of the wrist movement. The experimental trials consist of purely wrist flexion/extension or radial/ulnar deviation and the combination of two movements, as detailed in Table 6.1. Each trial starts from the neutral position and takes approximately 2 s for one defined movement cycle. Five trials containing five repetitions of each movement are recorded. One trial from each movement is used to optimize the parameters of the proposed musculoskeletal model-based approach for the ipsilateral case and contralateral case respectively.

The rest of the trials are used to validate the performance of the proposed model-based approach. A five-minute break is given between trials to prevent fatigue.

Table 6.1: Experimental protocol

Index	Movement set	Active DoF(s)
1	Sinusoidal movement	Wrist flexion/extension(WFE)
2	Sinusoidal movement	Radial/Ulnar Deviation (RUD)
3	Combined movement in a circular clockwise (CW)/Counterclockwise (CCW)	WFE and RUD

6.2.2 Data acquisition

EMG recording

The surface EMG signals are recorded by the Avanti Sensors (Delsys Trigno^{TM}) in this experiment. The EMG signals of five muscles ($i = 1, 2, \ldots, 5$) articulating the wrist joint are collected, including Flexor Carpi Radialis (FCR), Flexor Carpi Ulnaris (FCU), Extensor Carpi Radialis Longus (ECRL), Extensor Carpi Radialis Brevis (ECRB) and Extensor Carpi Ulnaris (ECU). EMG signals are recorded from the right forearm (right top corner in Fig. 6.1). The location of electrode placement are found by palpation and evaluated by performing contraction while looking at the signal prior to experiment. The skin is cleaned using an alcohol wipe to minimize the impedance prior to electrode placement (shaved if necessary). The EMG signals are acquired through the base station, sampled at 2000 Hz.

Wrist motion recording

The wrist kinematics data are captured using a 8-camera motion capture system (VICON Motion Systems Ltd. UK). To compute the wrist flexion/extension angle and ulnar/radial deviation angle, a coordinated system is adopted based on [175]. The reflective markers are attached symmetrically on the subject's forearms (seven markers at each limb). Four markers are allocated in hand area, including the radial head of the second metacarpal bone (RMC), the ulnar head of the fifth metacarpal bone (UMC), the radial styloid (STR) and the ulnar styloid (STU). Two markers are placed over the lateral (MEP) and medial epicondyles (LEP) of the humerus. Two markers are positioned on the acromio-clavicular join (SHO) and three markers are attached on the 7^{th} spinous process (C7), right clavicle (CLAV) and xiphoid (STE) respectively. The qualities of the movements data are evaluated after each trial, trials containing the markers' trajectory with the excessive gaps are abandoned. The kinematic data are sampled at 250 Hz and low-pass filtered.

6.2.3 Data processing

EMG processing

The recorded EMG signals are filtered using a 4^{th} order Butterworth band-pass filter (pass band at 20 Hz and 450 Hz) to remove the movement artefact and dc offset. The filtered signals are fully rectified and low-pass filtered by a 4^{th} order Butterworth low-pass filter at a corner frequency of 4 Hz. To interpret the envelope of the muscles activities between 0 and 1, the filtered signals are normalized by the MVCs. The resultant enveloped signals $e_i(t)$ are the inputs for the musculoskeletal model-based approach.

Figure 6.1: The placement of electrodes (right) and markers position of the right limb (left), along with the corresponding coordinate system. Markers on each limb are attached symmetrically.

Kinematics data processing

Similar to [175], the coordinate system (Figure 6.1) can be described in the following.

1) The original point **O** is defined as the centre of the wrist, at the midpoint between the STR and STU.

2) The y-axis is located along with the centre axis of the forearm, the positive direction points to the proximal joint.

3) The x-axis is perpendicular to the palm, the positive direction points inward. Then the z-axis is determined by the right-hand rule, orthogonal to the y-axis and x-axis. The positive direction points upward.

The midpoint between the RMC and UMC is denoted by H, allocating on the y-z plane. Thus the wrist joint angles θ_j $(j = 1, 2)$ for wrist flexion/extension

and radial/ulnar deviation can be calculated by the following equations.

$$\theta_1 = \arctan\left(\frac{H_x}{H_y}\right) \tag{6.1}$$

$$\theta_2 = \arctan\left(\frac{H_z}{H_y}\right) \tag{6.2}$$

where H_x, H_y and H_z are the projections of H on x-axis, y-axis and z-axis respectively. θ_1 and θ_2 represent the wrist flexion/extension and radial/ulnar deviation respectively. The positive directions correspond to the wrist flexion and ulnar deviation respectively. The surface EMG signals and kinematic data are synchronized in VICON Nexus software through a trigger module. The synchronized signals are resampled to 100 Hz for computing the muscle activation levels.
As elaborated in Figure 6.2, the filtered enveloped signal are recorded from the right side. The wrist kinematics are recorded from the both sides of the forearm, optimizing the physiological parameters for each case. Then the optimized model of the contralateral case is validated using the validation trials and is compared with ipsilateral case.

6.2.4 Musculoskeletal model-based approach

The wrist joint kinematics are estimated through the proposed musculoskeletal model-based approach for ipsilateral and contralateral cases respectively, which comprises the muscle activation dynamics, the muscle-tendon model and the joint kinematics estimation model. The muscle activation dynamics computes the muscle activation levels of the wrist muscles. Then the muscle force are calculated in response to muscle activation level and current states of muscle-fibre length. The joint angles are estimated with the combination of the skeletal properties through the forward dynamics.

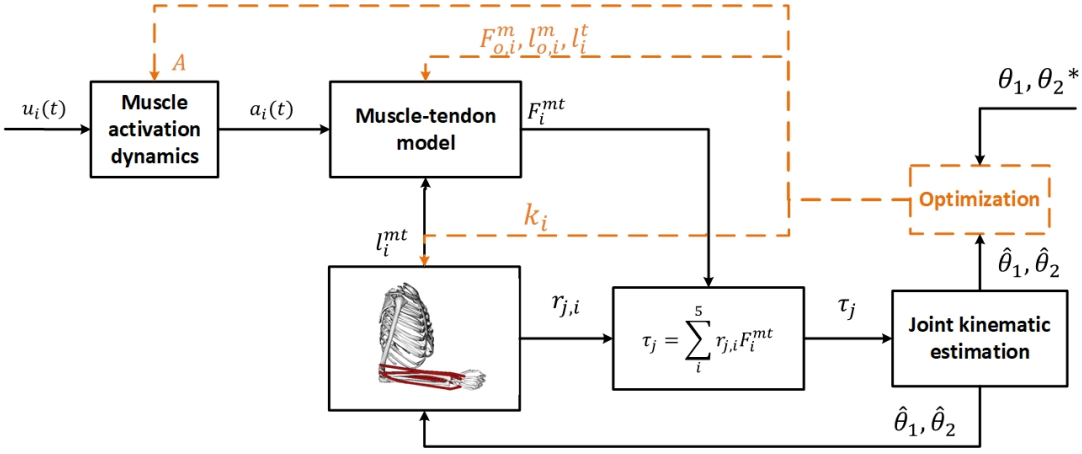

Figure 6.2: The flowchart of the EMG-driven musculoskeletal model: the enveloped EMG signals are taken from the right limb, computing the wrist joint angles through muscle activation dynamics and musculoskeletal model. The wrist angles are taken from the ipsi and contralateral sides are used to optimize the parameters, as shown in the dashed block.

Muscle activation dynamics

The muscle activation $a_i(t)$ is obtained through the non-linear transformation of the filtered enveloped signal $e_i(t)$ [119], which can be formed as

$$a_i(t) = \frac{e^{Au_i(t)} - 1}{e^A - 1} \tag{6.3}$$

where A is the non-linear shape factor.

Muscle-tendon model

For each muscle, the muscle-tendon model is modelled as an elastic tendon connected in series with a muscle fibre (Hill's muscle model). The muscle fibre contains the contractile element (CE) in parallel with passive element (PE). In this study, the tendon is assumed as a rigid elements, thus the muscle-tendon force F_i^{mt} can be computed by the sum of active force $F_{CE,i}$ and passive force

$F_{PE,i}$

$$F_i^{mt} = (F_{CE,i} + F_{PE,i}) \cos \phi_i \tag{6.4}$$

$$F_{CE,i} = F_{o,i}^m f_a(\bar{l}_{i,a}^m) f(\overline{v}_i) a_i(t) \tag{6.5}$$

$$F_{PE,i} = F_{o,i}^m f_p(\bar{l}_i^m) \tag{6.6}$$

where $F_{CE,i}$ is the active force generated by CE, including the function $f_a(\bar{l}_{i,a}^m)$ and $f(\overline{v}_i)$ to account for the active force-length curve and the force-velocity curve respectively. $F_{o,i}^m$ is the maximum isometric force. The force-length curve and force-velocity curve can be expressed as

$$f_a(\bar{l}_{i,a}^m) = e^{-(\bar{l}_{i,a}^m - 1)^2 k_0^{-1}} \tag{6.7}$$

$$f(\overline{v}_i) = \begin{cases} \frac{0.3(\overline{v}_i + 1)}{-\overline{v}_i + 0.3} & \overline{v}_i \leq 0 \\ \frac{2.34\overline{v}_i + 0.039}{1.3\overline{v}_i + 0.039} & \overline{v}_i > 0 \end{cases} \tag{6.8}$$

where $\bar{l}_{i,a}^m$ is equal to $\bar{l}_{i,a}^m = l_i^m / (l_{o,i}^m(\lambda(1 - a_i(t)) + 1)$ [94]. l_i^m and $l_{o,i}^m$ are the current state of muscle fibre length and optimal fibre length respectively. The coefficient k_0 is set to 0.45 in order to approximate the force-length curve [120]. For the force-velocity curve, $\overline{v}_i$ is obtained by normalization of muscle contraction velocity v_i to $l_{o,i}^m$/sec [87], in which v_i is the derivative of the muscle fibre length with respect to time.

Furthermore, $F_{PE,i}$ is the passive force generated by the PE in muscle fibre. The passive force-length relationship $f_p(\bar{l}_i^m)$ denotes if the muscle fibre length exceeds the optimal muscle fibre length, which be presented as

$$f_p(\bar{l}_i^m) = \frac{e^{10(\bar{l}_i^m - 1)}}{e^5} \tag{6.9}$$

where l_i^m is the normalization of muscle fibre length with respect to $l_{o,i}^m$.

The pennation angle ϕ_i is angle between the tendon and muscle fibre. It changes as the muscle contraction, which is obtained by

$$\phi_i = \sin^{-1}\left(\frac{l_{o,i}^m \sin \phi_{o,i}}{l_i^m}\right) \tag{6.10}$$

in which $\phi_{o,i}$ represents the optimal pennation angle.

In order to obtain the current states of the muscle fibre length, a large combinations of wrist movement involving wrist flexion/extension and radial/ulnar deviation simultaneously are simulated by restricting other DoFs to the experimental posture [96]. The simulated results are exported to generate the polynomial equation of the muscle-tendon lengths l_i^{mt} with respect to the wrist joint angles. Then the muscle fibre length can be obtained by

$$l_i^m = (k_i l_i^{mt}(\theta) - l_i^t)\cos^{-1}\phi_i \tag{6.11}$$

where l_i^{mt} and l_i^t are the muscle-tendon length and tendon length respectively. The scale coefficient k_i is introduced to account for the difference of the muscle-tendon length across subjects.

The moment arm is then obtained by the partial derivatives of the muscle-tendon length with respect to the corresponding joint angles

$$r_{j,i} = \frac{\partial l_i^{mt}}{\partial \theta_j} \tag{6.12}$$

where $r_{j,i}$ represents the moment arm of ith muscle with respect to the jth joint angle. Therefore, the corresponding wrist joint torques can be computed by

$$\tau_j = \sum_{i=1}^{5} r_{j,i} F_i^{mt} \tag{6.13}$$

where τ_j is a 2×1 vector, representing the joint torques at wrist flexion/extension and ulnar/radial deviation respectively.

Joint kinematics estimation model

The wrist joint is modelled as a universal joint. The axis of radial/ulnar deviation is believed to be slightly distal to the axis of wrist flexion/extension [181]. Nevertheless, the distance between the axes is small and has the negligible effects

on the wrist dynamic [182]. The equation of motion is computed by.

$$\tau_j = M\ddot{\theta}_j + C\dot{\theta}_j + K\theta_j + G \tag{6.14}$$

where matrix M is the inertia term, which estimated according tos the subject's body weight and height [183]; Matrix C and K are the damping and stiffness parameters respectively [162]. G is the gravitational term which only has the effects on radial/ulnar deviation in this study. $\ddot{\theta}_j$, $\dot{\theta}_j$ and θ_j are the joint accelerations, joint velocities and joint angles respectively. Therefore, the joint torques (τ_j) are computed through the current states of muscle-tendon model together and muscle activation level. The joint accelerations are forward integrated to estimate the next state of wrist joint angles, using the $4th$ order Runge-Kutta method.

Parameters optimization

As discussed in previous chapters, the proposed model-based approach contains several parameters that represent the characterization of the subject's muscle properties [119]. These parameters vary across subjects due to the different conditions of the anatomical status, e.g., skin condition. Thus, the maximum isometric muscle force, optimal muscle fibre length, tendon length and scale coefficient k_i are optimized for each subject for either ipsilateral case and contralateral cases. Besides, the non-linear shape factor is also included.

It is worthy to note that although these parameters are not available in amputees, these parameters still can be optimized via contralateral case for the phantom limb that can constrain the estimated movements within the physiologically feasible RoMs.

For each subject, the nominal value of these parameters are assigned according to [126]. The boundaries for each parameters are the in Chapter Three

(Table 3.2), which are constrained within the physiological range [96]. The genetic algorithm is applied in this study to optimize these parameters for each subject and their movements,by finding the minimum value of the cost function. The cost function is written as

$$\chi = [F^m_{o,i}, l^m_{o,i}, l^t_i, k_i, A]^T \tag{6.15}$$

$$\hat{\chi} = \arg\min_{\chi}\{f(\chi)\} \tag{6.16}$$

where

$$f(\chi) = \frac{1}{N}\sum_{j=1}^{2}\sum_{n=1}^{N}(\theta_j - \hat{\theta}_j) \tag{6.17}$$

where $f(\chi)$ is the objective function that minimizes the difference between the estimated joint angles and measured joint angles. θ_j and $\hat{\theta}_j$ are the measured joint angles and estimated joint angles respectively, and N is the number of samples.

6.2.5 Performance index

To quantify the estimation performance of the proposed EMG-driven model, the coefficient of determination (R^2) and normalized root-mean-square-error (NRMSE) are used as the metric for each DoF, which can be expressed as

$$R^2_j = 1 - \frac{\mathrm{Var}(\theta_j - \hat{\theta}_j)}{\mathrm{Var}(\theta_j)} \tag{6.18}$$

$$\mathrm{NRMSE_j} = \frac{\sqrt{\sum_{n=1}^{N}(\theta_j - \hat{\theta}_j)^2}}{\theta_{max,j} - \theta_{min,j}} \tag{6.19}$$

where θ_j and $\hat{\theta}_j$ represent the jth measured joint angle and the jth estimated joint angle respectively. $\theta_{max,j}$ and $\theta_{min,j}$ are the maximum and minimum value of the jth measured joint angle. In equation (6.18), the numerator represents the mean-square-error (MSE) and denominator is the total variance [173]. The NRMSE and R^2 quantify the difference in terms of amplitude and correlation

between the estimated joint angles and the measured joint angles. Higher values of R^2 and lower NRMSE indicate the musculoskeletal model-based approach can estimate the joint angle accurately. In addition, separate one-way ANOVAs are conducted for each DoF to evaluate the differences between the ipsilateral case and contralateral case in terms of the R^2 and NRMSE. Statistical significance value is set to $p = 0.05$.

6.3 Results

For each subject, the wrist kinematic data are collected bilaterally and the EMG signal is collected from the dominant side are used to calibrate the muscle-tendon parameters. The estimated results for the ipsilateral case and contralateral case across the single DoF movement and combined movement trials are illustrated in Figure 6.3.

The one-way ANOVA analysis indicates that there is no statistical difference between the ipsilateral case and the contralateral case. The p values are 0.27 and 0.77 for wrist flexion/extension (WFE) and radial/ulnar deviation (RUD) respectively. In the single activation trial, the mean R^2 and mean NRMSE in the case of ipsi(contra)lateral are: 0.905(0.895), 0.118(0.141); 0.887(0.875), 0.138(0.131) for the WFE and RUD respectively. In the combined motion trials, mean R^2 and mean NRMSE are 0.856 (0.838) and 0.143 (0.138) for WFE. For the RUD, the mean R^2 and mean NRMSE are 0.791 (0.784) and 0.157 (0.176).

The estimation performance of the contralateral case are summarised in Table 6.2, in terms of the R^2 and NRMSE for each subject. Results indicate the proposed EMG-driven musculoskeletal model can provide an accurate wrist joint kinematics estimation. When one DoF is activated, the estimation performance is better than the performance when the combined movements are performed, e.g., in the

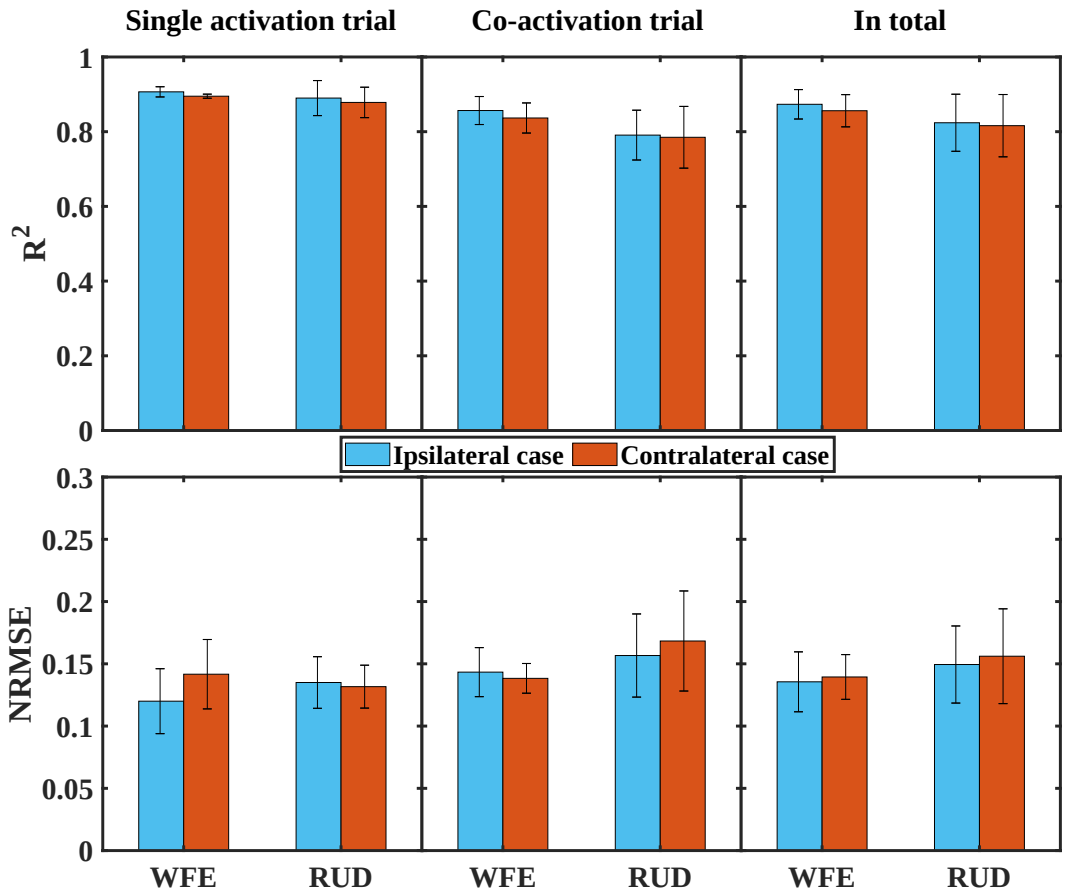

Figure 6.3: Comparison of the estimation performance between the ipsilateral and contralateral case in the single activation trials and combined movement trials. Top panel and bottom panel present the R^2 and NRMSE respectively. WFE and RUD correspond to the wrist flexion/extension and radial/ulnar deviation respectively.

contralateral case, the R^2 of WFE is 0.90 in the single movement trial and is 0.84 in the combined trial.

One representative example for comparison between the ipsilateral case and contralateral case is given in Figure 6.6. For the ipsilateral case, the R^2 (NRMSE) are 0.91 (0.08) for WFE and 0.85 (0.12) for RUD, respectively. For the contralat-

eral case, the R^2 (NRMSE) are 0.89 (0.09) and 0.82 (0.12) for WFE and RUD respectively.

Table 6.2: Estimation performance across all subjects in the contralateral case

Subject	**Trial**	R^2		**NRMSE**	
		WFE	**RUD**	**WFE**	**RUD**
S1	T1/T2	0.90	0.85	0.14	0.14
	T3	0.79	0.85	0.14	0.17
	T4	0.81	0.80	0.13	0.14
S2	T1/T2	0.90	0.90	0.11	0.11
	T3	0.84	0.85	0.14	0.12
	T4	0.88	0.82	0.12	0.16
S3	T1/T2	0.89	0.92	0.18	0.12
	T3	0.93	0.57	0.12	0.16
	T4	0.86	0.78	0.15	0.26
S4	T1/T2	0.89	0.89	0.17	0.13
	T3	0.79	0.74	0.13	0.18
	T4	0.85	0.73	0.15	0.23
S5	T1/T2	0.90	0.90	0.12	0.13
	T3	0.83	0.88	0.14	0.13
	T4	0.80	0.84	0.14	0.15
S6	T1/T2	0.89	0.81	0.13	0.16
	T3	0.83	0.81	0.16	0.17
	T4	0.83	0.75	0.14	0.15
Mean		0.86	0.82	0.14	0.16
Std.		0.04	0.08	0.02	0.04

Std. = standard deviation

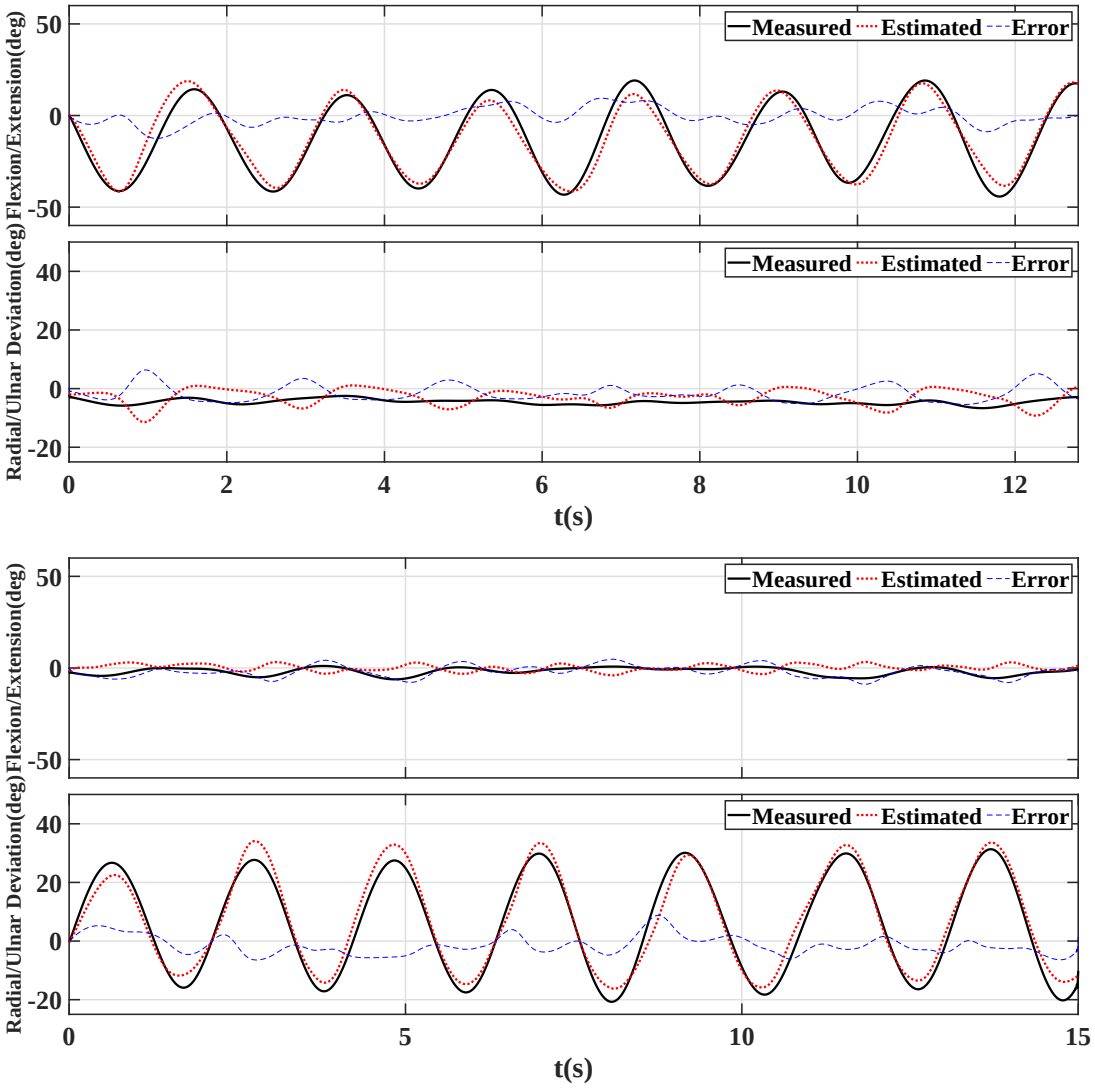

Figure 6.4: Estimation performance of the representative subject for single DoF in the contralateral case. The R^2 and NRMSE for the corresponding trials are: (left) 0.95 (0.07) for WFE, (right) 0.96 (0.08) for RUD. Errors are presented in blue dashed line

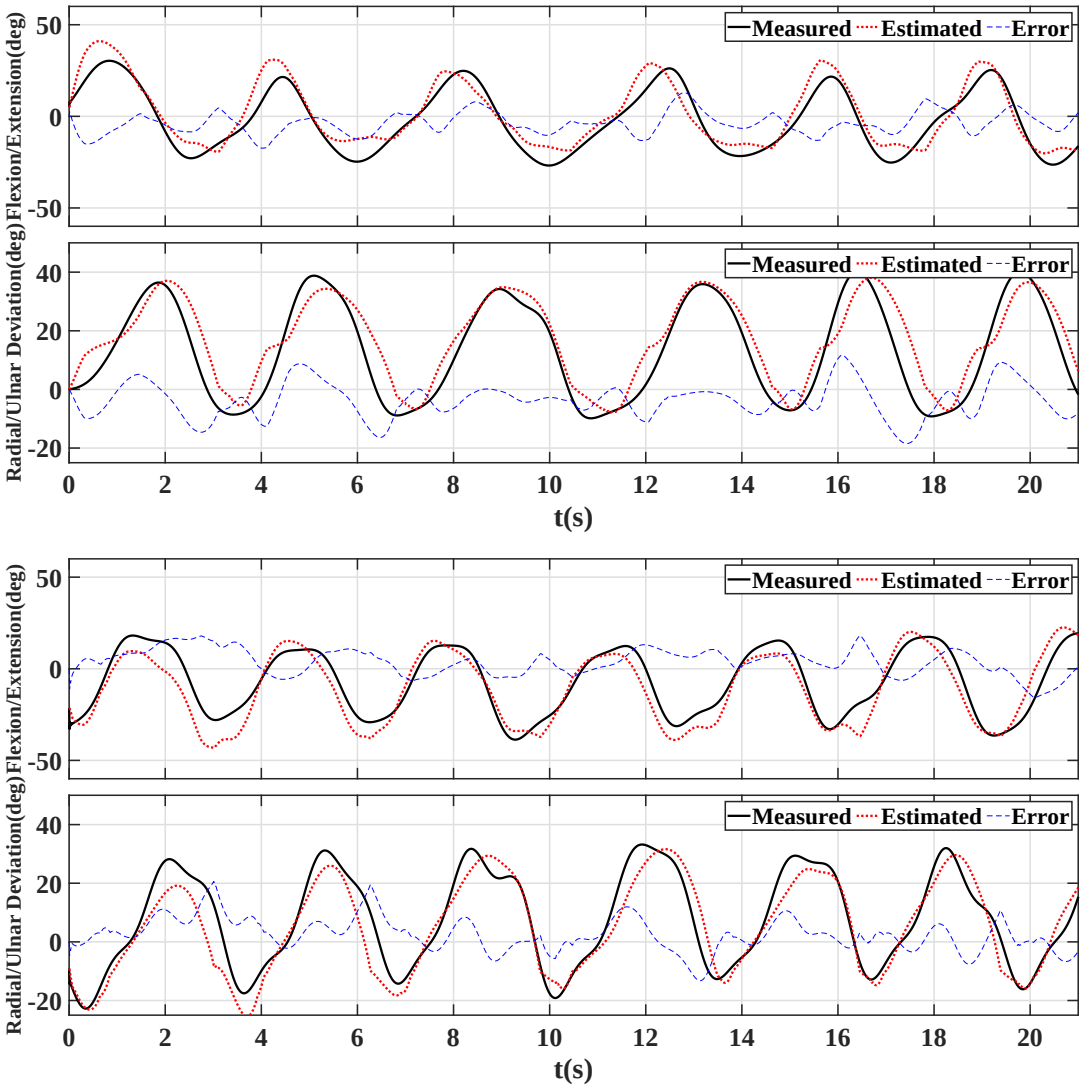

Figure 6.5: Estimation performance of the representative subject for co-contraction in the contralateral case. (Left) 0.84 (0.10) for WFE and 0.87 (0.11) for RUD and (Right) 0.86 (0.12) for WFE and 0.89 (0.10) for RUD.

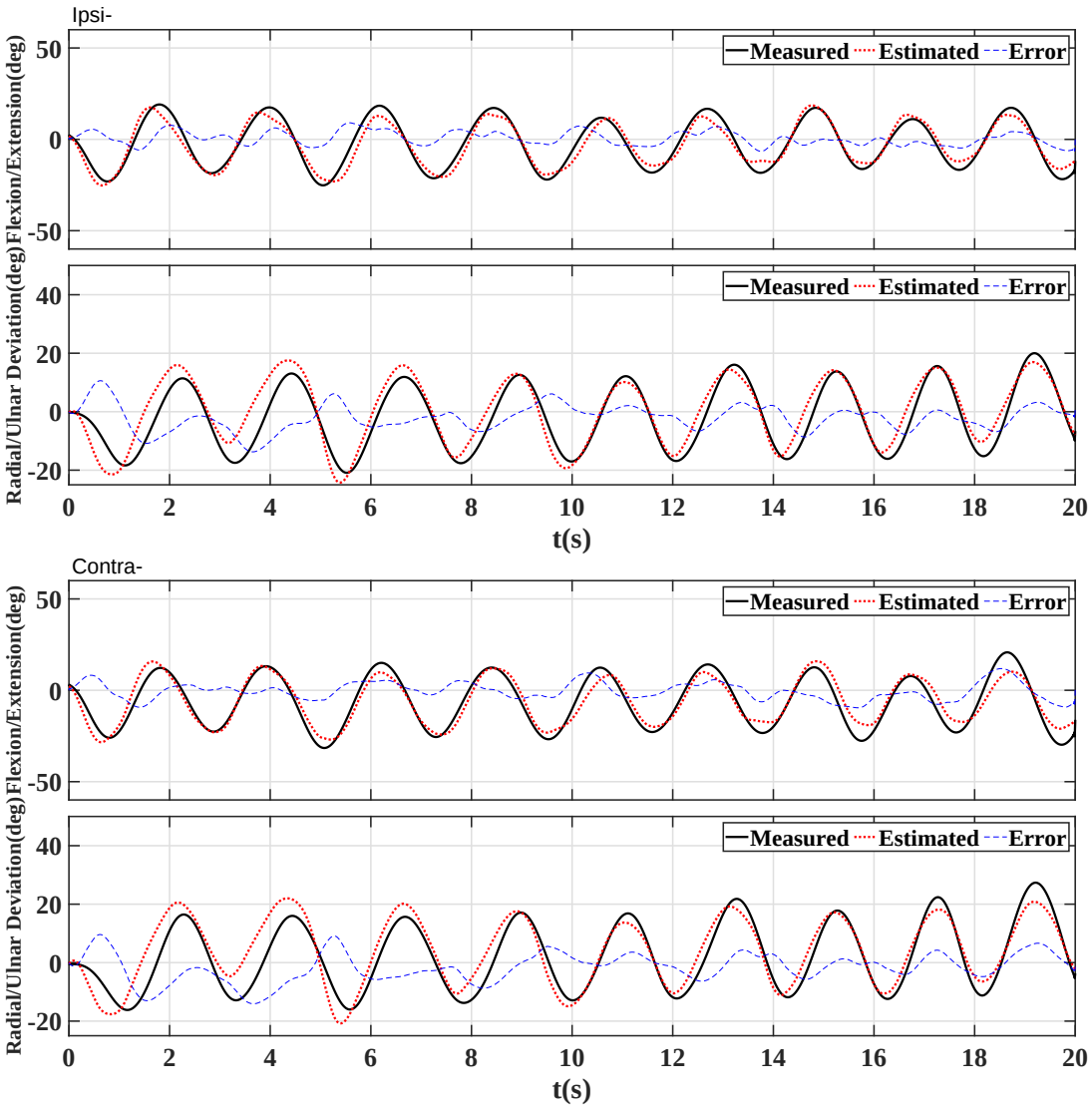

Figure 6.6: Representative example for comparison between the ipsilateral case (Top) and contralateral case (Bottom). Red dash line denotes the estimated WFE angles (top figures) and RUD angles (bottom figures), black line denote the measured joint angles. For ipsilateral case, the R^2 (NRMSE) are 0.91 (0.08) for WFE and 0.85 (0.12) for RUD, respectively. For contralateral case, the R^2 (NRMSE) are 0.89 (0.09) and 0.82 (0.12) for WFE and RUD respectively. Errors are presented in blue dashed line.

6.4 Discussion

6.4.1 Mirrored bilateral movement

The EMG signal and kinematic data are collected when the subjects perform the wrist movements using the mirrored bilateral movements train strategy. The proposed musculoskeletal model-based approach is used to estimate the multiple DoF wrist kinematics of the contralateral side using the EMG signals captured from the ipsilateral side. Muscle activations are computed from the wrist primary muscles. The experiments are conducted on the able-bodied subjects to show the feasibility of the proposed method.

The proposed musculoskeletal model-based approach is tested on the able-bodied subjects, laying the groundwork for future research on amputees. Nevertheless, it has been shown that the amputees can voluntarily produce the muscle activities to experience different movements after amputation. This suggests that the phantom arm remains the functionalities of expressing the preserved limb movements by generating relevant motor commands as if the limb is still there [179, 184]. Therefore, the EMG signals from amputees can be applied into the proposed model-based approach to estimate the phantom limb's kinematics. The experimental results demonstrate that the proposed model-based approach is able to estimate the wrist joint angles of contralateral side by using the EMG signals from ipsilateral side using the mirrored bilateral movements. This approach provides the accurate joint angular movements estimation in the contralateral case (Figure 6.3), which can be replicated for the unilateral amputees. In addition, to obtain the accurate estimation based on the user's intention, the model-based approach requires the parameters to be optimized by the objective function (equation (**??**)) and the training data. The mirrored bilateral movement training strategy plays the crucial role in the proposed approach to facilitate the para-

meter optimization, in which the kinematic data are unavailable from amputated side [174, 180].

6.4.2 Model performance

The experimental results demonstrate that the proposed EMG-driven model can respond to the able-bodied subject's intention in the simultaneous and proportional wrist joint movements. It reflects the biological process from the EMG signals to the wrist kinematics, interpreting the internal muscle active/passive force and the joint torques [131]. In the contralateral cases, the mean R^2 are 0.86 ($\pm$0.04) and 0.82 ($\pm$0.08) for WFE and RUD respectively, which is slightly lower than the ipsilateral case. Both cases have the similar NRMSE, which are 0.14 ($\pm$0.02) and 0.16 ($\pm$0.04) for ipsi and contralateral cases respectively.

For the single DoF movement trials, the estimation performance shows a high correlation and lower NRMSE than the combined movement trials. One potential issue is that the performance is affected by the crosstalk, which leads to the model treats the crosstalk signals as the muscle activities and generates the muscle force. Moreover, the passive tendon force is another issue that results in estimation errors. Besides, the subject may slightly involve the forearm pronation/supination when the combined movements are performed, which the muscle activities may deviated [19]. The primary wrist muscles are selected in this study. For the single DoF movements, the selected wrist muscles act as the antagonist and agonist pair. For example, the FCR and FCU are the flexor group and activated simultaneously. These muscles are active alone when both DoFs are actuated [139, 185]. For the amputees, it may be difficult to locate the targeted muscles after amputation. Some studies applied the High-density (HD) EMG electrodes to record the muscle activities from the amputated side[174, 175]. Therefore, the activities of the targeted muscles of the missing limb can be clustered and identified by the spatial

information [130, 139], and estimated through the muscle synergy technique [186]. State-of-the-art myoelectric control schemes are mostly based on machine learning techniques, extracting features from the captured EMG signals, training the numerical transfer functions, and then to estimate the joint angles correspondingly [174]. Although it cannot be compared with data-driven approaches, the estimation performance shows similar performance compared with the model-free approaches in terms of R^2. Muceli *et al.* reported that the overall R^2 for all DoFs has over 0.79 [174]. Jiang *el al.* showed higher R^2 in wrist flexion/extension and radial/ulnar deviation movement when only DoF was close to the maximum range of motion (mean $R^2 = 0.88$ for contralateral case) [175]. However, machine learning techniques requires a large amount of datasets to maximise the estimation performance. Pan *et al.,* reported that for the same training data, the model-based approach is significantly better performance than the artificial neural network (ANN) and linear regression (LR) algorithm [131]. Furthermore, it is proved that the musculoskeletal model-based approach is robust to the different postures. In addition, the proposed approach has a similar performance compared with [185], who proposed a neural regression mode combined with a generic musculoskeletal model to estimate the wrist joint kinematics. The mean R^2 is 0.8 for the able-bodied subjects in their study. Although they also estimated the forearm pronation/supination, the related muscles are pronator teres and musculus supinator mainly, and the effects on the flexion and deviation moments are excluded [185].

The proposed model-based approach contains several physiological parameters, which affect the model output significantly, i.e., isometric maximum force, muscle fibre length, tendon length and non-linear shape factor. The pennation angle is set to constant due to the fact it has minor effect on the model output [127]. These parameters cannot be obtained from amputees. Nevertheless, the pro-

posed model can be established for the phantom arm using the mirrored bilateral movement training strategy. The parameters are optimized through the genetic algorithm with an average optimization time of 20 minutes offline. In addition, the muscle-tendon lengths of selected muscles are determined by the regression algorithm, including the complicated combination of the wrist movements with respect to wrist flexion/extension and radial/ulnar deviation. Other approaches to generate the subject-specific muscle-tendon model by scaling the model based on the recorded data [39], where the scaling process is not suitable for the amputees. To account for the subject-specificity, the scaling coefficient is introduced for the muscle-tendon length.

The tendon compliance could hurdle the real-time application of the musculoskeletal model-based approach, i.e., numerical stiffness in muscle-tendon model [95]. The tendon is assuming stiff enough in this study. The proposed model-based approach still guarantee accurate wrist joint angles estimation in response to the surface EMG signals. An average offline computation time of a 20 seconds trial is 0.556 seconds on a desktop computer with a quad-core processor and 32GB RAM. It is indicated that the proposed model has the capability of real-time application.

6.4.3 Limitations

The proposed strategy is experimentally verified on the able-bodied subjects to show the feasibility of estimating the accurate wrist joint angles. However, there are some limitations to the current study, including 1) the performance of the proposed approach and mirrored bilateral training strategy are only tested on with a limited number of subjects. We will recruit more subjects including amputated patients for further investigation. 2) two DoFs are included in this study. We will further develop and verify the musculoskeletal model-based approach for

the movements of hand open/close and forearm rotation.

6.5 Chapter summary

In this Chapter, we proposed a musculoskeletal model to estimate the 2 DoFs wrist kinematics of the contralateral limb based on the muscle activities from the ipsilateral limb using the mirrored bilateral movements. The proposed model interpreted the biological process from the muscle activities to wrist joint angles. In the contralateral case, the proposed approach shows that the mean R^2 are 0.86 and 0.82 for the wrist flexion/extension and radial/ulnar deviation respectively. Results indicate the potential solution for simultaneous and proportional control of wrist kinematics for the unilateral amputee. Future work includes the extensions of kinematics estimation of hand open/close and forearm rotation and further validation on the amputated patient.

Chapter 7

Conclusions and Future work

This research presented the design and development of EMG-driven subject-specific musculoskeletal models for the wrist joint and eventually incorporated the EMG-driven model into the wrist robot to improve its control performance. The following research objectives were achieved. Firstly, a EMG-driven musculoskeletal model was developed for wrist flexion/extension motion, and the estimation accuracy was validated experimentally. Secondly, a sensitivity analysis was conducted to identify the influence of the physiological parameters on the estimation performance. Thirdly, a direct collocation method was proposed to optimize the subject-specific parameters efficiently. Its computational speed was evaluated and compared with the computational speed when the genetic algorithm was applied. Fourthly, the EMG-driven musculoskeletal model was incorporated with two active assistive control strategies to validate its applicability and practicality. The internal muscular states were used to identify the wrist joint stiffness which aided the adaptation method of control strategies. The performance of the control strategies were experimentally evaluated. Finally, the multiple DoF wrist EMG-driven musculoskeletal model was developed to predict the wrist flexion/extension and ulnar/radial deviation using the mirrored bilateral training strategy. The estimation accuracy was also experimentally validated. This

chapter presents the research contributions and outlines the future work resulted from this research.

7.1 Conclusions and Contributions

Development of the EMG-driven musculoskeletal model for estimation continuous wrist motion

Current approaches of the EMG-based motion intention for wrist joint are based on the model-based approach. These approaches interpret the motion intention based on the numerical functions and fail to capture the underlying muscular and skeletal information that is used for robot-aided wrist rehabilitation. Furthermore, the model-free approaches require a large amount of training data to map the EMG signal to motion intention. Chapter 3 presented the development of an EMG-driven musculoskeletal model for the wrist joint to overcome these limitations. This model comprises three sub-models to explicitly elucidate the relationships from the muscle activities to muscle force and eventually to joint motion. The genetic algorithm was utilized to obtain the subject-specific parameters, and these parameters were bound within the range to realize the physiological joint movement. With the assumption of the rigid tendon element, this model showed the feasibility of real-time computation. Experimental validation yielded that the proposed model has high predictive accuracy. This model-based approach provides valuable insights to understand the transformation between the muscle contraction and the resultant joint motion. In addition, only one calibration trial was utilized to obtain the subject-specific parameters, which indicated that this model-based approach can facilitate the rehabilitation setup process. The sensitivity analysis was also conduced in Chapter 3 to investigate the effects of physiological parameters on the estimation accuracy. It was found that the

tendon length and muscle-tendon length had high sensitivities. The optimal fibre length, maximum isometric force, moment arm and non-linear shape factor had moderate sensitivities, whereas the pennation angle had the lowest sensitivity.

Development of an effective optimization method of the wrist musculoskeletal model

The state-or-art optimization methods for the musculoskeletal model required a long period to obtain the subject-specific parameters, which leads to barriers for implementing the model-based approach in the practical scenario. Chapter 4 presented the development of an effective optimisation method to optimize the subject-specific parameters in the wrist EMG-driven musculoskeletal model and to increase the optimization speed significantly. The direction collocation method transcribed the muscle activation model, the EMG signal, the muscle activation, and joint kinematics of the wrist EMG-driven musculoskeletal model into the control and state variables. Together with constraints imposed by dynamics in the EMG-driven model, the resultant non-linear programming problem was solved efficiently by the IPOPT solver. Experimental results demonstrated that the use of the direction collocation method achieved the similar predictive accuracy to the use of the genetic algorithm. The computational speed was significantly greater than the genetic algorithm, as the optimization time were 1697 s and 75 s for the direct collocation method and the genetic algorithm respectively. This suggested that the direct collocation method has the potential to be implemented in the practical scenario. The proposed method also could be beneficial for those EMG-driven musculoskeletal models which require subject-specific parameters.

EMG-driven musculoskeletal model-based control strategies for a wrist exoskeleton

Incorporating the EMG-based approaches for the control of the wrist rehabilitation robot provides an intuitive response to the subject's motion intention. It is also suggested to incorporate the biomechanical property with the active assistive control strategy to improve the control performance [53, 110–112]. It is a challenging task to evaluate the joint stiffness in real-time. It requires time-consuming experimental work to establish the relationship between the joint stiffness, joint position and EMG signal, and the stiffness profile is varied across subjects. Chapter 5 provided a solution for the real-time estimation of wrist joint stiffness without additional cost. Furthermore, this chapter presented the development of the EMG-driven musculoskeletal model-based control strategies for a wrist exoskeleton to improve its control performance. It is the first time that the EMG-driven musculoskeletal model-based control strategies have been implemented for the wrist rehabilitation robot. Experimental validation was conducted on 12 healthy subjects. The mean passive and active joint stiffness were 0.78 Nm/rad (Std = 0.55) and 10.53 Nm/rad (std = 3.22) respectively, which were within the range of measurements reported in the literature. Results indicated that the model-based approach is capable to estimate the joint stiffness in real-time.
The adaptive cooperative control strategy was proposed, which included a PID-based position controller and an admittance controller. This control strategy was proposed to modify the reference trajectory based on the subjects' motion intention. The admittance parameters were adapted in response to the wrist joint stiffness. Experimental results demonstrated that the proposed control strategy not only achieved adequate tracking accuracy but also adapted the robot's behaviour by the consideration of the subjects' motion intention and wrist joint impedance. The proposed ACC showed the potential to enhance the training efficacy and

safety for robot-aided wrist rehabilitation. This chapter also proposed the assist-as-needed control strategy. An admittance controller was combined with a force controller to deliver the assistance. In this study, subjects were encouraged to participate the exercise by tracking a virtual trajectory. The desired trajectory was computed based on the muscular effort through the admittance controller. The robot's assistance was determined through the kinematic errors and was adapted by the joint impedance. Experimental evaluation was conducted with the adaptive parameter and with the constant parameters. Results demonstrated the proposed control strategy was able to provide the compliant assistance in accordance with subject's wrist joint stiffness. To concluded, the proposed EMG-driven musculoskeletal model control strategies provide a novel solution to incorporate subjects' motion intention and biomechanical characteristics into the robot-aided wrist rehabilitation robot.

Development of the EMG-driven musculoskeletal model for estimation multiple wrist DoFs

In Chapter 6, the EMG-driven musculoskeletal model was developed to estimate the 2 DoFs of wrist kinematics. The aim was to exploit the use of mirrored bilateral movement to estimate the wrist kinematics of the contralateral limb according to the muscle activities recorded from the ipsilateral limb. It provided a solution for the prothesis calibration. Results showed that the model-based approach provides high predictive accuracy in the contralateral case. The mean R^2 were 0.86 and 0.82 for the wrist flexion/extension and radial/ulnar deviation respectively, which indicated the potential solution for simultaneous and proportional control of wrist kinematics for the unilateral amputee. This study could also be applied for robot-aided wrist rehabilitation as discussed in previous chapters. The development of the wrist EMG-driven musculoskeletal model in this study

paves the way for future implementation on multiple DoFs wrist rehabilitation robots.

7.2 Future work

Further research should be undertaken to improve the performance of EMG-driven musculoskeletal models for robot-aided wrist rehabilitation.

1) In this research, electrodes were used to capture the muscle activities. For human wrist joint, these muscles are mainly attached at forearm. The signal quality is influenced by the muscle shift and cross-talk during the movement tasks. Future work will apply the high-density electrode, e.g., 8-by-8 array electrodes, to capture the muscle activities. More information, such as the temporal and spatial characteristics, can be obtained to establish a greater degree of accuracy in determining the muscle activation levels of the wrist primary muscles.

2) The proposed models in this thesis are 'open-loop' estimation models. Future work will explore the use of the afferent signals, e.g., the muscle spindle model and Golgi Tendon Organ model, as feedback signals to improve the estimation performance.

3) In Chapter 2, sensitivity analysis yielded the estimation accuracy was highly sensitive to the muscle-tendon length. Future work can applied magnetic Resonance Imaging technique or ultrasound technique to generate the 3D model for the subject-specific muscle-tendon length. The regression algorithm can be used to reliably interpret the 3D model with a low computational cost.

4) In Chapter 5, the model-based approach was used to estimate the wrist joint stiffness in flexion/extension. Experimental evaluation conducted on 12

healthy subjects demonstrated the feasibility of the proposed method. Future work will provide the model-based joint stiffness estimation in two-dimension, i.e., wrist flexion/extension and ulnar/radial deviation.

5) Chapter 5 presented the model-based assist-as-needed control strategy. Further improvements of the force control performance to the PAM-driven wrist exoskeleton will be carried out including PAM modelling technique and the robot's dynamics. The adaptation method will be further adjusted to provide the optimal performance based on the wrist joint impedance. Future work will implement the model-based control strategies for multiple DoFs wrist rehabilitation robots based on the developed EMG-driven musculoskeletal model in Chapter 6.

6) The EMG-driven musculoskeletal models developed in this thesis were experimentally validated on the healthy subjects. However, patients with neurological disorders may have the abnormal activation patterns and different muscular properties. Future work will recruit patients with neurological disorders to investigate the performance of the proposed model-based control strategies.

7) Further work will carry on the evaluations of the model for different sessions in the rehabilitation program using the EMG-driven musculoskeletal model. This is because that the rehabilitation is a long-time program. The EMG activation pattern varies, i.e., the EMG signal is different among the training sessions [33]. In addition, EMG signal may also vary between days. Therefore, the proposed models should be re-optimized when the estimation accuracy degrades at a certain level. Furthermore, the proposed model may provide insights into evaluating the patient's impairment at the muscular level according to the re-optimized physiological parameters between different sessions. For

instance, evaluation of the varied physiological parameters, such as isometric force, joint stiffness, provides a new perspective to assess the patient's rehabilitation outcomes.

Bibliography

[1] Health Information Translations. Assisted arm range of motion exercises. [EB/OL], 2017. https://www.healthinfotranslations.org Accessed 02 July, 2021.

[2] NHS Foundation Trust. Wrist stability and strengthening. [EB/OL]. https://www.chelwest.nhs.uk/services/therapy-services/hand-therapy Accessed 02 July, 2021.

[3] Hermano Igo Krebs, Bruce T Volpe, Dustin Williams, James Celestino, Steven K Charles, Daniel Lynch, and Neville Hogan. Robot-aided neurorehabilitation: a robot for wrist rehabilitation. *IEEE transactions on neural systems and rehabilitation engineering*, 15(3):327–335, 2007.

[4] Jakob Oblak, Imre Cikajlo, and Zlatko Matjačić. Universal haptic drive: A robot for arm and wrist rehabilitation. *IEEE Transactions on Neural Systems and Rehabilitation Engineering*, 18(3):293–302, 2009.

[5] Dong Xu, Mingming Zhang, Han Xu, Jianming Fu, Xiaolong Li, and Sheng Q Xie. Interactive compliance control of a wrist rehabilitation device (WRed) with enhanced training safety. *Journal of healthcare engineering*, 2019, 2019.

[6] Abhishek Gupta, Marcia K O'Malley, Volkan Patoglu, and Charles Burgar. Design, control and performance of ricewrist: a force feedback wrist exoskeleton for rehabilitation and training. *The International Journal of Robotics Research*, 27(2):233–251, 2008.

[7] John A Martinez, Paul Ng, Son Lu, McKenzie S Campagna, and Ozkan Celik. Design of wrist gimbal: A forearm and wrist exoskeleton for stroke rehabilitation. In *2013 IEEE 13th international conference on rehabilitation robotics (ICORR)*, pages 1–6. IEEE, 2013.

[8] Leiyu Zhang, Jianfeng Li, Ying Cui, Mingjie Dong, Bin Fang, and Pengfei Zhang. Design and performance analysis of a parallel wrist rehabilitation robot (PWRR). *Robotics and Autonomous Systems*, 125:103390, 2020.

[9] Domenico Chiaradia, Luca Tiseni, Michele Xiloyannis, Massimiliano Solazzi, Lorenzo Masia, and Antonio Frisoli. An assistive soft wrist exosuit for flexion movements with an ergonomic reinforced glove. *Frontiers in Robotics and AI*, 7:182, 2021.

[10] Hyungmin Choi, Brian Byunghyun Kang, Bong-Keun Jung, and Kyu-Jin Cho. Exo-Wrist: A soft tendon-driven wrist-wearable robot with active anchor for dart-throwing motion in hemiplegic patients. *IEEE Robotics and Automation Letters*, 4(4):4499–4506, 2019.

[11] Tomohito Higuma, Kazuo Kiguchi, and Jumpei Arata. Low-profile two-degree-of-freedom wrist exoskeleton device using multiple spring blades. *IEEE Robotics and Automation Letters*, 3(1):305–311, 2017.

[12] Wei Meng, Bo Sheng, Michael Klinger, Quan Liu, Zude Zhou, and Sheng Q Xie. Design and control of a robotic wrist orthosis for joint rehabilitation. In

2015 IEEE International Conference on Advanced Intelligent Mechatronics (AIM), pages 1235–1240. IEEE, 2015.

[13] Domenico Formica, Steven K Charles, Loredana Zollo, Eugenio Guglielmelli, Neville Hogan, and Hermano I Krebs. The passive stiffness of the wrist and forearm. *Journal of neurophysiology*, 108(4):1158–1166, 2012.

[14] Stan Durand, Christian Pierre-Yves Rohan, Taya Hamilton, Wafa Skalli, and Hermano Igo Krebs. Passive wrist stiffness: the influence of handedness. *IEEE Transactions on Biomedical Engineering*, 66(3):656–665, 2018.

[15] Hans W Axelson and K-E Hagbarth. Human motor control consequences of thixotropic changes in muscular short-range stiffness. *The Journal of physiology*, 535(1):279–288, 2001.

[16] Andrew B Leger and Theodore E Milner. Passive and active wrist joint stiffness following eccentric exercise. *European journal of applied physiology*, 82(5):472–479, 2000.

[17] Autumn L Pando, Hyunglae Lee, Will B Drake, Neville Hogan, and Steven K Charles. Position-dependent characterization of passive wrist stiffness. *IEEE Transactions on Biomedical Engineering*, 61(8):2235–2244, 2014.

[18] Melinda Rybski. *Kinesiology for occupational therapy*, volume 1. Slack Incorporated, 2004.

[19] Steven Knight Charles. *It's all in the wrist: a quantitative characterization of human wrist control*. PhD thesis, Massachusetts Institute of Technology, 2008.

[20] Stroke Association et al. *State of the nation: stroke statistics*. Stroke Association (SA), 2016.

[21] Peter Langhorne, Fiona Coupar, and Alex Pollock. Motor recovery after stroke: a systematic review. *The Lancet Neurology*, 8(8):741–754, 2009.

[22] Preeti Raghavan. Upper limb motor impairment after stroke. *Physical Medicine and Rehabilitation Clinics*, 26(4):599–610, 2015.

[23] Peter Langhorne, Julie Bernhardt, and Gert Kwakkel. Stroke rehabilitation. *The Lancet*, 377(9778):1693–1702, 2011.

[24] Ho Shing Lo and Sheng Quan Xie. Exoskeleton robots for upper-limb rehabilitation: State of the art and future prospects. *Medical engineering & physics*, 34(3):261–268, 2012.

[25] Hermano Igo Krebs, Jerome Joseph Palazzolo, Laura Dipietro, Mark Ferraro, Jennifer Krol, Keren Rannekleiv, Bruce T Volpe, and Neville Hogan. Rehabilitation robotics: Performance-based progressive robot-assisted therapy. *Autonomous robots*, 15(1):7–20, 2003.

[26] Olivier Lambercy, Ludovic Dovat, Roger Gassert, Etienne Burdet, Chee Leong Teo, and Theodore Milner. A haptic knob for rehabilitation of hand function. *IEEE Transactions on Neural Systems and Rehabilitation Engineering*, 15(3):356–366, 2007.

[27] XL Hu, KY Tong, R Song, XJ Zheng, KH Lui, WWF Leung, S Ng, and SSY Au-Yeung. Quantitative evaluation of motor functional recovery process in chronic stroke patients during robot-assisted wrist training. *Journal of Electromyography and Kinesiology*, 19(4):639–650, 2009.

[28] V Squeri, L Masia, P Giannoni, G Sandini, and P Morasso. Wrist rehabilitation in chronic stroke patients by means of adaptive, progressive robot-aided therapy. *IEEE transactions on neural systems and rehabilitation engineering*, 22(2):312–325, 2013.

[29] Roberto Colombo, Fabrizio Pisano, Alessandra Mazzone, Carmen Delconte, Silvestro Micera, M Chiara Carrozza, Paolo Dario, and Giuseppe Minuco. Design strategies to improve patient motivation during robot-aided rehabilitation. *Journal of neuroengineering and rehabilitation*, 4(1):1–12, 2007.

[30] Olivier Lambercy, Ludovic Dovat, Hong Yun, Seng Kwee Wee, Christopher WK Kuah, Karen SG Chua, Roger Gassert, Theodore E Milner, Chee Leong Teo, and Etienne Burdet. Effects of a robot-assisted training of grasp and pronation/supination in chronic stroke: a pilot study. *Journal of neuroengineering and rehabilitation*, 8(1):1–12, 2011.

[31] Craig D Takahashi, Lucy Der-Yeghiaian, Vu Le, Rehan R Motiwala, and Steven C Cramer. Robot-based hand motor therapy after stroke. *Brain*, 131(2):425–437, 2008.

[32] V Reggie Edgerton and Roland R Roy. Robotic training and spinal cord plasticity. *Brain research bulletin*, 78(1):4–12, 2009.

[33] Xiao Ling Hu, Kai-yu Tong, Rong Song, Xiu Juan Zheng, and Wallace WF Leung. A comparison between electromyography-driven robot and passive motion device on wrist rehabilitation for chronic stroke. *Neurorehabilitation and neural repair*, 23(8):837–846, 2009.

[34] Paweł Maciejasz, Jörg Eschweiler, Kurt Gerlach-Hahn, Arne Jansen-Troy, and Steffen Leonhardt. A survey on robotic devices for upper limb rehabilitation. *Journal of neuroengineering and rehabilitation*, 11(1):1–29, 2014.

[35] Mohammadhossein Saadatzi, David C Long, and Ozkan Celik. Comparison of human-robot interaction torque estimation methods in a wrist rehabilitation exoskeleton. *Journal of Intelligent & Robotic Systems*, 94(3):565–581, 2019.

[36] James Pau. *A physiological model driven neuromuscular interface for exoskeleton assisted rehabilitation.* PhD thesis, ResearchSpace@ Auckland, 2013.

[37] Luzheng Bi, Cuntai Guan, et al. A review on emg-based motor intention prediction of continuous human upper limb motion for human-robot collaboration. *Biomedical Signal Processing and Control*, 51:113–127, 2019.

[38] Jie Liu, Sang Hoon Kang, Dali Xu, Yupeng Ren, Song Joo Lee, and Li-Qun Zhang. EMG-based continuous and simultaneous estimation of arm kinematics in able-bodied individuals and stroke survivors. *Frontiers in neuroscience*, 11:480, 2017.

[39] Massimo Sartori, David G. Llyod, and Dario Farina. Neural data-driven musculoskeletal modeling for personalized neurorehabilitation technologies. *IEEE Transactions on Biomedical Engineering*, 63(5):879–893, 2016. doi: 10.1109/TBME.2016.2538296.

[40] Ye Ma, Shengquan Xie, and Yanxin Zhang. A patient-specific EMG-driven neuromuscular model for the potential use of human-inspired gait rehabilitation robots. *Computers in biology and medicine*, 70:88–98, 2016.

[41] Weiqun Wang, Weiguo Shi, Zeng-Guang Hou, Badong Chen, Xu Liang, Shixin Ren, Jiaxing Wang, and Liang Peng. Prediction of human voluntary torques based on collaborative neuromusculoskeletal modeling and adaptive

learning. *IEEE Transactions on Industrial Electronics*, 68(6):5217–5226, 2020.

[42] Zeeshan O Khokhar, Zhen G Xiao, and Carlo Menon. Surface emg pattern recognition for real-time control of a wrist exoskeleton. *Biomedical engineering online*, 9(1):1–17, 2010.

[43] Rong Song, Kai-yu Tong, Xiaoling Hu, and Wei Zhou. Myoelectrically controlled wrist robot for stroke rehabilitation. *Journal of neuroengineering and rehabilitation*, 10(1):1–8, 2013.

[44] Yihui Zhao, Zhiqiang Zhang, Zhenhong Li, Zhixin Yang, Abbas A Dehghani-Sanij, and Shengquan Xie. An EMG-driven musculoskeletal model for estimating continuous wrist motion. *IEEE Transactions on Neural Systems and Rehabilitation Engineering*, 28(12):3113–3120, 2020.

[45] Richard A Berger. The anatomy and basic biomechanics of the wrist joint. *Journal of hand therapy*, 9(2):84–93, 1996.

[46] Frank H Netter. Atlas of human anatomy. philadelphia, pa: Saunders. *Elsevier*, 548:547, 2006.

[47] Ge Wu, Frans CT Van der Helm, HEJ DirkJan Veeger, Mohsen Makhsous, Peter Van Roy, Carolyn Anglin, Jochem Nagels, Andrew R Karduna, Kevin McQuade, Xuguang Wang, et al. ISB recommendation on definitions of joint coordinate systems of various joints for the reporting of human joint motion part II: shoulder, elbow, wrist and hand. *Journal of biomechanics*, 38(5):981–992, 2005.

[48] Carolee J Winstein, Dorian K Rose, Sylvia M Tan, Rebecca Lewthwaite, Helena C Chui, and Stanley P Azen. A randomized controlled comparison

of upper-extremity rehabilitation strategies in acute stroke: a pilot study of immediate and long-term outcomes. *Archives of physical medicine and rehabilitation*, 85(4):620–628, 2004.

[49] K-C Lin, C-Y Wu, T-H Wei, Chang Gung, C-Y Lee, and J-S Liu. Effects of modified constraint-induced movement therapy on reach-to-grasp movements and functional performance after chronic stroke: a randomized controlled study. *Clinical rehabilitation*, 21(12):1075–1086, 2007.

[50] Ann M Hammer and Birgitta Lindmark. Effects of forced use on arm function in the subacute phase after stroke: a randomized, clinical pilot study. *Physical Therapy*, 89(6):526–539, 2009.

[51] Gert Kwakkel, Caroline Winters, Erwin EH Van Wegen, Rinske HM Nijland, Annette AA Van Kuijk, Anne Visser-Meily, Jurriaan De Groot, Erwin De Vlugt, J Hans Arendzen, Alexander CH Geurts, et al. Effects of unilateral upper limb training in two distinct prognostic groups early after stroke: the explicit-stroke randomized clinical trial. *Neurorehabilitation and neural repair*, 30(9):804–816, 2016.

[52] James H Cauraugh and Jeffery J Summers. Neural plasticity and bilateral movements: a rehabilitation approach for chronic stroke. *Progress in neurobiology*, 75(5):309–320, 2005.

[53] Shahid Hussain, Prashant K Jamwal, Paulette Van Vliet, and Mergen H Ghayesh. State-of-the-art robotic devices for wrist rehabilitation: Design and control aspects. *IEEE Transactions on Human-Machine Systems*, 50 (5):361–372, 2020.

[54] Andrew J McDaid. Development of an anatomical wrist therapy exoskel-

eton (aw-tex). In *2015 IEEE International Conference on Rehabilitation Robotics (ICORR)*, pages 434–439. IEEE, 2015.

[55] Ning Li, Tie Yang, Yang Yang, Peng Yu, Xiujuan Xue, Xingang Zhao, Guoli Song, Imad H Elhajj, Wenxue Wang, Ning Xi, et al. Bioinspired musculoskeletal model-based soft wrist exoskeleton for stroke rehabilitation. *Journal of Bionic Engineering*, 17(6):1163–1174, 2020.

[56] Yin-Yu Su, Ying-Lung Yu, Ching-Hui Lin, and Chao-Chieh Lan. A compact wrist rehabilitation robot with accurate force/stiffness control and misalignment adaptation. *International Journal of Intelligent Robotics and Applications*, 3(1):45–58, 2019.

[57] George Andrikopoulos, George Nikolakopoulos, and Stamatis Manesis. Design and development of an exoskeletal wrist prototype via pneumatic artificial muscles. *Meccanica*, 50(11):2709–2730, 2015.

[58] Nicholas W Bartlett, Valentina Lyau, William A Raiford, Dónal Holland, Joshua B Gafford, Theresa D Ellis, and Conor J Walsh. A soft robotic orthosis for wrist rehabilitation. *Journal of Medical Devices*, 9(3), 2015.

[59] Harald Aschemann and Dominik Schindele. Comparison of model-based approaches to the compensation of hysteresis in the force characteristic of pneumatic muscles. *IEEE Transactions on Industrial Electronics*, 61(7): 3620–3629, 2013.

[60] James Hope and Andrew McDaid. Development of wearable wrist and forearm exoskeleton with shape memory alloy actuators. *Journal of Intelligent & Robotic Systems*, 86(3-4):397, 2017.

[61] Kang Xiang Khor, Patrick Jun Hua Chin, Che Fai Yeong, Eileen Lee Ming Su, Aqilah Leela T Narayanan, Hisyam Abdul Rahman, and Qamer Iqbal

Khan. Portable and reconfigurable wrist robot improves hand function for post-stroke subjects. *IEEE Transactions on Neural Systems and Rehabilitation Engineering*, 25(10):1864–1873, 2017.

[62] Stefan Hesse, Gotthard Schulte-Tigges, Matthias Konrad, Anita Bardeleben, and Cordula Werner. Robot-assisted arm trainer for the passive and active practice of bilateral forearm and wrist movements in hemiparetic subjects. *Archives of physical medicine and rehabilitation*, 84(6):915–920, 2003.

[63] Kai Keng Ang, Cuntai Guan, Kok Soon Phua, Chuanchu Wang, Longjiang Zhou, Ka Yin Tang, Gopal J Ephraim Joseph, Christopher Wee Keong Kuah, and Karen Sui Geok Chua. Brain-computer interface-based robotic end effector system for wrist and hand rehabilitation: results of a three-armed randomized controlled trial for chronic stroke. *Frontiers in neuroengineering*, 7:30, 2014.

[64] Hyung Seok Nam, Sukgyu Koh, Yoon Jae Kim, Jaewon Beom, Woo Hyung Lee, Shi-Uk Lee, and Sungwan Kim. Biomechanical reactions of exoskeleton neurorehabilitation robots in spastic elbows and wrists. *IEEE Transactions on Neural Systems and Rehabilitation Engineering*, 25(11):2196–2203, 2017.

[65] Craig G McDonald, Jennifer L Sullivan, Troy A Dennis, and Marcia K O'Malley. A myoelectric control interface for upper-limb robotic rehabilitation following spinal cord injury. *IEEE Transactions on Neural Systems and Rehabilitation Engineering*, 28(4):978–987, 2020.

[66] Ali Utku Pehlivan, Fabrizio Sergi, and Marcia K O'Malley. A subject-adaptive controller for wrist robotic rehabilitation. *IEEE/ASME Transactions on Mechatronics*, 20(3):1338–1350, 2014.

[67] Ali Utku Pehlivan, Dylan P Losey, and Marcia K O'Malley. Minimal assist-as-needed controller for upper limb robotic rehabilitation. *IEEE Transactions on Robotics*, 32(1):113–124, 2015.

[68] Erhan Akdoğan, Mehmet Emin Aktan, Ahmet Taha Koru, M Selçuk Arslan, Murat Atlıhan, and Banu Kuran. Hybrid impedance control of a robot manipulator for wrist and forearm rehabilitation: Performance analysis and clinical results. *Mechatronics*, 49:77–91, 2018.

[69] Patricia Staubli, Tobias Nef, Verena Klamroth-Marganska, and Robert Riener. Effects of intensive arm training with the rehabilitation robot armin ii in chronic stroke patients: four single-cases. *Journal of neuroengineering and rehabilitation*, 6(1):1–10, 2009.

[70] Domenico Buongiorno, Edoardo Sotgiu, Daniele Leonardis, Simone Marcheschi, Massimiliano Solazzi, and Antonio Frisoli. Wres: a novel 3 dof wrist exoskeleton with tendon-driven differential transmission for neuro-rehabilitation and teleoperation. *IEEE Robotics and Automation Letters*, 3 (3):2152–2159, 2018.

[71] Farshid Amirabdollahian, Serdar Ates, Angelo Basteris, Alfredo Cesario, Jaap Buurke, H Hermens, Dennis Hofs, Ellinor Johansson, Gail Mountain, Nasrin Nasr, et al. Design, development and deployment of a hand/wrist exoskeleton for home-based rehabilitation after stroke-script project. *Robotica*, 32(8):1331–1346, 2014.

[72] Laura Marchal-Crespo and David J Reinkensmeyer. Review of control strategies for robotic movement training after neurologic injury. *Journal of neuroengineering and rehabilitation*, 6(1):1–15, 2009.

[73] Kevin M Lynch and Frank C Park. *Modern Robotics*. Cambridge University Press, 2017.

[74] Amy A Blank, James A French, Ali Utku Pehlivan, and Marcia K O'Malley. Current trends in robot-assisted upper-limb stroke rehabilitation: promoting patient engagement in therapy. *Current physical medicine and rehabilitation reports*, 2(3):184–195, 2014.

[75] Xiaoyu Liu, Yuanjie Zhu, Hongqiang Huo, Pengxu Wei, Lizhen Wang, Aoran Sun, Chaoyi Hu, Xiaofei Yin, Zeping Lv, and Yubo Fan. Design of virtual guiding tasks with haptic feedback for assessing the wrist motor function of patients with upper motor neuron lesions. *IEEE Transactions on Neural Systems and Rehabilitation Engineering*, 27(5):984–994, 2019.

[76] Qing Miao, Mingming Zhang, Jinghui Cao, and Sheng Q Xie. Reviewing high-level control techniques on robot-assisted upper-limb rehabilitation. *Advanced Robotics*, 32(24):1253–1268, 2018.

[77] Lorenzo Masia, Maura Casadio, Psiche Giannoni, Giulio Sandini, and Pietro Morasso. Performance adaptive training control strategy for recovering wrist movements in stroke patients: a preliminary, feasibility study. *Journal of neuroengineering and rehabilitation*, 6(1):1–11, 2009.

[78] David A Winter. *Biomechanics and motor control of human movement*. John Wiley & Sons, 2009.

[79] John V Basmajian. Muscles alive. their functions revealed by electromyography. *Academic Medicine*, 37(8):802, 1962.

[80] Mamun Bin Ibne Reaz, M Sazzad Hussain, and Faisal Mohd-Yasin. Techniques of emg signal analysis: detection, processing, classification and applications. *Biological procedures online*, 8(1):11–35, 2006.

[81] Peter R Cavanagh and Paavo V Komi. Electromechanical delay in human skeletal muscle under concentric and eccentric contractions. *European journal of applied physiology and occupational physiology*, 42(3):159–163, 1979.

[82] Aaron J Young, Lauren H Smith, Elliott J Rouse, and Levi J Hargrove. Classification of simultaneous movements using surface EMG pattern recognition. *IEEE Transactions on Biomedical Engineering*, 60(5):1250–1258, 2012.

[83] Youngjin Na, Hyunjong Lee, and Suncheol Kwon. Investigating the effects of long-term contractions on myoelectric recognition of wrist movements from stroke patients. *International Journal of Precision Engineering and Manufacturing*, 21:1771–1779, 2020.

[84] Jie Liu, Yupeng Ren, Dali Xu, Sang Hoon Kang, and Li-Qun Zhang. EMG-based real-time linear-nonlinear cascade regression decoding of shoulder, elbow, and wrist movements in able-bodied persons and stroke survivors. *IEEE Transactions on Biomedical Engineering*, 67(5):1272–1281, 2019.

[85] Ergin Kilic. EMG based neural network and admittance control of an active wrist orthosis. *Journal of Mechanical Science and Technology*, 31(12):6093–6106, 2017.

[86] Kazuo Kiguchi and Yoshiaki Hayashi. An EMG-based control for an upper-limb power-assist exoskeleton robot. *IEEE Transactions on Systems, Man, and Cybernetics, Part B (Cybernetics)*, 42(4):1064–1071, 2012.

[87] Felix E Zajac. Muscle and tendon: properties, models, scaling, and application to biomechanics and motor control. *Critical reviews in biomedical engineering*, 17(4):359–411, 1989.

[88] Thomas S Buchanan, David G Lloyd, Kurt Manal, and Thor F Besier. Neuromusculoskeletal modeling: estimation of muscle forces and joint moments and movements from measurements of neural command. *Journal of applied biomechanics*, 20(4):367–395, 2004.

[89] Qi Shao, Daniel N Bassett, Kurt Manal, and Thomas S Buchanan. An emg-driven model to estimate muscle forces and joint moments in stroke patients. *Computers in biology and medicine*, 39(12):1083–1088, 2009.

[90] Massimo Sartori, Monica Reggiani, Dario Farina, and David G Lloyd. Emg-driven forward-dynamic estimation of muscle force and joint moment about multiple degrees of freedom in the human lower extremity. *PloS one*, 7(12): e52618, 2012.

[91] James WL Pau, Shane SQ Xie, and Andrew J Pullan. Neuromuscular interfacing: Establishing an EMG-driven model for the human elbow joint. *IEEE Transactions on biomedical engineering*, 59(9):2586–2593, 2012.

[92] Archibald Vivian Hill. The heat of shortening and the dynamic constants of muscle. *Proceedings of the Royal Society of London. Series B-Biological Sciences*, 126(843):136–195, 1938.

[93] Terry KK Koo and Arthur FT Mak. Feasibility of using emg driven neuromusculoskeletal model for prediction of dynamic movement of the elbow. *Journal of electromyography and kinesiology*, 15(1):12–26, 2005.

[94] David G Lloyd and Thor F Besier. An emg-driven musculoskeletal model to estimate muscle forces and knee joint moments in vivo. *Journal of biomechanics*, 36(6):765–776, 2003.

[95] Matthew Millard, Thomas Uchida, Ajay Seth, and Scott L Delp. Flexing

computational muscle: modeling and simulation of musculotendon dynamics. *Journal of biomechanical engineering*, 135(2), 2013.

[96] Scott L Delp, Frank C Anderson, Allison S Arnold, Peter Loan, Ayman Habib, Chand T John, Eran Guendelman, and Darryl G Thelen. Opensim: open-source software to create and analyze dynamic simulations of movement. *IEEE transactions on biomedical engineering*, 54(11):1940–1950, 2007.

[97] Scott L Delp and J Peter Loan. A graphics-based software system to develop and analyze models of musculoskeletal structures. *Computers in biology and medicine*, 25(1):21–34, 1995.

[98] Michael Damsgaard, John Rasmussen, Søren Tørholm Christensen, Egidijus Surma, and Mark De Zee. Analysis of musculoskeletal systems in the anybody modeling system. *Simulation Modelling Practice and Theory*, 14(8):1100–1111, 2006.

[99] Massimo Sartori, Monica Reggiani, Antonie J van den Bogert, and David G Lloyd. Estimation of musculotendon kinematics in large musculoskeletal models using multidimensional b-splines. *Journal of biomechanics*, 45(3): 595–601, 2012.

[100] Dustin L Crouch and He Huang. Lumped-parameter electromyogram-driven musculoskeletal hand model: A potential platform for real-time prosthesis control. *Journal of biomechanics*, 49(16):3901–3907, 2016.

[101] Christian Fleischer and Günter Hommel. A human–exoskeleton interface utilizing electromyography. *IEEE Transactions on Robotics*, 24(4):872–882, 2008.

[102] Guillaume Durandau, Dario Farina, Guillermo Asín-Prieto, Iris Dimbwadyo-Terrer, Sergio Lerma-Lara, Jose L Pons, Juan C Moreno, and Massimo Sartori. Voluntary control of wearable robotic exoskeletons by patients with paresis via neuromechanical modeling. *Journal of neuroengineering and rehabilitation*, 16(1):1–18, 2019.

[103] Shaowei Yao, Yu Zhuang, Zhijun Li, and Rong Song. Adaptive admittance control for an ankle exoskeleton using an emg-driven musculoskeletal model. *Frontiers in neurorobotics*, 12:16, 2018.

[104] Dustin L Crouch and He Helen Huang. Musculoskeletal model-based control interface mimics physiologic hand dynamics during path tracing task. *Journal of neural engineering*, 14(3):036008, 2017.

[105] Dimitra Blana, Edward K Chadwick, Antonie J van den Bogert, and Wendy M Murray. Real-time simulation of hand motion for prosthesis control. *Computer methods in biomechanics and biomedical engineering*, 20 (5):540–549, 2017.

[106] Massimo Sartori, Guillaume Durandau, Strahinja Došen, and Dario Farina. Robust simultaneous myoelectric control of multiple degrees of freedom in wrist-hand prostheses by real-time neuromusculoskeletal modeling. *Journal of neural engineering*, 15(6):066026, 2018.

[107] Francesco M Colacino, Rustighi Emiliano, and Brian R Mace. Subject-specific musculoskeletal parameters of wrist flexors and extensors estimated by an emg-driven musculoskeletal model. *Medical engineering & physics*, 34(5):531–540, 2012.

[108] Xu Zhang and Ping Zhou. High-density myoelectric pattern recognition

toward improved stroke rehabilitation. *IEEE Transactions on Biomedical Engineering*, 59(6):1649–1657, 2012.

[109] Xugang Xi, Wenjun Jiang, Xian Hua, Huijiao Wang, Chen Yang, Yun-Bo Zhao, Seyed M Miran, and Zhizeng Luo. Simultaneous and continuous estimation of joint angles based on surface electromyography state-space model. *IEEE Sensors Journal*, 21(6):8089–8099, 2021.

[110] Neville Hogan and Stephen P Buerger. Impedance and interaction control. In *Robotics and automation handbook*, pages 375–398. CRC press, 2018.

[111] Fares J Abu-Dakka and Matteo Saveriano. Variable impedance control and learningâ€"a review. *Frontiers in Robotics and AI*, 7, 2020.

[112] Mingming Zhang, Sheng Q Xie, Xiaolong Li, Guoli Zhu, Wei Meng, Xiaolin Huang, and Allan J Veale. Adaptive patient-cooperative control of a compliant ankle rehabilitation robot (CARR) with enhanced training safety. *IEEE Transactions on Industrial Electronics*, 65(2):1398–1407, 2017.

[113] Jinxian Qi, Guozhang Jiang, Gongfa Li, Ying Sun, and Bo Tao. Intelligent human-computer interaction based on surface emg gesture recognition. *Ieee Access*, 7:61378–61387, 2019.

[114] Ryan J Downey, Manelle Merad, Eric J Gonzalez, and Warren E Dixon. The time-varying nature of electromechanical delay and muscle control effectiveness in response to stimulation-induced fatigue. *IEEE Transactions on Neural Systems and Rehabilitation Engineering*, 25(9):1397–1408, 2016.

[115] Di Ao, Rong Song, and JinWu Gao. Movement performance of human–robot cooperation control based on emg-driven hill-type and proportional models for an ankle power-assist exoskeleton robot. *IEEE Transactions on Neural Systems and Rehabilitation Engineering*, 25(8):1125–1134, 2016.

[116] Zhang Lei. An upper limb movement estimation from electromyography by using bp neural network. *Biomed Signal Process Control*, 49:434–439, 2019.

[117] Ulysse Côté-Allard, Cheikh Latyr Fall, Alexandre Drouin, Alexandre Campeau-Lecours, Clément Gosselin, Kyrre Glette, François Laviolette, and Benoit Gosselin. Deep learning for electromyographic hand gesture signal classification using transfer learning. *IEEE Transactions on Neural Systems and Rehabilitation Engineering*, 27(4):760–771, 2019.

[118] Edward K Chadwick, Dimitra Blana, Antonie J van den Bogert, Robert F Kirsch, et al. A real-time, 3-d musculoskeletal model for dynamic simulation of arm movements. *IEEE Transactions on Biomedical Engineering*, 56(4): 941–948, 2008.

[119] Thomas S Buchanan, David G Lloyd, Kurt Manal, and Thor F Besier. Neuromusculoskeletal modeling: estimation of muscle forces and joint moments and movements from measurements of neural command. *Journal of applied biomechanics*, 20(4):367–395, 2004.

[120] Darryl G Thelen. Adjustment of muscle mechanics model parameters to simulate dynamic contractions in older adults. *J. Biomech. Eng.*, 125(1): 70–77, 2003.

[121] Lisa Margaret Schutte. *Using musculoskeletal models to explore strategies for improving performance in electrical stimulation-induced leg cycle ergometry*. PhD thesis, Stanford University, 1993.

[122] John W Ramsay, Betsy V Hunter, and Roger V Gonzalez. Muscle moment arm and normalized moment contributions as reference data for musculoskeletal elbow and wrist joint models. *J Biomech*, 42(4):463–473, 2009.

[123] John J Craig. *Introduction to robotics: mechanics and control, 3/E*. Pearson Education India, 2009.

[124] Theodore E Milner and Caroline Cloutier. Damping of the wrist joint during voluntary movement. *Experimental brain research*, 122(3):309–317, 1998.

[125] Richard L Lieber, Babak M Fazeli, and Michael J Botte. Architecture of selected wrist flexor and extensor muscles. *J HAND SURG*, 15(2):244–250, 1990.

[126] Katherine R Saul, Xiao Hu, Craig M Goehler, Meghan E Vidt, Melissa Daly, Anca Velisar, and Wendy M Murray. Benchmarking of dynamic simulation predictions in two software platforms using an upper limb musculoskeletal model. *Computer methods in biomechanics and biomedical engineering*, 18 (13):1445–1458, 2015.

[127] Carol Y Scovil and Janet L Ronsky. Sensitivity of a Hill-based muscle model to perturbations in model parameters. *Journal of biomechanics*, 39 (11):2055–2063, 2006.

[128] D Stegeman and H Hermens. Standards for surface electromyography: The european project surface EMG for non-invasive assessment of muscles (seniam). *Enschede: Roessingh Research and Development*, pages 108–12, 2007.

[129] Milad Masjedi and Lynsey D Duffell. Dynamic analysis of the upper limb during activities of daily living: Comparison of methodologies. *Proc Inst Mech Eng H*, 227(12):1275–1283, 2013.

[130] Kostas Nizamis, Noortje HM Rijken, Robbert Van Middelaar, João Neto, Bart FJM Koopman, and Massimo Sartori. Characterization of forearm

muscle activation in duchenne muscular dystrophy via high-density electromyography: a case study on the implications for myoelectric control. *Frontiers in neurology*, 11:231, 2020.

[131] Lizhi Pan, Dustin L Crouch, and He Huang. Comparing EMG-based human-machine interfaces for estimating continuous, coordinated movements. *IEEE Transactions on Neural Systems and Rehabilitation Engineering*, 27(10):2145–2154, 2019.

[132] Jianda Han, Qichuan Ding, Anbin Xiong, and Xingang Zhao. A state-space EMG model for the estimation of continuous joint movements. *IEEE Transactions on Industrial Electronics*, 62(7):4267–4275, 2015.

[133] Dimitra Blana, Antonie J Van Den Bogert, Wendy M Murray, Amartya Ganguly, Agamemnon Krasoulis, Kianoush Nazarpour, and Edward K Chadwick. Model-based control of individual finger movements for prosthetic hand function. *IEEE Transactions on Neural Systems and Rehabilitation Engineering*, 28(3):612–620, 2020.

[134] Vincenzo Carbone, MM van der Krogt, Hubertus FJM Koopman, and N Verdonschot. Sensitivity of subject-specific models to hill muscle–tendon model parameters in simulations of gait. *J Biomech*, 49(9):1953–1960, 2016.

[135] Friedl De Groote, Anke Van Campen, Ilse Jonkers, and Joris De Schutter. Sensitivity of dynamic simulations of gait and dynamometer experiments to hill muscle model parameters of knee flexors and extensors. *J Biomech*, 43(10):1876–1883, 2010.

[136] Yoann Blache, Benjamin Michaud, Isabelle Rogowski, Karine Monteil, and Mickaël Begon. Sensitivity of shoulder musculoskeletal model predictions to

muscle–tendon properties. *IEEE Transactions on Biomedical Engineering*, 66(5):1309–1317, 2018.

[137] CR Winby, DG Lloyd, and TB Kirk. Evaluation of different analytical methods for subject-specific scaling of musculotendon parameters. *Journal of biomechanics*, 41(8):1682–1688, 2008.

[138] Luca Modenese, Elena Ceseracciu, Monica Reggiani, and David G Lloyd. Estimation of musculotendon parameters for scaled and subject specific musculoskeletal models using an optimization technique. *J Biomech*, 49(2): 141–148, 2016.

[139] Massimo Sartori, Justin Van De Riet, and Dario Farina. Estimation of phantom arm mechanics about four degrees of freedom after targeted muscle reinnervation. *IEEE Transactions on Medical Robotics and Bionics*, 1(1): 58–64, 2019.

[140] Domenico Buongiorno, Michele Barsotti, Francesco Barone, Vitoantonio Bevilacqua, and Antonio Frisoli. A linear approach to optimize an emg-driven neuromusculoskeletal model for movement intention detection in myo-control: A case study on shoulder and elbow joints. *Frontiers in neurorobotics*, 12:74, 2018.

[141] John T Betts. *Practical methods for optimal control and estimation using nonlinear programming*. SIAM, 2010.

[142] Sina Porsa, Yi-Chung Lin, and Marcus G Pandy. Direct methods for predicting movement biomechanics based upon optimal control theory with implementation in opensim. *Annals of biomedical engineering*, 44(8):2542–2557, 2016.

[143] Matthew L Kaplan and Jean H Heegaard. Predictive algorithms for neuromuscular control of human locomotion. *Journal of Biomechanics*, 34(8): 1077–1083, 2001.

[144] Friedl De Groote, Allison L Kinney, Anil V Rao, and Benjamin J Fregly. Evaluation of direct collocation optimal control problem formulations for solving the muscle redundancy problem. *Annals of biomedical engineering*, 44(10):2922–2936, 2016.

[145] Yi-Chung Lin and Marcus G Pandy. Three-dimensional data-tracking dynamic optimization simulations of human locomotion generated by direct collocation. *Journal of biomechanics*, 59:1–8, 2017.

[146] Antoine Falisse, Sam Van Rossom, Ilse Jonkers, and Friedl De Groote. Emg-driven optimal estimation of subject-specific hill model muscle–tendon parameters of the knee joint actuators. *IEEE Transactions on Biomedical Engineering*, 64(9):2253–2262, 2016.

[147] Antonie J van den Bogert, Dimitra Blana, and Dieter Heinrich. Implicit methods for efficient musculoskeletal simulation and optimal control. *Procedia Iutam*, 2:297–316, 2011.

[148] Jeffrey Berning, Gerard E Francisco, Shuo-Hsiu Chang, Benjamin J Fregly, and Marcia K O'Malley. Myoelectric control and neuromusculoskeletal modeling: Complementary technologies for rehabilitation robotics. *Current Opinion in Biomedical Engineering*, page 100313, 2021.

[149] Nicola Lotti, Michele Xiloyannis, Guillaume Durandau, Elisa Galofaro, Vittorio Sanguineti, Lorenzo Masia, and Massimo Sartori. Adaptive model-based myoelectric control for a soft wearable arm exosuit: A new generation

of wearable robot control. *IEEE Robotics & Automation Magazine*, 27(1): 43–53, 2020.

[150] Eric T Wolbrecht, Vicky Chan, David J Reinkensmeyer, and James E Bobrow. Optimizing compliant, model-based robotic assistance to promote neurorehabilitation. *IEEE Transactions on Neural Systems and Rehabilitation Engineering*, 16(3):286–297, 2008.

[151] M. Sharifi, A. Zakerimanesh, J. K. Mehr, A. Torabi, V. K. Mushahwar, and M. Tavakoli. Impedance variation and learning strategies in human-robot interaction. *IEEE Transactions on Cybernetics*, pages 1–14, 2021. ISSN 2168-2275. doi: 10.1109/TCYB.2020.3043798.

[152] Toru Tsumugiwa, Ryuichi Yokogawa, and Kei Hara. Variable impedance control based on estimation of human arm stiffness for human-robot cooperative calligraphic task. In *Proceedings 2002 IEEE International Conference on Robotics and Automation (Cat. No. 02CH37292)*, volume 1, pages 644–650. IEEE, 2002.

[153] Peidong Liang, Chenguang Yang, Zhijun Li, and Ruifeng Li. Writing skills transfer from human to robot using stiffness extracted from semg. In *2015 IEEE international conference on cyber technology in automation, control, and intelligent systems (CYBER)*, pages 19–24. IEEE, 2015.

[154] Zhijun Li, Zhicong Huang, Wei He, and Chun-Yi Su. Adaptive impedance control for an upper limb robotic exoskeleton using biological signals. *IEEE Transactions on Industrial Electronics*, 64(2):1664–1674, 2016.

[155] Theodore E Milner and Caroline Cloutier. Compensation for mechanically unstable loading in voluntary wrist movement. *Experimental Brain Research*, 94(3):522–532, 1993.

[156] Andrea Zonnino and Fabrizio Sergi. Model-based analysis of the stiffness of the wrist joint in active and passive conditions. *Journal of biomechanical engineering*, 141(4), 2019.

[157] Lei Cui, Eric J Perreault, Huub Maas, and Thomas G Sandercock. Modeling short-range stiffness of feline lower hindlimb muscles. *Journal of biomechanics*, 41(9):1945–1952, 2008.

[158] Mark Halaki, Nicholas O'Dwyer, and Ian Cathers. Systematic nonlinear relations between displacement amplitude and joint mechanics at the human wrist. *Journal of biomechanics*, 39(12):2171–2182, 2006.

[159] John ZZ Chew, Simon C Gandevia, and Richard C Fitzpatrick. Postural control at the human wrist. *The Journal of physiology*, 586(5):1265–1275, 2008.

[160] Alfred C Schouten, Erwin de Vlugt, JJ Bob van Hilten, and Frans CT van der Helm. Design of a torque-controlled manipulator to analyse the admittance of the wrist joint. *Journal of neuroscience methods*, 154(1-2): 134–141, 2006.

[161] Asbjørn Klomp, Jurriaan H De Groot, Erwin De Vlugt, Carel GM Meskers, J Hans Arendzen, and Frans CT Van Der Helm. Perturbation amplitude affects linearly estimated neuromechanical wrist joint properties. *Ieee Transactions on Biomedical Engineering*, 61(4):1005–1014, 2013.

[162] Kyungbin Park, Pyung-Hun Chang, and Sang Hoon Kang. In vivo estimation of human forearm and wrist dynamic properties. *IEEE Transactions on Neural Systems and Rehabilitation Engineering*, 25(5):436–446, 2016.

[163] Robert Riener, Lars Lunenburger, Saso Jezernik, Martin Anderschitz, Gery Colombo, and Volker Dietz. Patient-cooperative strategies for robot-aided

treadmill training: first experimental results. *IEEE transactions on neural systems and rehabilitation engineering*, 13(3):380–394, 2005.

[164] Mohammad Habibur Rahman, Md Jahidur Rahman, OL Cristobal, Maarouf Saad, Jean-Pierre Kenné, and Philippe S Archambault. Development of a whole arm wearable robotic exoskeleton for rehabilitation and to assist upper limb movements. *Robotica*, 33(1):19–39, 2015.

[165] Prashant Jamwal. *Design analysis and control of wearable ankle rehabilitation robot*. PhD thesis, ResearchSpace@ Auckland, 2011.

[166] Rui Wu, He Zhang, Tao Peng, Le Fu, and Jie Zhao. Variable impedance interaction and demonstration interface design based on measurement of arm muscle co-activation for demonstration learning. *Biomedical Signal Processing and Control*, 51:8–18, 2019.

[167] Thomas R Kurfess. *Robotics and automation handbook*. CRC press, 2018.

[168] Yu Su, Mark H Fisher, Andrzej Wolczowski, G Duncan Bell, David J Burn, and Robert X Gao. Towards an EMG-controlled prosthetic hand using a 3-d electromagnetic positioning system. *IEEE transactions on instrumentation and measurement*, 56(1):178–186, 2007.

[169] Max Ortiz-Catalan, Bo Håkansson, and Rickard Brånemark. Real-time and simultaneous control of artificial limbs based on pattern recognition algorithms. *IEEE Transactions on Neural Systems and Rehabilitation Engineering*, 22(4):756–764, 2014.

[170] Andrea Tigrini, Luca Alberto Pettinari, Federica Verdini, Sandro Fioretti, and Alessandro Mengarelli. Shoulder motion intention detection through myoelectric pattern recognition. *IEEE Sens. Lett*, 5(8):1–4, 2021.

[171] S Micera, J Carpaneto, F Posteraro, L Cenciotti, Mirjana Popovic, and P Dario. Characterization of upper arm synergies during reaching tasks in able-bodied and hemiparetic subjects. *Clin Biomech*, 20(9):939–946, 2005.

[172] Lauren H Smith, Todd A Kuiken, and Levi J Hargrove. Evaluation of linear regression simultaneous myoelectric control using intramuscular emg. *IEEE Transactions on Biomedical Engineering*, 63(4):737–746, 2015.

[173] Johnny LG Nielsen, Steffen Holmgaard, Ning Jiang, Kevin B Englehart, Dario Farina, and Phil A Parker. Simultaneous and proportional force estimation for multifunction myoelectric prostheses using mirrored bilateral training. *IEEE Transactions on Biomedical Engineering*, 58(3):681–688, 2010.

[174] Silvia Muceli and Dario Farina. Simultaneous and proportional estimation of hand kinematics from EMG during mirrored movements at multiple degrees-of-freedom. *IEEE transactions on neural systems and rehabilitation engineering*, 20(3):371–378, 2011.

[175] Ning Jiang, Johnny LG Vest-Nielsen, Silvia Muceli, and Dario Farina. EMG-based simultaneous and proportional estimation of wrist/hand kinematics in uni-lateral trans-radial amputees. *J. Neuroeng. Rehabilitation*, 9(1):42, 2012.

[176] Janne M Hahne, Felix Biessmann, Ning Jiang, Hubertus Rehbaum, Dario Farina, Frank C Meinecke, K-R Müller, and Lucas C Parra. Linear and nonlinear regression techniques for simultaneous and proportional myoelectric control. *IEEE Transactions on Neural Systems and Rehabilitation Engineering*, 22(2):269–279, 2014.

[177] Janne M Hahne, Sven Dähne, Han-Jeong Hwang, Klaus-Robert Müller, and Lucas C Parra. Concurrent adaptation of human and machine improves simultaneous and proportional myoelectric control. *IEEE Transactions on Neural Systems and Rehabilitation Engineering*, 23(4):618–627, 2015.

[178] Qin Zhang, Te Pi, Runfeng Liu, and Caihua Xiong. Simultaneous and proportional estimation of multijoint kinematics from EMG signals for myocontrol of robotic hands. *IEEE ASME Trans Mechatron*, 25(4):1953–1960, 2020.

[179] Catherine Mercier, Karen T Reilly, Claudia D Vargas, Antoine Aballea, and Angela Sirigu. Mapping phantom movement representations in the motor cortex of amputees. *Brain*, 129(8):2202–2210, 2006.

[180] Shingo Oda. Motor control for bilateral muscular contractions in humans. *The Japanese journal of physiology*, 47(6):487–498, 1997.

[181] CP Neu, 3rd Crisco, JJ, and SW Wolfe. In vivo kinematic behavior of the radio-capitate joint during wrist flexion–extension and radio-ulnar deviation. *Journal of biomechanics*, 34(11):1429–1438, 2001.

[182] Steven K Charles and Neville Hogan. Dynamics of wrist rotations. *Journal of biomechanics*, 44(4):614–621, 2011.

[183] Paolo De Leva. Adjustments to zatsiorsky-seluyanov's segment inertia parameters. *Journal of biomechanics*, 29(9):1223–1230, 1996.

[184] Vilayanur S Ramachandran and William Hirstein. The perception of phantom limbs. the do hebb lecture. *Brain: a journal of neurology*, 121 (9):1603–1630, 1998.

[185] Tamas Kapelner, Massimo Sartori, Francesco Negro, and Dario Farina. Neuro-musculoskeletal mapping for man-machine interfacing. *Scientific reports*, 10(1):1–10, 2020.

[186] Di Ao, Mohammad S Shourijeh, Carolynn Patten, and Benjamin J Fregly. Evaluation of synergy extrapolation for predicting unmeasured muscle excitations from measured muscle synergies. *Frontiers in computational neuroscience*, 14:108, 2020.